


2014

MODELING DYNAMICS OF OZONE AND NITROGEN OXIDES AT SUMMIT, GREENLAND WITH A 1-D PROCESS-SCALE MODEL

Keenan Anton Murray
Michigan Technological University

Follow this and additional works at: <https://digitalcommons.mtu.edu/etds>

 Part of the [Atmospheric Sciences Commons](#), [Environmental Chemistry Commons](#), and the [Environmental Engineering Commons](#)
Copyright 2014 Keenan Anton Murray

Recommended Citation

Murray, Keenan Anton, "MODELING DYNAMICS OF OZONE AND NITROGEN OXIDES AT SUMMIT, GREENLAND WITH A 1-D PROCESS-SCALE MODEL", Dissertation, Michigan Technological University, 2014.

<https://digitalcommons.mtu.edu/etds/930>

Follow this and additional works at: <https://digitalcommons.mtu.edu/etds>

 Part of the [Atmospheric Sciences Commons](#), [Environmental Chemistry Commons](#), and the [Environmental Engineering Commons](#)

MODELING DYNAMICS OF OZONE AND NITROGEN OXIDES AT SUMMIT,
GREENLAND WITH A 1-D PROCESS-SCALE MODEL

By

Keenan Anton Murray

A DISSERTATION

Submitted in partial fulfillment of the requirements for the degree of

DOCTOR OF PHILOSOPHY

In Environmental Engineering

MICHIGAN TECHNOLOGICAL UNIVERSITY

2014

© 2014 Keenan A. Murray

This dissertation has been approved in partial fulfillment of the requirements for the Degree of DOCTOR OF PHILOSOPHY in Environmental Engineering.

Department of Civil & Environmental Engineering

Dissertation Advisor: *Paul V. Doskey*

Committee Member: *Louisa Kramer*

Committee Member: *Alex S. Mayer*

Committee Member: *Sarah. A. Green*

Department Chair: *David Hand*

To my loving girlfriend and supporting family

Table of Contents

Chapter 1. Preface	5
Chapter 2. Abstract	6
Chapter 3. Introduction.....	8
Chapter 4. Modeling Dynamics of Ozone and Nitrogen Oxides at Summit, Greenland with a 1-D Process-Scale Model. I. Model Presentation and Chemical Dynamics During a Spring Ozone Intrusion Event	12
Chapter 5. Modeling Dynamics of Ozone and Nitrogen Oxides at Summit, Greenland with a 1-D Process-Scale Model. II. Temporal Variations of Snowpack Chemistry.....	91
Chapter 6. Modeling Dynamics of Ozone and Nitrogen Oxides at Summit, Greenland with a 1-D Process-Scale Model. III. Comparison of Measured Fluxes with Modeled Exchange with Snow	129
Chapter 7. Conclusions	153

Chapter 1. Preface

Chapter 4, *Modeling Dynamics of Ozone and Nitrogen Oxides at Summit, Greenland with a 1-D Process-Scale Model. I. Model Presentation and Chemical Dynamics During a Spring Ozone Intrusion Event*, is a planned submission to Atmospheric Environment. Brian Seok and Laurens Ganzeveld initially developed a parameterized model to attempt to replicate measurements of ozone and nitrogen oxides collected by Louisa Kramer, Brie Van Dam, and Detlev Helmig. The parameterized model was incapable of reproducing chemical trends in the snowpack, but was a first step in model development. Paul Doskey and Keenan Murray decided a process-scale model was required to replicate chemical measurements in the snowpack. The model was developed by Keenan Murray with the assistance of Laurens Ganzeveld and is presented in this paper. Rao Kotamarthi and Alex Mayer are acknowledged for assistances with initial process-scale model development.

Chapter 5, *Modeling Dynamics of Ozone and Nitrogen Oxides at Summit, Greenland with a 1-D Process-Scale Model. II. Temporal Variations of Snowpack Chemistry*, is a planned submission to Atmospheric Environment. Keenan Murray, Laurens Ganzeveld, and Brian Seok developed the process-scale model used to investigate temporal variations of snowpack chemistry. Louisa Kramer, Brie Van Dam, and Detlev Helmig provided meteorological and chemical measurements from Summit, Greenland used in the model and for model analysis. Paul Doskey provided insight of important chemical processes in snowpack and provided Keenan Murray with guidance in the paper development. Rao Kotamarthi is acknowledged for assistance with initial process-scale model development.

Chapter 6, *Modeling Dynamics of Ozone and Nitrogen Oxides at Summit, Greenland with a 1-D Process-Scale Model. III. Comparison of Measured Fluxes with Modeled Exchange with Snow*, is a planned submission to Atmospheric Environment. Keenan Murray, Laurens Ganzeveld, and Brian Seok developed the process-scale model used to estimate the surface exchange of NO_x and ozone. Louisa Kramer, Brie Van Dam, and Detlev Helmig provided meteorological and chemical measurements from Summit, Greenland used in the model and for calculating chemical fluxes of NO_x and ozone. Paul Doskey provided insight of important chemical processes in snowpack and provided Keenan Murray with guidance in the paper development. Rao Kotamarthi is acknowledged for assistance with initial process-scale model development.

Chapter 2. Abstract

This work presents a 1-D process scale model used to investigate the chemical dynamics and temporal variability of nitrogen oxides (NO_x) and ozone (O_3) within and above snowpack at Summit, Greenland for March-May 2009 and estimates surface exchange of NO_x between the snowpack and surface layer in April-May 2009. The model assumes the surface of snowflakes have a Liquid Like Layer (LLL) where aqueous chemistry occurs and interacts with the interstitial air of the snowpack. Model parameters and initialization are physically and chemically representative of snowpack at Summit, Greenland and model results are compared to measurements of NO_x and O_3 collected by our group at Summit, Greenland from 2008-2010.

The model paired with measurements confirmed the main hypothesis in literature that photolysis of nitrate on the surface of snowflakes is responsible for nitrogen dioxide (NO_2) production in the top ~50 cm of the snowpack at solar noon for March – May time periods in 2009. Nighttime peaks of NO_2 in the snowpack for April and May were reproduced with aqueous formation of peroxyntiric acid (HNO_4) in the top ~50 cm of the snowpack with subsequent mass transfer to the gas phase, decomposition to form NO_2 at nighttime, and transportation of the NO_2 to depths of 2 meters. Modeled production of HNO_4 was hindered in March 2009 due to the low production of its precursor, hydroperoxy radical, resulting in underestimation of nighttime NO_2 in the snowpack for March 2009. The aqueous reaction of O_3 with formic acid was the major sink of O_3 in the snowpack for March-May, 2009. Nitrogen monoxide (NO) production in the top ~50

cm of the snowpack is related to the photolysis of NO_2 , which underrepresents NO in May of 2009. Modeled surface exchange of NO_x in April and May are on the order of 10^{11} molecules $\text{m}^{-2} \text{s}^{-1}$. Removal of measured downward fluxes of NO and NO_2 in measured fluxes resulted in agreement between measured NO_x fluxes and modeled surface exchange in April and an order of magnitude deviation in May. Modeled transport of NO_x above the snowpack in May shows an order of magnitude increase of NO_x fluxes in the first 50 cm of the snowpack and is attributed to the production of NO_2 during the day from the thermal decomposition and photolysis of peroxyntic acid with minor contributions of NO from HONO photolysis in the early morning.

Chapter 3. Introduction

Nitrogen oxides ($\text{NO}_x = \text{NO} + \text{NO}_2$) and ozone (O_3) chemistry are intricately intertwined by the NO_x cycle. The NO_x cycle is represented by two chemical reactions, the photolysis of nitrogen dioxide (NO_2) to form O_3 and nitrogen monoxide (NO) and the reaction of NO with O_3 to form NO_2 . These reactions combined do not create or destroy NO_x nor ozone and occur at fast rates. Perturbing the NO_x cycle by introducing NO_2 or NO from an outside source causes production and destruction of O_3 , respectively. Since O_3 is a green house gas and a major oxidizing agent in the troposphere, understanding its' production and consumption is required for determining current and future anthropogenic impacts.

Depletion of ozone and production of nitrogen oxides in sunlit Arctic snowpack have been the focus of several field studies. Ozone is a greenhouse gas and an important tropospheric oxidant that is directly linked with the NO_x cycle. Relative levels of nitrogen dioxide (NO_2) and nitric oxide (NO) and mixing ratios of hydroperoxyl radical (HO_2) and organic peroxy radicals (RO_2) generated by oxidation of carbon monoxide, methane, and nonmethane hydrocarbons regulate production/destruction of O_3 . Thus, accurately representing the dynamics of O_3 and NO_x chemistry within sunlit snowpack in process-scale models is required to forecast impacts of climate change on the tropospheric chemistry of the Arctic.

Our research group and collaborators at University of Colorado, Boulder, measured a comprehensive suite of continuous of O_3 , NO_x , and temperature data within and above

the snowpack and wind speed/direction and irradiance at Summit, Greenland from June 2008 to July 2010. Chemical and temperature measurements were made at 2 heights above the surface and up to 14 intervals within the snowpack to a depth of 2.8 m. Observations during the sunlit season reveal higher and lower levels of NO_x and O_3 , respectively, deep in the snowpack compared to the surface layer. Ozone exhibits a diurnal cycle with peak concentrations in the evenings that diminish deeper in the snowpack. The diurnal cycle in NO shows a peak near solar noon located within the upper 50 cm of the snowpack. The profile of NO_2 sometimes exhibits 2 peaks in a diurnal cycle with the first peak observed at solar noon near the surface and the second peak in the evening extending deeper into the snowpack.

While chemical measurements reveal the snowpack is a chemically active environment, the physical and chemical mechanisms are poorly understood. Production of NO_x in snowpack is theorized to occur through photolysis of nitrate (NO_3^-) on the surface of snowflakes. Atmospheric chemists generally assume the NO_x terminating reaction of NO_2 with hydroxyl radical (OH) produces nitric acid (HNO_3) removing NO_x from the atmosphere by deposition. However, above snowpack, HNO_3 deposition is hypothesized to be the main source of NO_3^- for NO_2 production within the snowpack. Thus, photolysis of NO_3^- in snowpack might represent an important pathway for recycling NO_x back to the atmosphere. However, due to the dependence of nitrate photolysis on irradiance, nitrate photolysis cannot be the direct source of observed NO_2 peaks at nighttime within the snowpack.

The 1-D process-scale model presented in this work is used to test hypothetical sources of NO_x and analyze chemical dynamics within the snowpack. The model uses similar proposed chemical and physical processes defined in a previously published process-scale model capable of replicating measurements of NO , bromide monoxide, and O_3 1.5 meters above the snowpack at Summit, Greenland over a three day period. The model components include (1) a Liquid Like Layer on the surface of snowflakes where aqueous chemistry occurs, (2) mass transfer of chemical species between the aqueous and gas phases within the snowpack, (3) transport of chemical species in the interstitial air of snowpack by diffusion and “wind pumping”, which is vertical advection in the snowpack caused by wind over the snowpack micro-topography producing pressure perturbations, and (4) transport of chemical species in the overlying atmosphere by turbulent kinetic energy and concentration gradients. The included chemistry is extensive, including NO_x , HO_x , O_x , halogen, and organic chemistry in the gas and aqueous phases.

Here we present the 1-D process-scale model and the analysis of the chemical dynamics in the snowpack responsible for the observed trends of NO_x and O_3 in and above snowpack at Summit, Greenland. Temporal variations of chemical dynamics are analyzed by using the model to represent three 15-day episodes in March, April, and May. These months were chosen as they represent time periods when daily peak irradiance is less than 350 W m^{-2} , the sun rises and sets in a 24-hour period, and the sun does not set, respectively. Modeled surface exchange of NO_x from the snowpack will be compared to measurements made above the snowpack for the April and May time periods.

Chapter 4. Modeling Dynamics of Ozone and Nitrogen Oxides at Summit, Greenland with a 1-D Process-Scale Model. I. Model Presentation and Chemical Dynamics During a Spring Ozone Intrusion Event^a

Keenan A. Murray¹, Louisa J. Kramer^{2,3}, Paul V. Doskey^{1,3,4,*}, Laurens Ganzeveld⁵, Brian Seok⁶, Brie Van Dam⁶, and Detlev Helmig⁶

¹Department of Civil and Environmental Engineering, Michigan Technological University, Houghton, MI, USA

²Department of Geological and Mining Engineering and Sciences, Michigan Technological University, Houghton, MI, USA

³Atmospheric Sciences Program, Michigan Technological University, Houghton, MI, USA

⁴School of Forest Resources and Environmental Science, Michigan Technological University, Houghton, MI, USA

⁵Department of Environmental Sciences, Wageningen University, Wageningen, Netherlands

⁶Institute of Arctic and Alpine Research, University of Colorado at Boulder, CO, USA

kmurray@mtu.edu, lkramer@mtu.edu, pvdoskey@mtu.edu*, Laurens.Ganzeveld@wur.nl, seok@Colorado.edu, Brie.Vandam@Colorado.EDU, Detlev.Helmig@Colorado.EDU

*Corresponding author. Phone: +1 906-487-2745

^a The material contained in this chapter is part of a planned submission to the Atmospheric Environment Journal.

Abstract

Observed trends of nitrogen dioxide (NO_2), nitric oxide (NO), and ozone (O_3) in snowpack interstitial air at Summit, Greenland were best replicated with a 1-D process-scale model that included aqueous-phase chemistry confined to a Liquid Like Layer (LLL) on the surface of snowflakes. Aqueous-phase oxidation of formic acid was a major removal process for O_3 with a maximum consumption rate of about 10^6 - 10^7 molec cm^{-3} s^{-1} . The maximum production rate of nitrogen dioxide (NO_2) by photolysis of nitrate (NO_3^-) was approximately 10^8 molec cm^{-3} s^{-1} , which was responsible for daily observations of maxima in NO_2 mixing ratios near solar noon. Maximum levels of NO_2 were observed deep in the snowpack at night and were attributed to aqueous- and gas-phase decomposition of peroxyntic acid in the upper 50 cm of the snowpack, which was responsible for about 10^8 molec cm^{-3} s^{-1} of NO_2 . The NO in snowpack interstitial air is confined to upper levels of the snowpack and observed profiles of NO mixing ratios are consistent with photolysis of gaseous NO_2 . Production of nitrogen oxides (NO_x) from NO_3^- photolysis was estimated to be two orders of magnitude larger than nitrite photolysis and supports the hypothesis that NO_3^- photolysis is the primary source of NO_x within sunlit snowpack in the Arctic.

Keywords: nitrogen monoxide, nitrogen dioxide, NO_x , ozone, 1-D process-scale model, Summit, Greenland

1. Introduction

Depletion of ozone (O_3) and production of nitrogen oxides (NO_x) in sunlit Arctic snowpack have been the focus of several field studies (Beine et al., 2002; Dibb et al., 2002; Helmig et al., 2007a; Honrath et al., 2000). Ozone is a greenhouse gas and an important tropospheric oxidant that is directly linked with the NO_x cycle. Relative levels of nitrogen dioxide (NO_2) and nitric oxide (NO) and mixing ratios of hydroperoxyl radical (HO_2) and organic peroxy radicals (RO_2) generated by oxidation of carbon monoxide, methane, and nonmethane hydrocarbons regulate production/destruction of O_3 . Thus, accurately representing the dynamics of O_3 and NO_x chemistry within sunlit snowpack in process-scale models is required to forecast impacts of climate change on the tropospheric chemistry of the Arctic.

Thomas et al. (2011) coupled the 1-D atmospheric boundary layer model MISTRA to a 1-D snowpack chemistry model and developed MISTRA-SNOW to reproduce NO_x , halogen, and O_3 profiles above and within snowpack at Summit, Greenland. Observed trends in NO, O_3 , and bromine monoxide (BrO) 1.5 meters above the snowpack for 10-13 June 2008 were replicated by MISTRA-SNOW; however, comparisons between modeled and measured chemical profiles in the snowpack were not made due to a lack of observations.

Van Dam et al. (2014) report a comprehensive suite of continuous measurements of O_3 , NO_x , and temperature within and above snowpack and wind speed/direction and irradiance at Summit, Greenland from June 2008 to July 2010. Chemical and temperature measurements were made at 2 heights above the surface and up to 14 intervals within the snowpack to a depth of 2.8 m. Observations during the sunlit season reveal higher and lower levels of NO_x and O_3 , respectively, deep in the snowpack compared to the surface layer. Ozone exhibits a diurnal cycle with peak concentrations in the evenings that diminish deeper in the snowpack. The diurnal cycle of NO shows a peak near solar noon located within the upper 50 cm of the snowpack. The profile of NO_2 sometimes exhibits 2 peaks in a diurnal cycle with the first peak observed at solar noon near the surface and the second peak in the evening extending deeper into the snowpack.

Production of NO_x in snowpack is theorized to occur through photolysis of nitrate (NO_3^-) on the surface of snowflakes (Dibb et al., 2002; Honrath et al., 2000; Jacobi et al., 2004). Nitric acid (HNO_3), which is produced through reaction of NO_2 with hydroxyl radical (OH), is the likely source of NO_3^- in snow and is typically considered a major sink of NO_x . Thus, photolysis of NO_3^- in snowpack might represent an important pathway for recycling NO_x back to the atmosphere. Observations in the snowpack at Summit, Greenland reveal peaks of NO and NO_2 at solar noon near the surface of the snowpack (Van Dam et al., 2014). The observations suggest NO_3^- as a potential source of NO_x near

the surface of the snowpack. However, photolysis of NO_3^- cannot directly produce the observed nighttime peaks of NO_2 . Oxidation of NO_2 by HO_2 and RO_2 produces a complex mixture of peroxyxynitric acid (HNO_4) and organic peroxy nitrates like peroxyacyl nitrate (PAN) that are thermally unstable and decompose forming NO_2 . Other dark reactions that may be responsible for nighttime production of NO_2 include aqueous-phase reaction of O_3 and nitrite (NO_2^-) and gaseous decomposition of dinitrogen pentoxide (N_2O_5).

Here we reproduce measured profiles of NO_x and O_3 in the sunlit snowpack of Summit, Greenland during a stratospheric O_3 intrusion event (Van Dam et al., 2014) with a 1-D process-scale model that incorporates physical and chemical processes identified by *Thomas et al. (2011)* in MISTRA-SNOW. The 1-D process scale model incorporates non-uniform representations of several snowpack parameters and modified representations of mass transfer and advection in the snowpack. The focus of the modeling experiment is 15-30 April 2009 when a stratospheric O_3 intrusion event elevated O_3 mixing ratios approximately 30 ppbv above the annual average of 44-50 ppbv reported by *Helmig et al. (2007b)* for the period 2000-2005 and surface wind speeds reached a maximum of about 17 m s^{-1} .

2. Model description

Key snowpack processes represented in MISTRA-SNOW, i.e., diffusion, advection in snowpack generated by surface winds and microtopography (windpumping), a Liquid Like Layer (LLL) on the surface of snowflakes, gas- and aqueous-phase chemistry in snowpack, and mass transfer between the phases (Thomas et al., 2011) were included in the 1-D process-scale model (Fig. 4.1). The Finite Volume Method with Crank-Nicholson discretization of the various physical processes was applied. The model allows for changes in the number and thickness of snowpack layers and is guided by measurements of surface layer O₃, surface and boundary layer temperatures, irradiance, and wind speed. The model domain includes 3 m of the atmosphere above the surface and the upper 3 m of the snowpack, which are each divided into 20 layers. Layers near the snowpack-atmosphere interface are the most narrow and increase in thickness near the boundaries.

Physical representation of snow

The specific surface area and radius of snowflakes, which are geometrically represented as spheres, are determined empirically based upon a user defined snow density profile (Domine et al., 2008) and are calculated as follows:

$$SSA = -308.2 \text{LOG}_{10}(\rho_{snow}) - 205.96 \quad (1)$$

$$r = \frac{3}{SSA \rho_{snow}} \quad (2)$$

where SSA is the specific surface area ($\text{cm}^2 \text{g}^{-1}$), r is the radius (cm), and ρ_{snow} is the snow density (g cm^{-3}). Snowpack porosity is calculated by mass balance and the density of snow and ice according to the following:

$$\phi = 1 - \frac{\rho_{snow}}{\rho_{ice}} \quad (3)$$

where Φ is snowpack porosity and ρ_{ice} is the ice density (g cm^{-3}). The density gradient used in the analysis is assumed to be linear from the surface of the snowpack to a depth of 3 m and ranges from 0.3 to 0.5 g cm^{-3} with the lowest density at the surface of the snowpack. The values are based on reported values of rounded grains in windpacked snow (Domine et al., 2008) and model iterations.

Aqueous or aqueous-like chemistry is assumed to occur on the surface of snowflakes in a thin Liquid-Like Layer (LLL), which is reported to vary in thickness from 1 to 30 nm

(Rosenberg, 2005). The initial LLL thickness in the model is 30 nm and is adjusted online for changes in solute concentration and temperature as follows (Cho et al., 2002):

$$\theta \approx \frac{M_{H_2O}RT_f}{1000\Delta H_f^o} \left(\frac{T}{T_f - T} \right) C_T^o \quad (4)$$

where θ is the mass fraction of liquid to solid water, M_{H_2O} is the molecular weight of water (g mol^{-1}), R is the ideal gas constant ($\text{J K}^{-1} \text{mol}^{-1}$), T_f is the freezing point temperature of water (K), ΔH_f^o is the enthalpy of fusion (J kg^{-1}), and C_T^o is the total solute concentration in melted snow ($m, \text{mole}_{\text{solute}} \text{kg}_{\text{solvent}}^{-1}$), which is based upon the initialized LLL thickness. Through various model runs it was determined the changes in solute concentrations and temperature do not greatly affect LLL thickness.

Atmosphere and snowpack temperature profiles

The temperature profile in the atmosphere is guided by measurements (Van Dam et al., 2014). Snowpack surface temperature is estimated by linear interpolation of measurements across the atmosphere-snow interface, which is reasonable as the top ~50 cm of the snowpack is directly affected by the temperature of the overlying atmosphere (Fig. 4.2). The estimated surface temperature is used to estimate temporal variations in the temperature profile as follows (Thomas et al., 2011):

$$\frac{\partial T}{\partial t} = \frac{\partial}{\partial z} \left(\frac{k_{eff}}{\rho_{snow} C_p} \frac{\partial T}{\partial z} \right) \quad (5)$$

Where T is the temperature (K), t is time (s), k_{eff} is the thermal conductivity ($\text{W m}^{-1} \text{K}^{-1}$), and C_p is the heat capacity of snow ($\text{J g}^{-1} \text{K}^{-1}$). Thermal conductivity is set to $0.25 \text{ W m}^{-1} \text{K}^{-1}$ (Thomas et al., 2011) and heat capacity is estimated by a weighted average that is based upon Φ and heat capacities of air and ice.

Governing equations of the 1-D process-scale model

Temporal variations in concentrations of chemical species are calculated as follows:

$$\frac{\partial C_g}{\partial t} = -\nabla \cdot (U_{\text{firn}} C_g) + \nabla \cdot (D_g C_g) - L k_{mt} \left(C_g - \frac{C_a}{H} \right) + P - D \quad (6)$$

$$\frac{\partial C_a}{\partial t} = k_{mt} \left(C_g - \frac{C_a}{H} \right) + P - D \quad (7)$$

where C_g and C_a are concentrations (molec cm⁻³) of chemical species in the gas- and aqueous-phases, respectively, U_{firn} is the vertical advective velocity in the snowpack (m s⁻¹), D_g is the effective diffusion coefficient (m² s⁻¹), L is the volumetric ratio of LLL to interstitial air, k_{mt} is the mass transfer coefficient (m³ aqueous m⁻³ air s⁻¹), H is the dimensionless Henry's law constant (vol_{air} vol_{water}⁻¹), and P and D are the chemical production and destruction of the species, respectively. Toyota and McConnell developed the following equations to estimate vertical advective velocity in snowpack based upon measured wind speeds above the snowpack (Toyota, 2005):

$$U_{firn} = \frac{6k\rho_{air}}{\pi\mu\lambda_{surf}} \frac{h}{\lambda_{surf}} \frac{\sqrt{\alpha^2 + 1}}{\alpha} u_{10}^2 (C_1 \exp\left(\frac{z}{\delta}\right) - C_2 \exp\left(-\frac{z}{\delta}\right)) \quad (8)$$

$$\delta = \frac{1}{2} \frac{\alpha}{\sqrt{\alpha^2 + 1}} \lambda_{surf} \quad (9)$$

$$C_1 = \frac{\exp\left(\frac{H_s}{\delta}\right)}{\exp\left(\frac{H_s}{\delta}\right) + \exp\left(-\frac{H_s}{\delta}\right)} \quad C_2 = \frac{\exp\left(-\frac{H_s}{\delta}\right)}{\exp\left(\frac{H_s}{\delta}\right) + \exp\left(-\frac{H_s}{\delta}\right)} \quad (10) (11)$$

where k is the permeability of the snowpack (m^2), ρ_{air} is the density of air (kg m^{-3}), μ is the dynamic viscosity of air ($\text{kg m}^{-1} \text{s}^{-1}$), λ_{surf} is the relief wavelength of the microtopography (m), h is the relief amplitude of the microtopography (m), α is the horizontal aspect ratio of the microtopography (dimensionless), u_{10} is the wind speed at an elevation of 10 m above the surface of the snowpack (m s^{-1}), z is the depth in the snowpack (m), and H_s is the depth of the ventilated snowpack (m). Values of the advection parameters are given in Table 4.1. The depth of O_3 intrusion in the modeled profile was used to select the values of H_s , h , and λ_{surf} .

The effective diffusion coefficient is based upon molecular diffusion and is calculated as follows:

$$D_g = D_{g,mol} * \frac{\tau}{\phi} \quad (12)$$

where $D_{g,mol}$ is the molecular diffusion coefficient ($\text{m}^2 \text{s}^{-1}$) and τ is the tortuosity.

Tortuosity was set at a constant value of $2/\pi$ due to the assumed spherical shape of a snowflake. To estimate k_{mt} , mass transfer between snowpack interstitial air and the surface of an assumed, spherical snowflake is treated the same as mass transfer between a water droplet and the atmosphere (Sander, 1999) as follows:

$$k_{mt} = \left(\frac{r^2}{3D_{g,mol}} + \frac{4r}{3v\alpha} \right)^{-1} \quad (13)$$

where r is the radius of the snowflake (m), v is the molecular velocity (m s^{-1}), and α is an accommodation coefficient (dimensionless), which represents the probability that a molecule at the gas-aqueous interface crosses the interface. Accommodation coefficients included in the model can be found in the supplementary material.

Values of the eddy diffusivity in the atmospheric surface layer are based upon observed values of the friction velocity and Monin-Obukhov length and are calculated as follows (Businger et al., 1971; Dyer, 1974):

$$K_H = k u_* \frac{z}{\phi} \quad (14)$$

$$\phi = \left(1 - 14 \frac{z}{L}\right)^{-\frac{1}{4}} \quad L < 0 \quad (15)$$

$$\phi = 1 + \frac{4.6z}{L} \quad L > 0 \quad (16)$$

$$\phi = 1 \quad L = 0 \quad (17)$$

where K_H is the eddy diffusivity ($\text{m}^2 \text{s}^{-1}$), u_* is the friction velocity (m s^{-1}), L is the Monin-Obukhov length (m), and k is the Von Karman constant (0.4). If values of u_* and L are not available, default values of $5.0 \times 10^{-3} \text{ m s}^{-1}$ and 0, respectively, are used in the model to represent a neutral stability in the boundary layer.

The Kinetic PreProcessor (KPP; (Damiani et al., 2012)) was used to solve the chemical kinetic system. Light and dark aqueous-phase chemistry is added to the model, which currently uses the KPP default tropospheric chemistry with minor modifications. Changes and addition of gas-phase reaction rates are documented in the supplementary material. Reaction rates are corrected for temperature using the Arrhenius equation when values of the activation energy are available. Photolysis rates are calculated with the FAST-JX model (Stickler, 2013) and adjusted for cloud cover by the ratio of measured irradiance to

modeled clear sky conditions. Details of the kinetic and photolytic reactions and initial conditions of the model are in the supplementary material.

Photolysis rates are adjusted by assuming exponential decay of photolysis rates as a function of depth in the snowpack and calculated with the calculus average according to the following:

$$j_z = \frac{j_0}{z_2 - z_1} \int_{z_1}^{z_2} \exp\left(\frac{z}{\varepsilon}\right) \quad (18)$$

where j_z and j_0 are the photolysis rates at any depth and at the surface of the snowpack (s^{-1}), respectively, z is depth in the snowpack and z_1 and z_2 represent the edge depths of the Finite Volume (m), and ε is the e-fold depth of the photolysis rate (m). The e-fold depths for chemical species not listed in Table 4.2 were set to a default value of 10 cm. Values of e-fold depths for O_3 and NO_2 were determined iteratively with the model. The e-fold depth of NO_2 was found to directly affect the NO profile and will be discussed in further detail later in the paper.

Calculation of rates of production and consumption of key chemical species

Chemical rates of production and consumption of key species were calculated with the model and the fraction of the production and consumption per individual chemical pathway were determined as follows:

$$P_i = \frac{\text{production}_i}{\sum_k \text{production}_k} * 100 \quad (19)$$

$$C_i = \frac{\text{consumption}_i}{\sum_k \text{consumption}_k} * 100 \quad (20)$$

where all values are absolute, P_i and C_i are the fraction (%) of overall production and consumption contributed from each reaction i , and k is an index for the summation over all production or consumption reactions. Aqueous-phase reactions were adjusted by the volumetric ratio, L . Chemical reactions with significant reverse reactions are adjusted to reflect the impact of reverse reactions as follows:

$$P_i = \frac{production_i - consumption_i}{(\sum_k production_k) - consumption_i} * 100 \quad (21)$$

$$C_i = \frac{consumption_i - production_i}{(\sum_k consumption_k) - production_i} * 100 \quad (22)$$

The adjustments can result in negative values, which are instead reported as values of zero. The calculated P_i and C_i are shown on contour graphs to provide a sense of location and time when a chemical species is influenced by reaction i . A subplot of total production or consumption rates is supplied for determination of the significance of estimated P_i 's and C_i 's.

Model initialization

Measurements of surface O₃, wind speed, friction velocity, Monin-Obukhov length, surface and atmospheric temperature, and irradiance were used to guide the model. Model time steps were generally 6 s unless a stability criterion required smaller steps. The model was allowed to spin up 15 days to the period of the model experiment (15-30 April 2009) and is sufficient in length to allow the model to achieve a pseudo-equilibrium state. Initial conditions for chemical species concentrations are presented in Table 4.8 Suppl.

3. Results and discussion

The 1-D process-scale model was applied to the period 15 - 30 April 2009, which included a stratospheric O₃ intrusion event on April 17 (Van Dam et al., 2014). Mixing ratios of O₃ were approximately 30 ppb_v above the annual average of 43.8-50.3 ppb_v reported by *Helmig et al. (2007b)* for 2000-2005, which aided in identifying physical and chemical processes that regulated the dynamics of O₃ and NO_x within and above sunlit snowpack. Observations include profiles of temperature (Fig. 4.2), wind speed (Fig. 4.3), and O₃, NO₂, NO, and irradiance (Fig. 4.4). The upper 50 cm of the snowpack and overlying atmospheric surface layer respond to the diurnal cycle in temperature; however, temperatures deeper in the snowpack remained relatively constant during the 2-week period (Fig. 4.2). Positive and negative temperature gradients were observed between the deep snowpack and the snow surface with some gradients reaching a maximum of approximately 30°C. Wind speeds during the period were 0-17 m s⁻¹ (Fig. 4.3). Peaks in the NO and NO₂ profiles are observed at solar noon; however, there is a discontinuity in the NO₂ profile with elevated levels occurring deep in the snowpack during the night. The O₃ levels in snowpack are greatest during the stratospheric ozone intrusion event on 17 April 2009.

Ozone

Agreement between observed and modeled diurnal cycles of O₃ is rather poor (Fig. 4.5). The windpumping parameterization in the model accurately predicts O₃ profiles in snowpack interstitial air during the O₃ intrusion event on 17 April; however, values are overestimated on 15-20 April. Wind speeds during the 15-30 April period are large and attain speeds greater than 5 m s⁻¹ (Fig. 4.3). Overestimates for 15-20 April imply high wind speed does not always produce large advection (windpumping) within the snowpack. Model estimates of the O₃ profile on 21-23 April when wind speeds were less than 5 m s⁻¹ exhibit small intrusions of O₃. Nighttime intrusions of O₃ and small intrusions near solar noon are predicted during the period. However, minimum values of O₃ were observed near solar noon, which implies the model is overestimating the downward flux of O₃ and/or production of O₃ near the surface of the snowpack. The model predicted larger O₃ intrusions when wind speeds increased during the 23-30 April period.

Photolysis accounts for up to 50% of the consumption of O₃ in the top 50 cm of the snowpack during the daytime (Fig. 4.6) and produces O(¹D) and O₂. Subsequent reaction of O(¹D) with H₂O is an important source of OH at Summit, Greenland (Yang et al., 2002). There is net consumption of O₃ within the snowpack at all times of the day except

in the top 50 cm of the snowpack near solar noon when production rates of O₃ are on the same order of magnitude as consumption rates, which may explain model predictions of small O₃ intrusion during the day. Production of O₃ near solar noon is accelerated by oxidation of NO by HO₂ and methyl peroxy radical (CH₃O₂) that allows O₃ to accumulate. Thus, an important daytime, loss mechanism for O₃ is not represented in the model. Model runs initialized with ppb_v levels of halogens were able to reduce net production of O₃, however, the halogen concentrations are much higher than the observed levels (Thomas et al., 2011). The majority of O₃ consumption in the snowpack is from the aqueous reaction of O₃ with formic acid (HCOOH) that produces CO₂, OH, and HO₂ (Fig. 4.7). The net aqueous-phase consumption rate of O₃ via oxidation of HCOOH is 10⁶-10⁷ molec cm⁻³ s⁻¹.

. Nitrogen oxides

There is good agreement between model estimates and observations of the diurnal profiles of NO (Fig. 4.8) and NO₂ (Fig. 4.9) in snowpack interstitial air. The maximum depth of NO penetration into the snowpack was about 25 cm and is directly related to the e-fold depth of the photolysis of NO₂. Thus, an e-fold depth of 25 cm for NO₂ was used throughout the modeling experiment. Trends in model estimates of NO₂ mixing ratios do not agree with observations during the beginning of the episode when wind speeds are large. The model predicts NO₂ produced near the surface at solar noon is transported

deep into the snowpack; however, NO_2 mixing ratios above the snowpack are overestimated and NO_2 mixing ratios in snowpack interstitial air are underestimated at night. Model predictions of downward transport of NO_2 in the snowpack by windpumping overestimate NO_2 mixing ratios with increasing depth. However, enhanced advection by windpumping might remove NO_2 or NO_2 precursors by mechanisms not represented in the model. Surface temperatures during the day at the beginning of the period are much lower than the remainder of the period, which would increase solubility of chemical species in the LLL and reduce NO_2 production rates and mixing ratios in snowpack interstitial air. Also, thermodynamic and kinetic parameters in the model might be underestimated at lower temperatures. Model estimates of NO_2 mixing ratios above snowpack at night agree with the observations; however, model estimates during the day do not agree with the measurements, with the exception of high wind speed conditions during the beginning of the period. Enhanced emissions of NO_2 or NO_2 precursors during high wind speed conditions would bring model estimates of NO_2 mixing ratios above the daytime snowpack into better agreement with observations.

Photolysis of NO_3^- contributes up to 80% of the NO_2 production in the top 50 cm of the snowpack during the daytime (Fig. 4.10), which agrees with the hypothesis proposed by *Honrath et al. (2000)*. Other major sources of NO_2 are the reactions of CH_3O_2 with NO to form formaldehyde (HCHO), NO_2 , HO_2 and OH , and HO_2 with NO to form NO_2 . Oxidation of NO by HO_2 and CH_3O_2 allows O_3 mixing ratios to increase in the top 50 cm of the snowpack without affecting levels of NO_x . Production of NO_2 at the surface of the

snowpack exhibits a diurnal trend, with peak production rates on the order of 10^8 molec $\text{cm}^{-3} \text{s}^{-1}$. The profile of NO_2 production via NO_3^- photolysis mirrors the observed NO_2 and NO profiles in the top 50 cm of snowpack (Fig. 4.4).

The principal chemical pathway for nighttime production of NO_2 deep in the snowpack is thermal decomposition of HNO_4 , which produces NO_2 and HO_2 (Fig. 4.11). Trends in NO_2 production via the mechanism are the same as trends in the observed NO_2 profile (Fig. 4.9). The reaction also appears to play an important role in nighttime production of NO_2 in the surface layer of the snowpack. Peak nighttime production in the snowpack and surface layer above snowpack are on the order of 10^8 and 10^4 - 10^5 molec $\text{cm}^{-3} \text{s}^{-1}$, respectively, with higher nighttime production in the top 50 cm of the snowpack and in the surface layer during the beginning of the period. The NO_2 formed near the surface of the snowpack is apparently transported deep into the snowpack. The hypothesis is supported by model predictions of greater NO_2 production via HNO_4 decomposition in the surface layer above snowpack at the beginning of the period when high wind speeds appear to transport more HNO_4 , NO_2 , and HO_2 from the top 50 cm of the snowpack into overlying atmosphere. The discovery of the importance of peroxyntic acid in nighttime production of NO_2 implies further research of peroxyntic acid chemistry and measurements in and above the snowpack should be pursued.

The model includes HNO₄ production from the gas- or aqueous-phase reaction of NO₂ and HO₂ (Fig. 4.12, Fig. 4.13). The HNO₄ produced in the gas phase at night is readily decomposed to NO₂, which represents a null cycle for production of nighttime NO₂. However, HNO₄ produced in the aqueous phase or in the gas phase during the day can decompose during the night and produce NO₂. Production of HNO₄ during the day is about 10⁸ molec cm⁻³ s⁻¹ and occurs primarily in the aqueous phase in the upper 50 cm of the snowpack. Daytime production of HNO₄ coincides with aqueous-phase production of NO₂, which apparently partitions into snowpack interstitial air and is transported deep into the snowpack where maxima in NO₂ mixing ratios are observed. Production of the HNO₄ precursor, HO₂, in the upper 50 cm of the snowpack is 10⁶-10⁸ molec cm⁻³ s⁻¹ and exhibits a diurnal cycle with a maximum at solar noon. There are several sources of HO₂ in the gas and aqueous phases. In addition to decomposition of HNO₄, gas-phase oxidation of NO by CH₃O₂ produces NO₂ and methoxy radical (CH₃O) that reacts with O₂ to produce HCHO and HO₂. Also, reaction of gas-phase HCHO with OH produces the formyl radical (HCO) that rapidly combines with O₂ to produce HO₂. Aqueous-phase oxidation of hydrated HCHO by OH produces HCOOH and HO₂, with maximum production rates occurring near solar noon in the upper 10 cm of the snowpack. Aqueous-phase reaction of HCOOH with O₃ is another source of HO₂.

Other sources of NO₂ during the night might include reaction of NO₂⁻ with O₃ and decomposition of PAN and N₂O₅. However, model predictions indicate the pathways do not make significant contributions to accumulation of NO₂ in snowpack interstitial air

during the night. Simulated levels of PAN above and within snowpack are about 30 ppt_v. Measurements of PAN within the snowpack exhibited increasing levels with depth and were approximately 200 ppt_v at a depth of 25 cm (Ford et al., 2002), which indicates the model underestimates PAN production. Levels of N₂O₅ in the top 1.5 m of the snowpack are below 10 ppt_v and are higher in the surface layer and deep in the snowpack at ~20 ppt_v. However, decomposition of the observed mixing ratios of PAN and N₂O₅ is insufficient to support observed levels of NO₂ deep in snowpack at night.

The shape of the NO profile is directly related to the e-fold depth of NO₂ photolysis. Photolysis of NO₂ is the major chemical reaction that produces NO during the day (Fig. 4.14). Production of NO in the top ~10 cm of the snowpack during the day is on the order of 10⁶ molec cm⁻³ s⁻¹. The measured irradiance shows the sun is setting during the first week of the period, and thus, model estimates of very small NO production (Fig. 4.14) are slightly in error and result from either incorrect modeling of photolysis rates or an artifact created by filling contours on the plots. Production of NO from NO₂ photolysis at night is possible during late April when the sun does not completely set. Photolysis of NO₂⁻ contributes to NO production in the top 10 cm of the snowpack in the evening and early morning and represents the remaining contribution of NO production (Fig. 4.14). Overall production of NO is two orders of magnitude less than NO₂ production implying photolysis of NO₃⁻ is the primary source of NO_x within the snowpack.

4. Conclusions

A 1-D process-scale model of the chemical dynamics of NO_x and O_3 above and within snow was used to evaluate key processes that regulated levels of the chemical species in snowpack during a stratospheric O_3 intrusion event (15-30 April 2009). Physical and chemical processes identified by *Thomas et al. (2011)* in MISTRA-SNOW were incorporated in the 1-D process scale model. Important features of the model include the following: (1) aqueous-phase chemistry occurs in a LLL on the surface of snowflakes, (2) concentrations of chemical species in the LLL are constrained by measurements of chemical species in snowpack interstitial air, (3) chemical species are transported within snowpack interstitial air by diffusion and wind pumping that is derived from measurements of surface wind speeds, (4) fluxes of chemical species above snowpack are calculated as the product of the measured gradients in mixing ratios of the species and the eddy diffusivity derived from meteorological measurements, (4) interpolated measurements of snowpack surface temperatures are used to calculate the thermal flux and variations in snowpack temperature with depth, (5) modeled gradients in O_3 mixing ratios in the overlying atmosphere are represented by the measured gradients, and (6) measured irradiance is used to adjust photolysis rates calculated with FAST-JX.

The 1-D process-scale model was able to reproduce trends in diurnal profiles of mixing ratios of NO_x and O_3 in snowpack interstitial air at Summit, Greenland. Mixing ratios of

O₃ and NO_x in interstitial air deep in the snowpack were sometimes elevated when high surface wind speeds were observed. Windpumping at high surface wind speeds is predicted to transport chemical species deep into the snowpack; however, some observations indicate the windpumping parameterization in the model overestimates transport of O₃ and NO₂ at high wind speeds. The LLL plays an important role in O₃ destruction through reaction with HCOOH. The overall O₃ consumption rate is 10⁶-10⁷ molec cm⁻³ s⁻¹. Peak production of NO₂ during the day is about 10⁸ molec cm⁻³ s⁻¹ through photolysis of NO₃⁻, which is responsible for 80% of the NO₂ production in the upper 50 cm of the snowpack. Thermal decomposition of HNO₄ at night produces NO₂ deep in the snowpack and in the surface layer at rates of 10⁸ and 10⁴-10⁵ molec cm⁻³ s⁻¹, respectively. The NO₂ produced in the upper 50 cm of the snowpack during the night through thermal decomposition of HNO₄ is transported downward and is responsible for elevating mixing ratios of NO₂ in interstitial air of the deep snowpack. Production of NO in the upper 10 cm of the snowpack during the day is about 10⁶ molec cm⁻³ s⁻¹. Nearly all the NO is produced through photolysis of NO₂.

Acknowledgments

Keenan A. Murray acknowledges assistance from V. Rao Kotamarthi (Argonne National Laboratory) and Alex Mayer (Michigan Technological University) with modeling chemical dynamics of the atmospheric boundary layer and implementation of the Finite Volume method

and windpumping model. Partial funding through teaching assistantships was provided by Michigan Technological University. The Arctic System Science Program of the National Science Foundation provided funding for the study through grant NSF-OPP-07-13992.

References

- Beine, H.J., Dominé, F., Simpson, W., Honrath, R.E., Sparapani, R., Zhou, X., King, M., 2002. Snow-pile and chamber experiments during the Polar Sunrise Experiment 'Alert 2000': exploration of nitrogen chemistry. *Atmospheric Environment* 36, 2707-2719.
- Businger, J.A., Wyngaard, J.C., Izumi, Y., Bradley, E.F., 1971. Flux-Profile Relationships in the Atmospheric Surface Layer. *Journal of the Atmospheric Sciences* 28, 181-189.
- Cho, H., Shepson, P.B., Barrie, L.A., Cowin, J.P., Zaveri, R., 2002. NMR Investigation of the Quasi-Brine Layer in Ice/Brine Mixtures. *The Journal of Physical Chemistry B* 106, 11226-11232.
- Damiani, A., De Simone, S., Rafanelli, C., Cordero, R.R., Laurenza, M., 2012. Three years of ground-based total ozone measurements in the Arctic: Comparison with OMI, GOME and SCIAMACHY satellite data. *Remote Sensing of Environment* 127, 162-180.
- Dibb, J.E., Arsenault, M., Peterson, M.C., Honrath, R.E., 2002. Fast nitrogen oxide photochemistry in Summit, Greenland snow. *Atmospheric Environment* 36, 2501-2511.
- Domine, F., Albert, M., Huthwelker, T., Jacobi, H.W., Kokhanovsky, A.A., Lehning, M., Picard, G., Simpson, W.R., 2008. Snow physics as relevant to snow photochemistry. *Atmos. Chem. Phys.* 8, 171-208.

- Dyer, A.J., 1974. A review of flux-profile relationships. *Boundary-Layer Meteorol* 7, 363-372.
- Ford, K.M., Campbell, B.M., Shepson, P.B., Bertman, S.B., Honrath, R.E., Peterson, M., Dibb, J.E., 2002. Studies of Peroxyacetyl nitrate (PAN) and its interaction with the snowpack at Summit, Greenland. *Journal of Geophysical Research: Atmospheres* 107, ACH 6-1-ACH 6-10.
- Helmig, D., Bocquet, F., Cohen, L., Oltmans, S.J., 2007a. Ozone uptake to the polar snowpack at Summit, Greenland. *Atmospheric Environment* 41, 5061-5076.
- Helmig, D., Oltmans, S.J., Carlson, D., Lamarque, J.-F., Jones, A., Labuschagne, C., Anlauf, K., Hayden, K., 2007b. A review of surface ozone in the polar regions. *Atmospheric Environment* 41, 5138-5161.
- Honrath, R.E., Guo, S., Peterson, M.C., Dziobak, M.P., 2000. Photochemical production of gas phase NO_x from ice crystal NO₃⁻. *J. Geophys. Res.* 105, 24183-24190.
- Jacobi, H.-W., Bales, R.C., Honrath, R.E., Peterson, M.C., Dibb, J.E., Swanson, A.L., Albert, M.R., 2004. Reactive trace gases measured in the interstitial air of surface snow at Summit, Greenland. *Atmospheric Environment* 38, 1687-1697.
- Rosenberg, R., 2005. Why Is Ice Slippery? *Physics Today* 58, 50-55.
- Sander, R., 1999. Modeling Atmospheric Chemistry: Interactions between Gas-Phase Species and Liquid Cloud/Aerosol Particles. *Surveys in Geophysics* 20, 1-31.
- Stickler, G., Kyle, L., 2013. Educational Brief: Solar Radiation and the Earth System, National Aeronautics and Space Administration.
- Thomas, J.L., Stutz, J., Lefer, B., Huey, L.G., Toyota, K., Dibb, J.E., von Glasow, R., 2011. Modeling chemistry in and above snow at Summit, Greenland – Part 1:

Model description and results. *Atmospheric Chemistry and Physics* 11, 4899-4914.

Toyota, K., McConnell, J.C, 2005. One-dimensional modeling of air-snowpack interactions and bromine activation in the springtime Arctic air (Oral presentation), AGU Fall meeting.

Van Dam, B., Helmig, D., Doskey, P.V., Kramer, L., Murray, K., Ganzeveld, L., Toro, C., Seok, B., 2014. Multi-year observations of O₃ and NO_x dynamics in the Summit, Greenland snowpack.

Yang, J., Honrath, R.E., Peterson, M.C., Dibb, J.E., Sumner, A.L., Shepson, P.B., Frey, M., Jacobi, H.W., Swanson, A., Blake, N., 2002. Impacts of snowpack emissions on deduced levels of OH and peroxy radicals at Summit, Greenland. *Atmospheric Environment* 36, 2523-2534.

Tables

Table 4.1. Windpumping parameters.

Parameter	Value
λ_{surf}	33 m, based on recommended ratio of h/λ_{surf} (Cunningham, 1993)
h	1 m (from model iterations focused on ozone intrusion)
α	1 (Thomas et al., 2012)
H_s	2 m (from model iterations focused on ozone intrusion)
μ	$1.73 \text{ kg m}^{-1} \text{ s}^{-1}$
k	$17.5\text{e-}10 \text{ m}^2$ (Domine et al., 2008)

Table 4.2. Values of e-fold depths for chemical species.

Species	e-fold depth [cm]	Reference
NO_3^-	10.0	(Thomas et al., 2011)
H_2O_2	13.3	(Galbavy et al., 2007)
NO_2^-	16.3	(Galbavy et al., 2007)
O_3	15.0	(Model iterations)
NO_2	25.0	(Model iterations)

Figures

Fig. 4.1

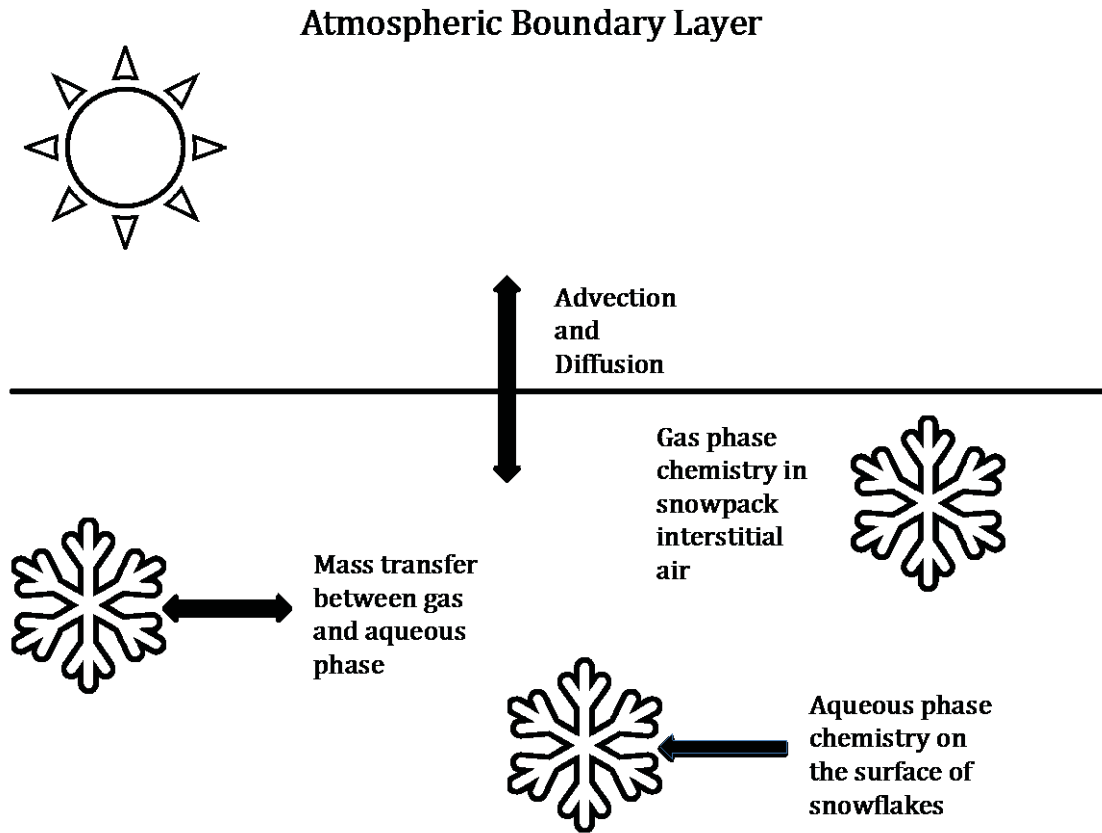


Fig. 4.1. Process diagram of chemical and physical processes included in the process-scale model.

Fig. 4.2

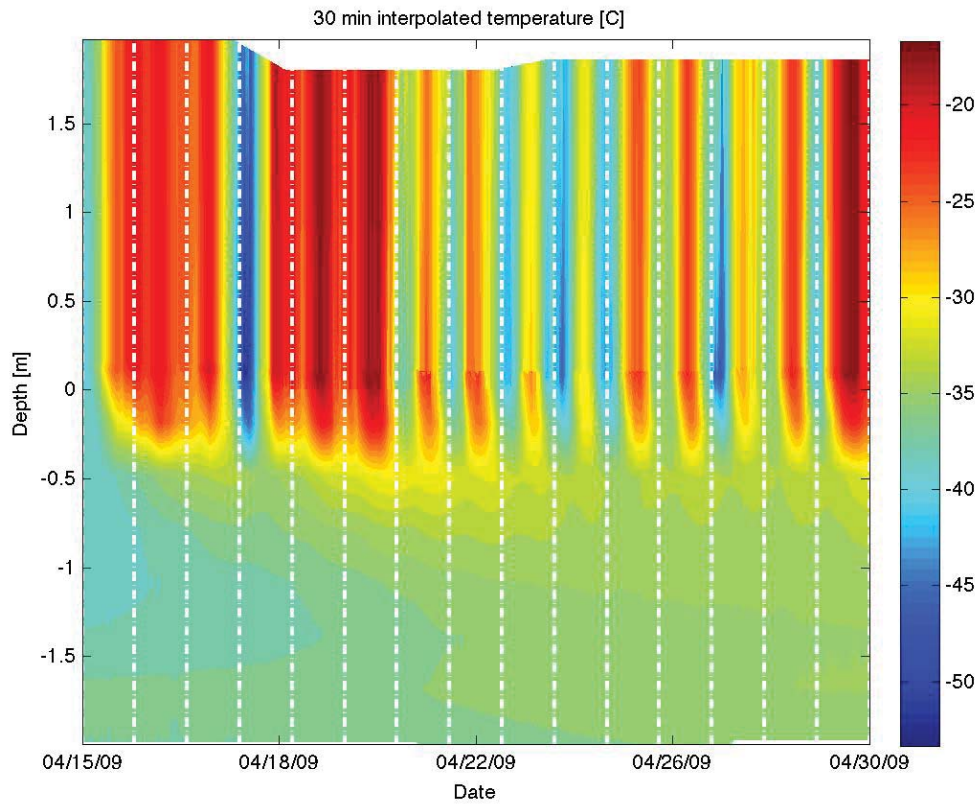


Fig. 4.2. The measured temperature profile above and within the snowpack for April 15th -30th, 2009. The temperature is in units of Celsius and negative depths represent the snowpack. Vertical white dashed lines represent midnight of each day.

Fig. 4.3

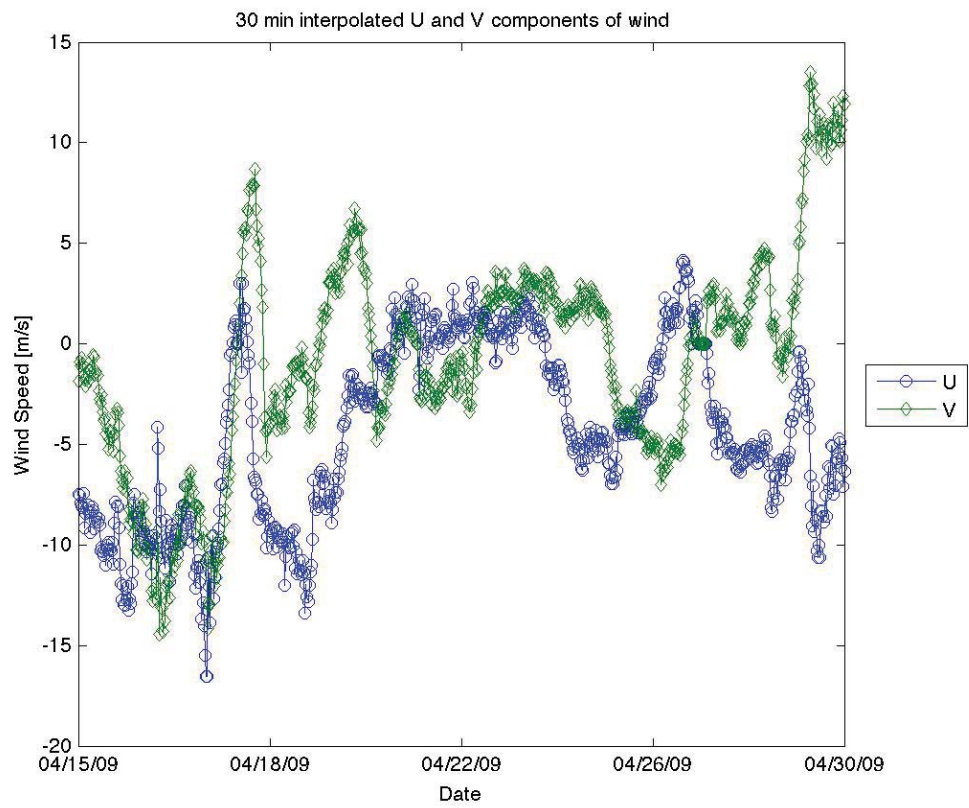


Fig. 4.3. The North/South (V) and East/West wind speeds (U) at Summit, Greenland April 15th-30th, 2009.

Fig. 4.4

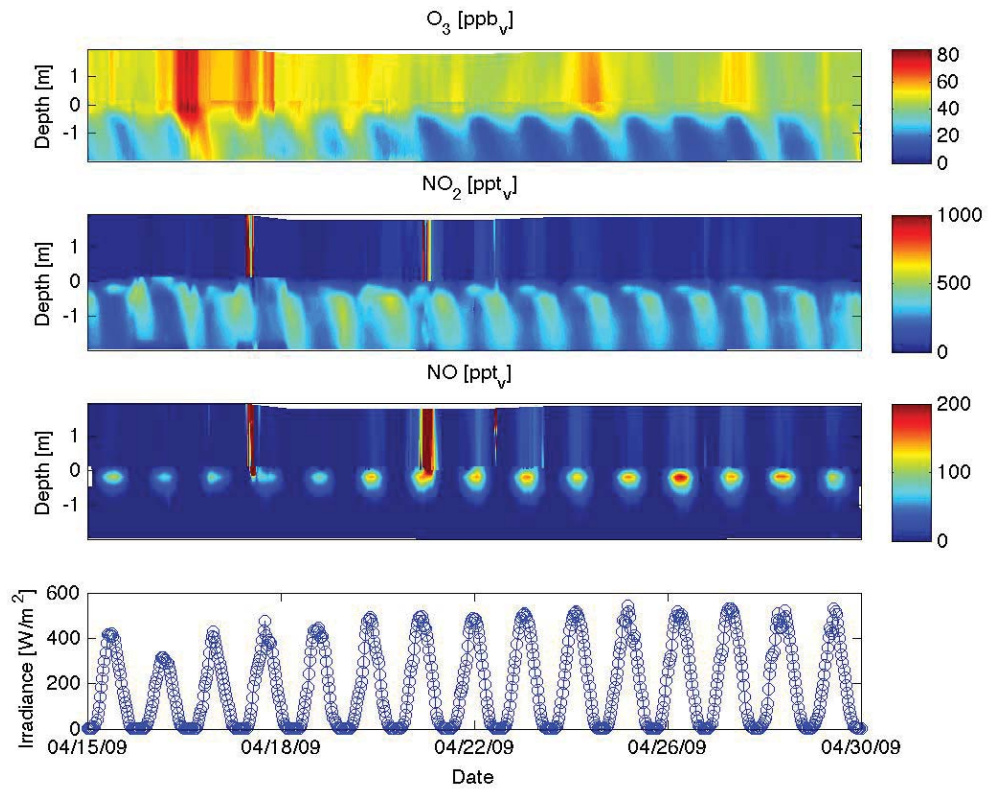


Fig. 4.4. Ozone, nitrogen monoxide, and nitrogen dioxide chemical profile observations at Summit, Greenland for April 15th-April 30th, 2009. Negative depths represent depths within the snowpack. The bottom plot contains the measured irradiance during the time period to provide a sense of time for the chemical observations.

Fig. 4.5

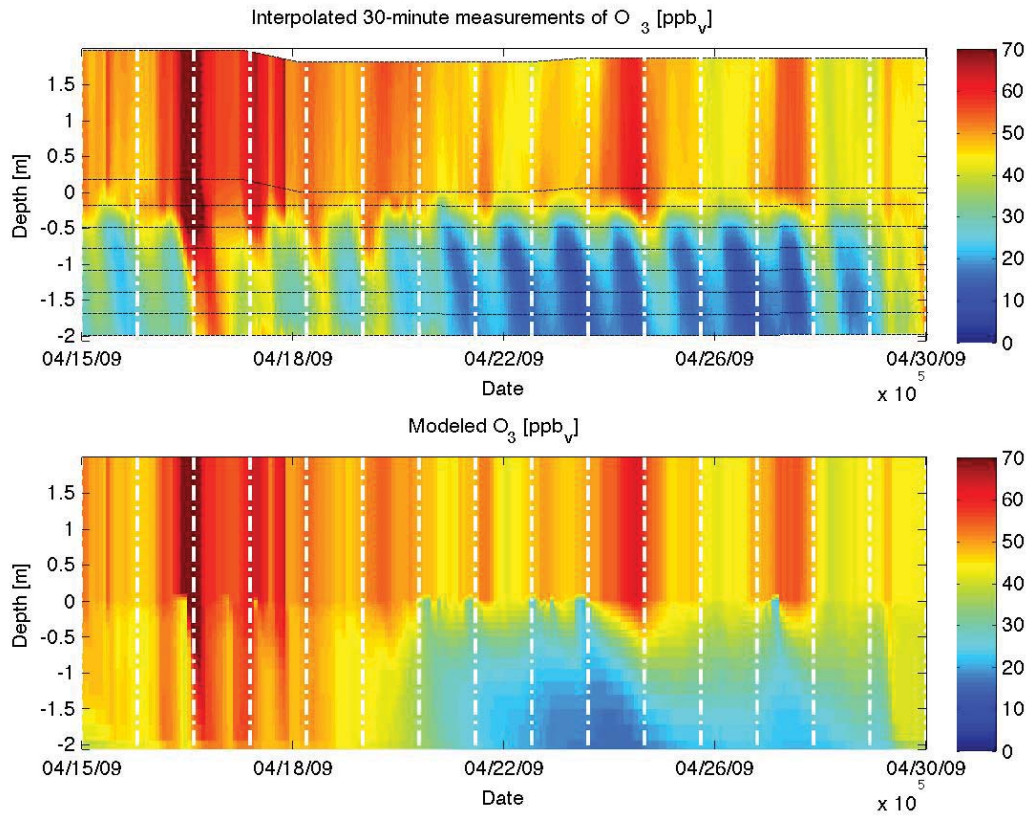


Fig. 4.5. Comparison of observed and modeled ozone profiles for April 15th-30th, 2009. Chemical profiles are in ppbv. Horizontal dashed black lines represent measurement heights. Vertical white dashed lines represent midnight of each day. Negative depths represent the snowpack.

Fig. 4.6

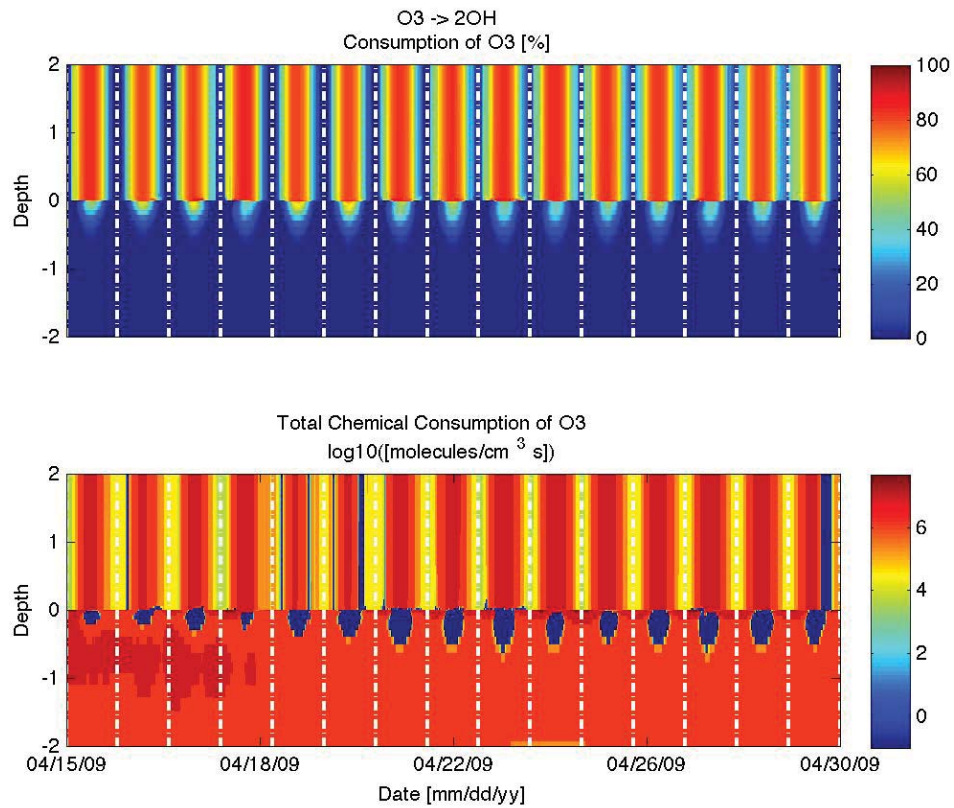


Fig. 4.6. Modeled consumption of ozone by the photolysis of ozone to form hydroxyl radical for April 15th -30th, 2009. The top graph shows the percent contribution of the reaction to consumption rates depicted in the bottom graph. Consumption rates are reported in $\log_{10}(\text{molec cm}^{-3} \text{ s}^{-1})$ to allow visualization of a range of consumption rates. Vertical white lines represent midnight of each day.

Fig. 4.7

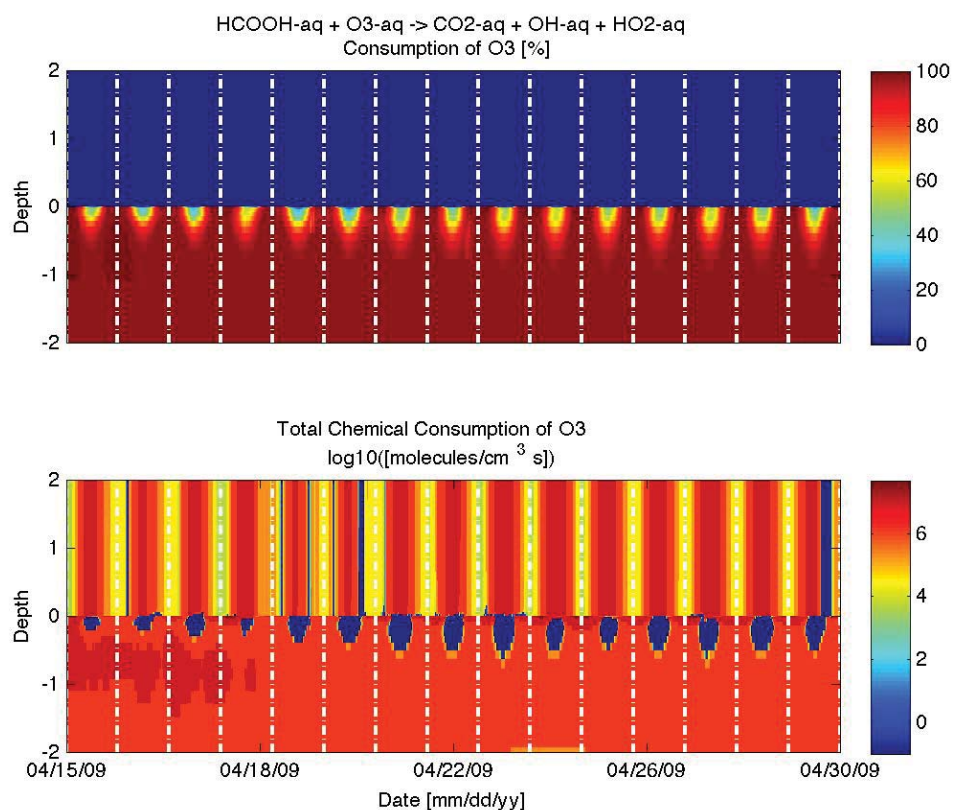


Fig. 4.7 Modeled consumption of ozone by the aqueous reaction of formic acid with ozone to form carbon dioxide, hydroxyl radical, and hydroperoxyl radical for April 15th - 30th, 2009. The top graph shows the percent contribution of the reaction to consumption rates depicted in the bottom graph. Consumption rates are reported in $\log_{10}(\text{molec cm}^{-3} \text{ s}^{-1})$ to allow visualization of a range of consumption rates. Vertical white lines represent midnight of each day.

Fig. 4.8

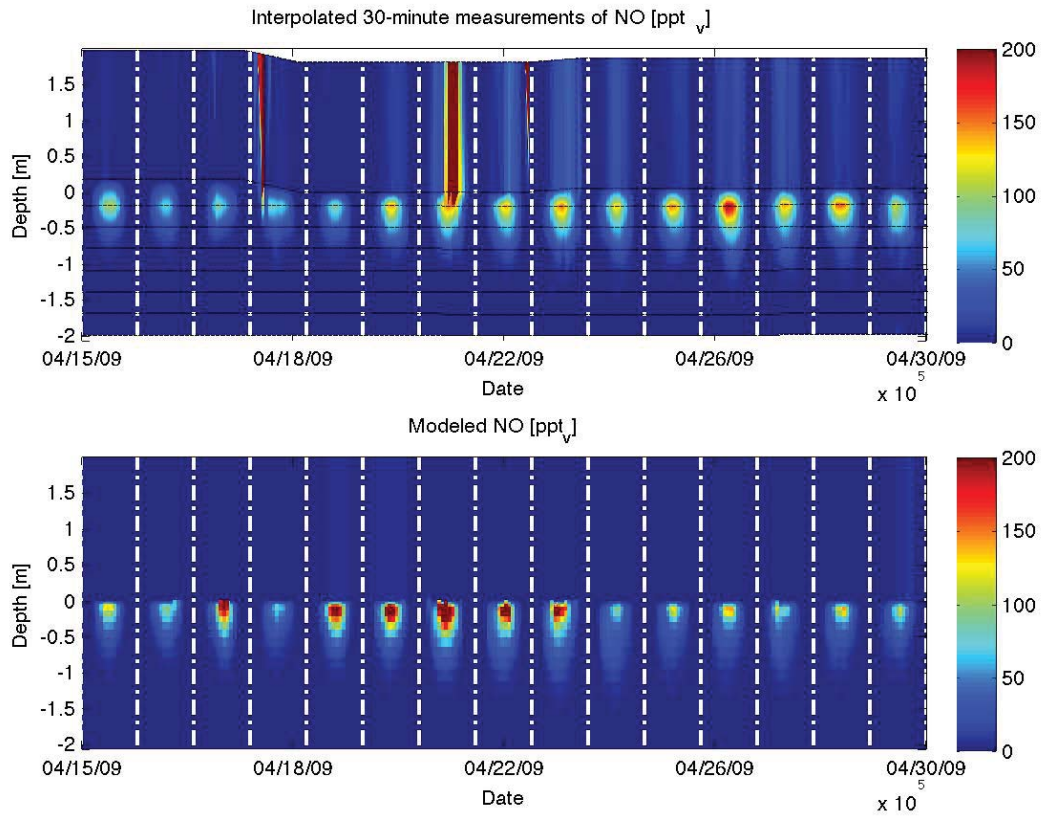


Fig. 4.8. Comparison of observed and modeled nitrogen monoxide profiles for April 15th-30th, 2009. Chemical profiles are in ppt_v. Horizontal dashed black lines represent measurement heights. Vertical white dashed lines represent midnight of each day. Negative depths represent the snowpack.

Fig. 4.9

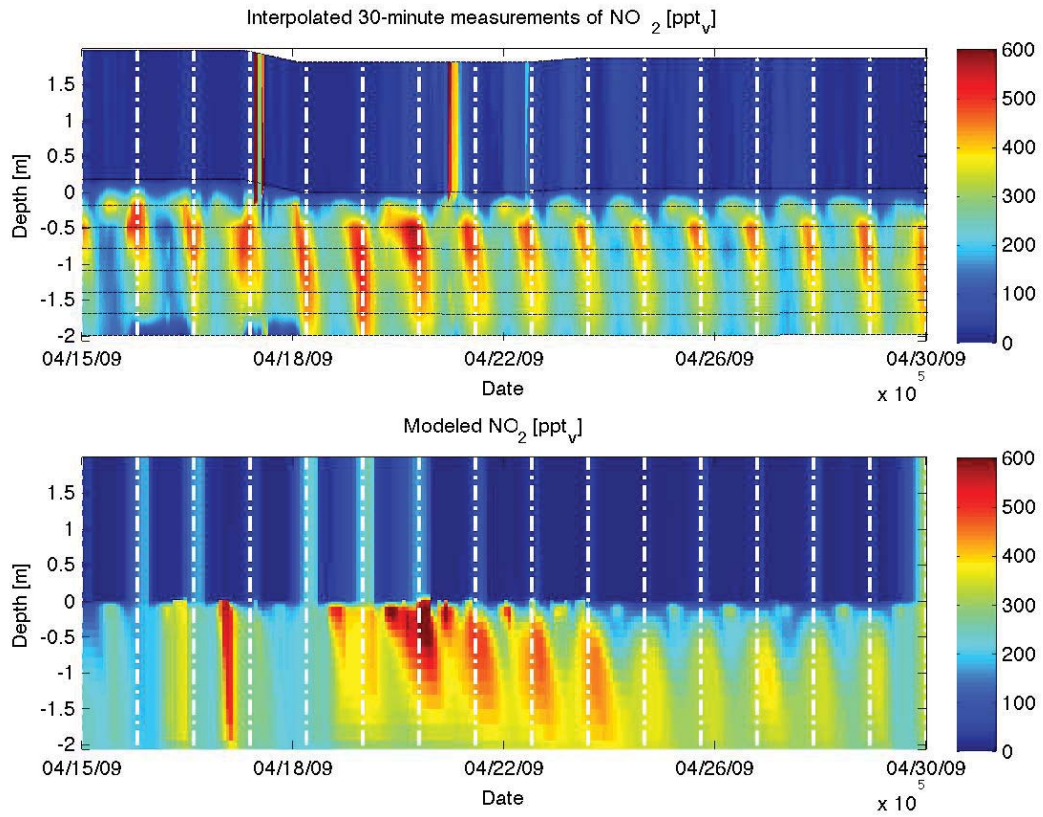


Fig. 4.9. Comparison of observed and modeled nitrogen dioxide profiles for April 11th - 30th, 2009. Chemical profiles are in ppt_v. Horizontal dashed black lines represent measurement heights. Vertical white dashed lines represent midnight of each day. Negative depths represent the snowpack.

Fig. 4.10

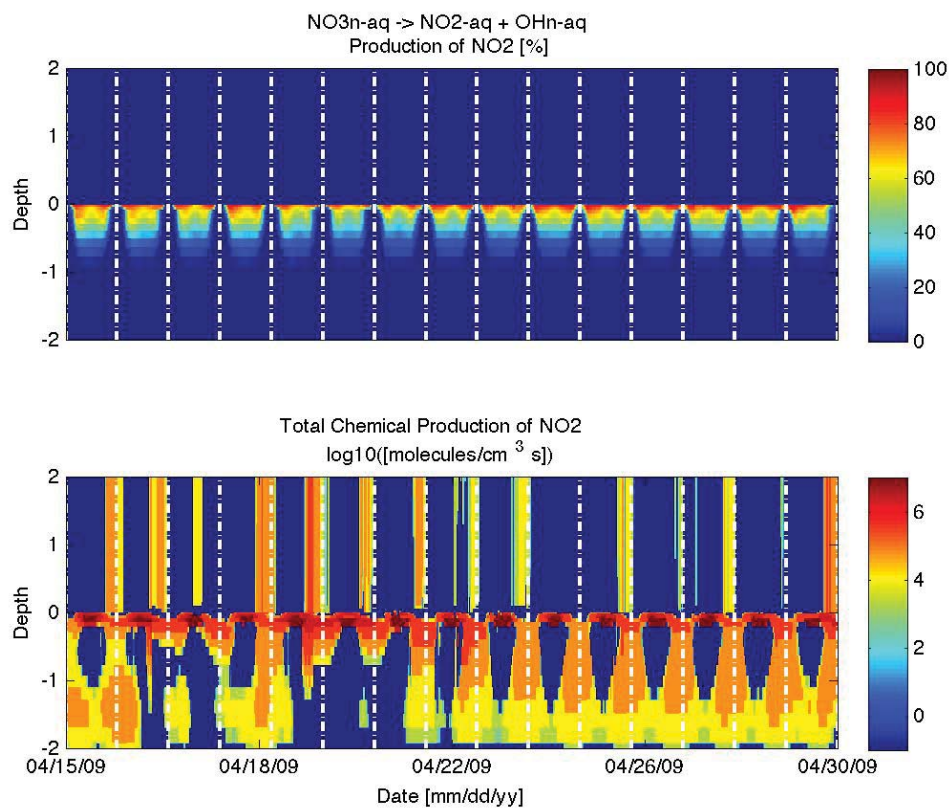


Fig. 4.10. Modeled production of nitrogen dioxide from the photolysis of nitrate ion to form nitrogen dioxide and hydroxide in the aqueous phase for April 15th-30th, 2009. The top graph shows the percent contribution of the reaction to production rates depicted in the bottom graph. Production rates are reported in $\log_{10}(\text{molec cm}^{-3} \text{ s}^{-1})$ to allow visualization of a range of production rates. Vertical white lines represent midnight of each day.

Fig. 4.11

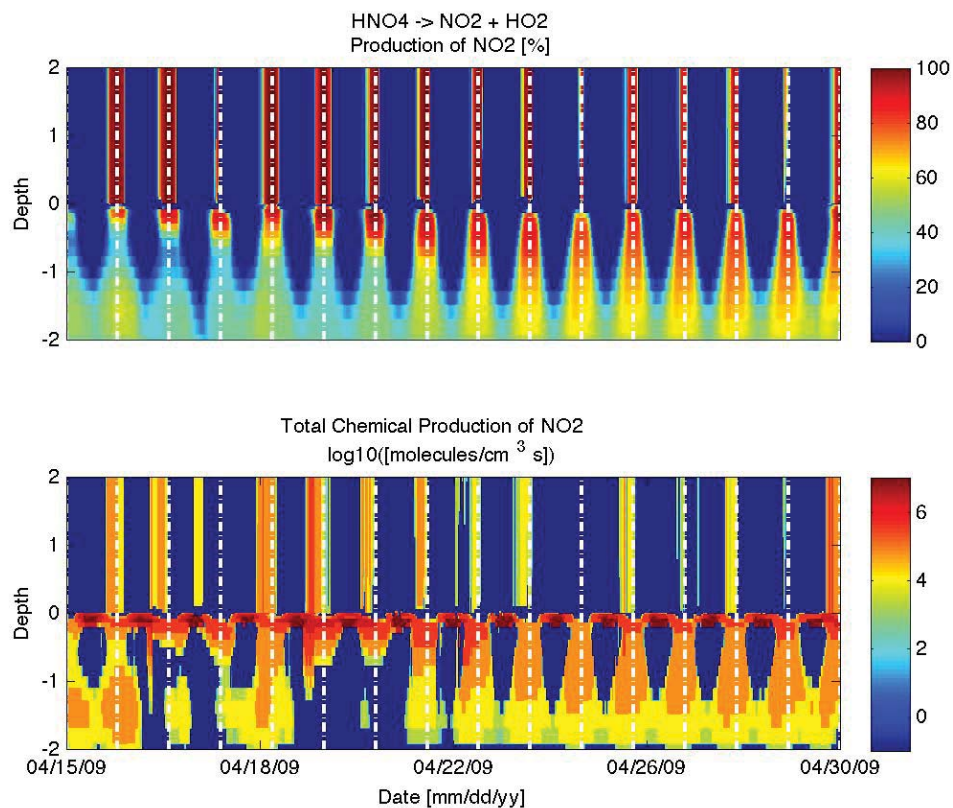


Fig. 4.11. Modeled production of nitrogen dioxide from the decomposition of peroxyntic acid to form hydroperoxyl radical and nitrogen dioxide for April 15th-30th, 2009. The top graph shows the percent contribution of the reaction to production rates depicted in the bottom graph. Production rates are reported in $\log_{10}(\text{molec cm}^{-3} \text{ s}^{-1})$ to allow visualization of a range of production rates. Vertical white lines represent midnight of each day.

Fig. 4.12

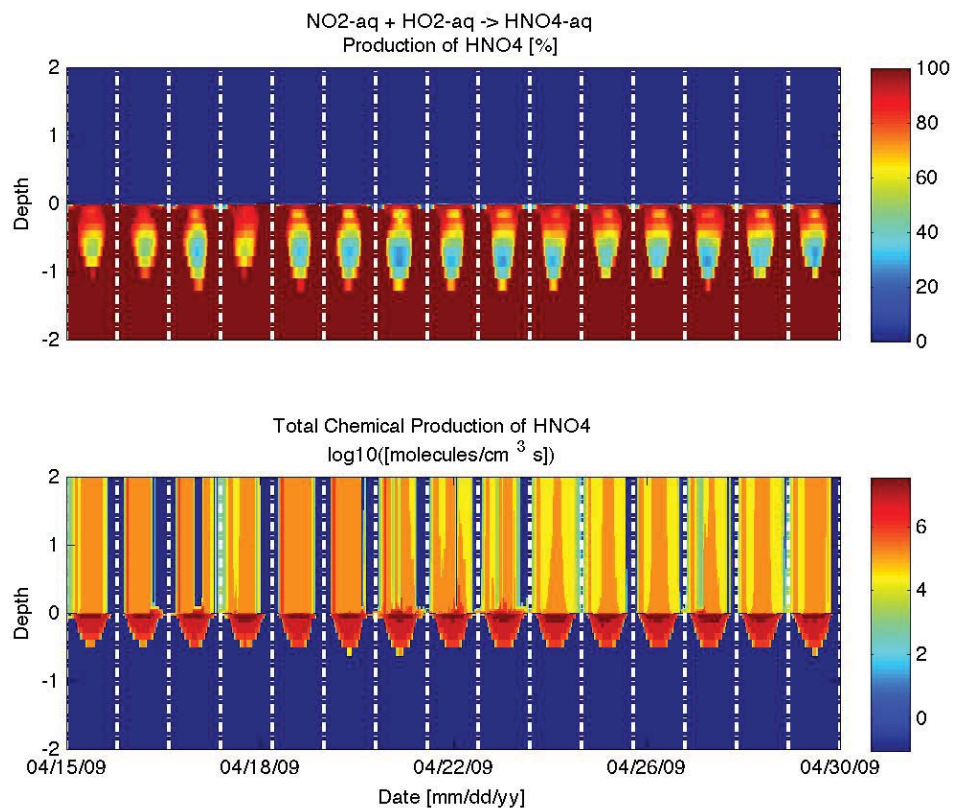


Fig. 4.12. Modeled production of peroxyntic acid from the aqueous reaction of nitrogen dioxide and hydroperoxyl radical for April 15th-30th, 2009. The top graph shows the percent contribution of the reaction to production rates depicted in the bottom graph. Production rates are reported in $\log_{10}(\text{molec cm}^{-3} \text{ s}^{-1})$ to allow visualization of a range of production rates. Vertical white lines represent midnight of each day.

Fig. 4.13

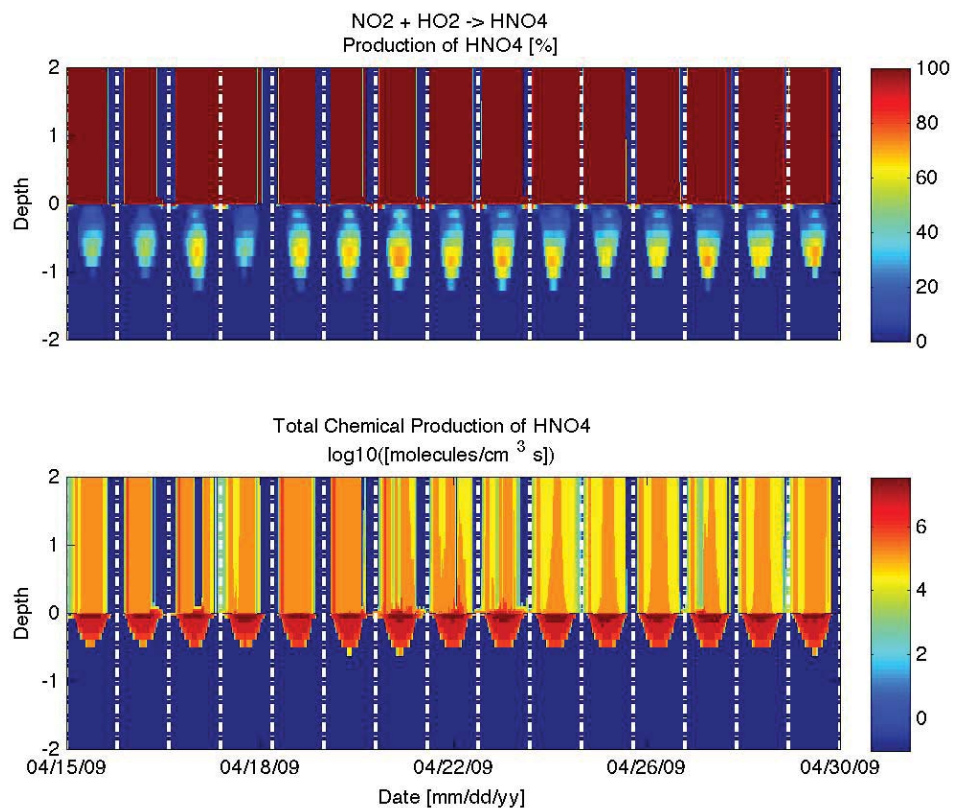


Fig. 4.13. Modeled production of peroxyntinic acid from the gas reaction of nitrogen dioxide and hydroperoxyl radical for April 15th-30th, 2009. The top graph shows the percent contribution of the reaction to production rates depicted in the bottom graph. Production rates are reported in $\log_{10}(\text{molec cm}^{-3} \text{ s}^{-1})$ to allow visualization of a range of production rates. Vertical white lines represent midnight of each day.

Fig. 4.14

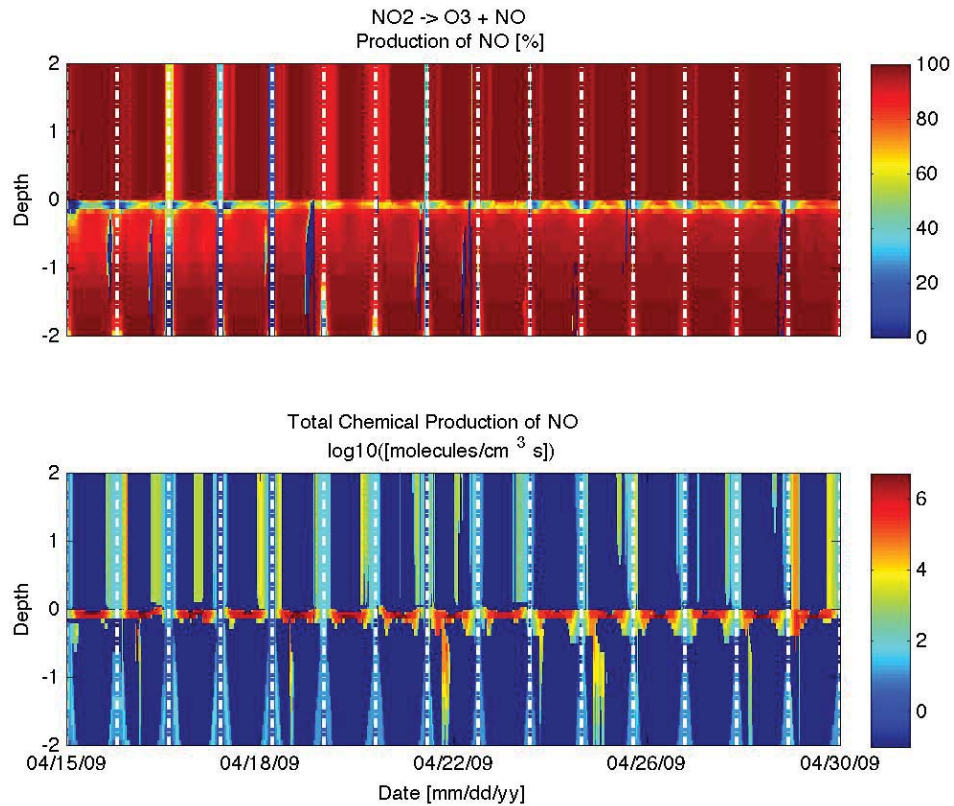


Fig. 4.14. Modeled production of nitrogen monoxide from the photolysis of nitrogen dioxide to form ozone and nitrogen monoxide for April 15th-30th, 2009. The top graph shows the percent contribution of the reaction to production rates depicted in the bottom graph. Production rates are reported in $\log_{10}(\text{molec cm}^{-3} \text{ s}^{-1})$ to allow visualization of a range of production rates. Vertical white lines represent midnight of each day.

Supplement for

Modeling Dynamics of Ozone and Nitrogen Oxides at Summit, Greenland with a 1-D
Process-Scale Model. I. Model Presentation and Chemical Dynamics During a Spring
Ozone Intrusion Event

This supplement includes the Henry's Law constant, mass transfer accommodation coefficients, gas and aqueous phase chemical reaction rates not included in the Kinetic PreProcessor default troposphere package, aqueous phase equilibrium equations, and initial chemical conditions.

5. Henry's law constants and mass transfer accommodation coefficients

Table 4.3 contains the standard Henry's Law (K_H^0) and mass transfer accommodation coefficient (α^0) used in the model. The Henry's Law constants (K_H) and mass transfer accommodation coefficients (α) are adjusted for temperature by the following equations:

$$K_H = K_H^0 \exp\left(-\frac{\Delta_{soln}H}{R}\left(\frac{1}{T} - \frac{1}{T^0}\right)\right)$$

$$\frac{d\frac{\alpha}{1-\alpha}}{d\frac{1}{T}} = -\frac{\Delta_{obs}H}{R}$$

where T is the temperature (K), T^0 is the reference temperature of 273.15 Kelvin, and $\Delta_{soln}H/R$ and $\Delta_{obs}H/R$ are values reported in Table 4.3.

6. Kinetic Aqueous Chemistry

Table 4.4 includes the kinetic aqueous chemistry in the model. The kinetic rate constants are calculated from the Arrhenius equation:

$$k = A \exp\left(-\frac{E_a}{RT}\right)$$

Where k is the rate constant, E_a is the activation energy of the reaction, A is the pre-factor, R is the gas constant, and T is the temperature (K). If the pre-factor is not listed, a special rate is used from the reference.

7. Aqueous Photolysis Chemistry

Table 4.5 includes the photochemical reactions in the aqueous phase. The rate constants are calculated online with the Fast-JX model (Wild et al., 2000).

8. Gas Phase Chemistry

Table 4.6 includes kinetic gas phase chemistry that are not the default troposphere package from the Kinetic PreProcessor (KPP). The kinetic rate constants are calculated from the Arrhenius equation:

$$k = A \exp\left(-\frac{E_a}{RT}\right)$$

Where k is the rate constant, E_a is the activation energy of the reaction, A is the pre-factor, R is the gas constant, and T is the temperature (K). If the pre-factor is not listed, a special rate is used from the reference.

9. Aqueous Equilibrium Constants

Table 4.7 includes the equilibrium parameters used in the aqueous chemistry. The equilibrium constants (K) are adjusted for temperature by the following equation:

$$K = K_{298} \exp\left(\frac{\Delta H}{R} \left(\frac{1}{T} - \frac{1}{T^0}\right)\right)$$

Where T is the temperature (K), T^0 is the reference temperature of 273.15 K, and $\Delta H/R$ is the enthalpy divided by the gas constant (K).

10. Initial chemical conditions

Table 4.8 provides values of species concentrations used to initialize the model. Some species are initialized at different concentrations or heights in or above the snowpack.

Tables

Table 4.3 Henry's Law constants and mass transfer coefficients

Species	K_H^0	$-\Delta_{\text{soln}}H/R$ [K]	α^0	$-\Delta_{\text{obs}}H/R$ [K]	Reference
O ₃	1.2E-2	2560	0.04	(water ice at 195- 262 K)	(Thomas et al., 2011)
O ₂	1.3E-3	1500	0.01	2000	(Thomas et al., 2011)
OH	3.0E1	4300	0.1	(water ice at 205- 253 K)	(Thomas et al., 2011)
HO ₂	3.9E3	5900	0.02	(at 275 K)	(Thomas et al., 2011)
H ₂ O ₂	1.0E5	6338	0.077	2769	(Thomas et al., 2011)
NO	1.9E-3	1480	5.0E-5	0	(Thomas et al., 2011)
NO ₂	6.4E-3	2500	1.0E-4	(water ice at 195	(Thomas et al.,

				K)	2011)
NO ₃	2.0	2000	4.0E-2	(at 273 K)	(Thomas et al., 2011)
N ₂ O ₅	2.1	3400	0.1	(at 195-300 K)	(Fried et al., 1994; Thomas et al., 2011)
HONO	4.9E1	4780	1.0E-3	(Water ice at 180- 200K)	(Thomas et al., 2011)
HNO ₃	1.7E5	8694	3.0E-3	(water ice at 220K)	(Thomas et al., 2011)
HNO ₄	1.2E4	6900	1.0E-1	(at 290 K)	(Thomas et al., 2011)
NH ₃	5.8E1	4085	6.0E-2	(at 295 K)	(Thomas et al., 2011)
CH ₃ OO	6.0	=HO2	0.01	2000	(Thomas et al., 2011)
ROOH	3.0E2	5322	4.6E-3	3273	(Thomas et al., 2011)

HCHO	7.0E3	6425	0.04	(at 260-270K)	(Thomas et al., 2011)
HCOO H	3.7E3	5700	1.4E-2	3978	(Thomas et al., 2011)
CO ₂	3.1E-2	2423	1.0E-2	2000	(Thomas et al., 2011)
HCl	1.2	9001	0.3	Water ice(191 211 K)	(Thomas et al., 2011)
HOCl	6.7E2	5682	=HOBr		(Thomas et al., 2011)
Cl ₂	9.1E-2	25000	1.0E-4	(water ice at 200K)	(Thomas et al., 2011)
HBr	1.3	10239	0.2	(water ice at 200K)	(Thomas et al., 2011)
HOBr	9.3E1	=HOCL	3.0E-3	(water ice at 223- 239 K)	(Thomas et al., 2011)
Br ₂	7.6E1	4094	3.8E-2	6546	(Thomas et al., 2011)

BrCl	9.4E-1	5600	1.5e-1	(at 270-285 K)	(Thomas et al., 2011)
CH ₄	1.3E-3		1.0E-1	0	(Thomas et al., 2011)

Table 4.4 Kinetic aqueous chemistry rates and activation energies

HO _x and O _x Reactions	n-order	A [M ¹⁻ⁿ s ⁻¹]	-E _a / R [K]	Reference
$O_3 + OH \rightarrow HO_2 + O_2$	2	1.1E8		(Thomas et al., 2011)
$O_3 + O_2^- \xrightarrow{H_2O} OH + OH^- + 2O_2$	2	1.5E9		(Thomas et al., 2011)
$OH + OH \rightarrow H_2O_2$	2	5.5E9		(Thomas et al., 2011)
$OH + HO_2 \rightarrow H_2O + O_2$	2	7.1E9		(Thomas et al., 2011)
$OH + O_2^- \rightarrow OH^- + O_2$	2	1.0E10		(Thomas et al., 2011)
$OH + H_2O_2 \rightarrow HO_2 + H_2O$	2	2.7E7	-1684	(Thomas et al., 2011)
$HO_2 + HO_2 \rightarrow H_2O_2 + O_2$	2	9.7E5	-2500	(Thomas et al., 2011)

$HO_2 + O_2^- \xrightarrow{H^+} H_2O_2$	2	1.0E8	-900	(Thomas et al., 2011)
$O + O_2 \rightarrow O_3$	2	4.0E9		(Thomas et al., 2011)
NO _y Reactions	n-order	A [M ¹⁻ⁿ s ⁻¹]	-E _a / R [K]	Reference
$HONO + OH \rightarrow NO_2 + H_2O$	2	1.0E9	-1500	(Rettich, 1978)
$HONO + H_2O_2 \xrightarrow{H^+} HNO_3 + H^+$ $+ H_2O$	3	4.6E3	-6800	(Thomas et al., 2011)
$NO_3 + OH^- \rightarrow NO_3^- + OH$	2	8.2E7	-2700	(Thomas et al., 2011)
$NO_2 + NO_2 \rightarrow HNO_3 + HONO$	2	1.0E8		(Thomas et al., 2011)
$NO_2 + HO_2 \rightarrow HNO_4$	2	1.8E9		(Thomas et al., 2011)
$NO_2^- + OH \rightarrow NO_2 + OH^-$	2	1.0E10	-1500	(Thomas et al., 2011)

$NO_2^- + O_3 \rightarrow NO_3^- + O_2$	2	5.0E5	-6950	(Thomas et al., 2011)
$NO_4^- \rightarrow NO_2^- + O_2$	1	7.70E20	-1.4E4	(Régimbal and Mozurkewich, 1997)
$O + NO_2^- \rightarrow NO_3^-$	2	1.48E9		(Thomas et al., 2011)
$O + NO_3^- \rightarrow NO_2^- + O_2$	2	2.24E8		(Thomas et al., 2011)
$NO + NO_2 \rightarrow 2NO_2^- + 2H^+$	2	2.0E8		(Thomas et al., 2011)
$NO + OH \rightarrow NO_2^- + H^+$	2	2.0E10		(Thomas et al., 2011)
$NO_2 + OH \rightarrow NO_3^- + H^+$	2	1.3E9		(Thomas et al., 2011)
$NO_2^- + NO_3 \rightarrow NO_2 + NO_3^-$	2	1.2E9	-1500	(Ross, 1979)
$NO_3 + HO_2 \rightarrow NO_3^- + H^+ + O_2$	2	4.5E9	-1500	(Jacob, 1986)

$NO_3 + O_2^- \rightarrow NO_3^- + O_2$	2	1.0E9	-1500	(Jacob, 1986)
$NO_3 + H_2O_2 \rightarrow NO_3^-$	2	1.0E6	-2800	(Chameides, 1984)
$O_3 + NO_2^- \xrightarrow{H^+} NO_2 + OH + O_2$	2	2.6E4	- 5142.3	(Chu and Anastasio, 2007)
$N_2O_5 \rightarrow 2HNO_3$	1	1.0		assumed
Organic Reactions	n-order	A [M ¹⁻ⁿ s ⁻¹]	-E _a / R [K]	Reference
$HCHO + OH \rightarrow HCOOH + HO_2$	2	7.7E8	-1020	(Thomas et al., 2011)
$HCOOH + OH \rightarrow HO_2 + CO_2$	2	1.1E8	-991	(Thomas et al., 2011)
$HCOO^- + OH \rightarrow OH^- + HO_2 + CO_2$	2	3.1E9	-1240	(Thomas et al., 2011)
$CH_3O_2 + HO_2 \rightarrow CH_3OOH$	2	4.3E5	-3000	(Jacob, 1986)

$CH_3O_2 + O_2^- \rightarrow CH_3OOH + OH^-$	2	5.0E7	-1600	(Jacob, 1986)
$CH_3OH + OH \rightarrow CH_3O_2$	2	9.7E8		(Thomas et al., 2011)
$CH_3OOH + OH \rightarrow CH_3O_2$	2	2.7E7	-1715	(Thomas et al., 2011)
$CH_3OOH + OH \rightarrow HCHO + OH$	2	1.1E7	-1715	(Thomas et al., 2011)
$CO_3^- + O_2^- \rightarrow HCO_3^- + OH^-$	2	6.5E8		(Thomas et al., 2011)
$CO_3^- + H_2O_2 \rightarrow HCO_3^-$	2	4.3E5		(Thomas et al., 2011)
$CO_3^- + HCOO^- \rightarrow 2HCO^- + HO_2$	2	1.5E5		(Thomas et al., 2011)
$HCO_3^- + OH \rightarrow CO_3^-$	2	8.5E6		(Thomas et al., 2011)
$DOM + OH \rightarrow HO_2$	2	5.0E9		(Thomas et al., 2011)

$HCOOH + NO_3 \xrightarrow{O_2} NO_3^- + H^+$ $+ CO_2 + HO_2$	2	2.1E5	-3200	(Dogliotti, 1967)
$HCOOH + O_3 \rightarrow CO_2 + HO_2$ $+ OH$	2	5.0	0	(Hoigne, 1983)
$HCOO^- + NO_3 \xrightarrow{O_2} NO_3^- + CO_2 +$ HO_2	2	6.0E7	-1500	(Jacob, 1986)
$CH_3OH + NO_3 \xrightarrow{O_2} NO_3^- + H^+$ $+ HCHO + HO_2$	2	1.0E6	-2800	(Dogliotti, 1967)
$HCO_3^- + O_2^- \rightarrow HO_2^- + CO_3^-$	2	1.5E6	0	(Schmidt, 1972)
Halogen Chemistry	n-order	A [M ¹⁻ⁿ s ⁻¹]	-E _a / R [K]	Reference
$Cl + H_2O_2 \rightarrow HO_2 + Cl^- + H^+$	2	2.0E9	0	(Thomas et al., 2011)
$2Cl \rightarrow Cl_2$	2	8.8E7	0	(Thomas et al., 2011)
$Cl^- + OH \rightarrow ClOH^-$	2	4.2E9	0	(Thomas et al.,

				2011)
$Cl^- + O_3 \rightarrow ClO^- + O_2$	2	3.0E-3	0	(Thomas et al., 2011)
$Cl^- + NO_3 \rightarrow NO_3^- + Cl$	2	9.3E6	-4330	(Thomas et al., 2011)
$Cl^- + HOCl + H^+ \rightarrow Cl_2$	3	2.2E4	-3508	(Thomas et al., 2011)
$Cl_2 \rightarrow Cl^- + HOCl + H^+$	2	2.2E1	-8012	(Thomas et al., 2011)
$Cl_2 + OH \rightarrow HOCl + Cl^-$	2	1.0E9	0	(Thomas et al., 2011)
$Cl_2^- + OH^- \rightarrow 2Cl^- + OH$	2	4.0E6	0	(Thomas et al., 2011)
$Cl_2^- + HO_2 \rightarrow 2Cl^- + H^+ + O_2$	2	3.1E9	0	(Thomas et al., 2011)
$Cl_2^- + O_2^- \rightarrow 2Cl^- + O_2$	2	6.0E9	0	(Thomas et al., 2011)
$Cl_2^- + H_2O_2 \rightarrow 2Cl^- + H^+ + HO_2$	2	7.0E5	-3340	(Thomas et al.,

				2011)
$Cl_2^- + NO_2^- \rightarrow 2Cl^- + NO_2$	2	6.0E7	0	(Thomas et al., 2011)
$Cl_2^- + CH_3O_2H$ $\rightarrow 2Cl^- + H^+$ $+ CH_3O_2$	2	7.0E5	-3340	(Thomas et al., 2011)
$2Cl_2^- \rightarrow Cl_2 + 2Cl^-$	2	6.2E9	0	(Thomas et al., 2011)
$Cl_2^- + Cl \rightarrow Cl^- + Cl_2$	2	2.7E9	0	(Thomas et al., 2011)
$ClOH^- \rightarrow Cl^- + OH$	1	6.0E9	0	(Thomas et al., 2011)
$ClOH^- + H^+ \rightarrow Cl + H_2O$	2	4.0E10	0	(Thomas et al., 2011)
$HOCl + HO_2 \rightarrow Cl + O_2$	2	7.5E6	0	(Thomas et al., 2011)
$Cl_2 + HO_2 \rightarrow Cl_2^- + H^+ + O_2$	2	1.0E9	0	(Thomas et al., 2011)

$Cl_2 + O_2^- \rightarrow Cl_2^- + O_2$	2	1.0E9	0	(Thomas et al., 2011)
$Cl^- + HNO_4 \rightarrow HOCl + NO_3^-$	2	1.4E-2	0	(Thomas et al., 2011)
$Br + OH^- \rightarrow BrOH^-$	2	1.3E10	0	(Thomas et al., 2011)
$Br^- + OH \rightarrow BrOH^-$	2	1.1E10	0	(Thomas et al., 2011)
$Br^- + O_3 \rightarrow BrO^- + O_2$	2	2.1E2	-4450	(Thomas et al., 2011)
$Br^- + NO_3 \rightarrow Br + NO_3^-$	2	3.8E9	0	(Thomas et al., 2011)
$Br^- + HOBr + H^+ \rightarrow Br_2$	3	1.6E10	0	(Thomas et al., 2011)
$Br_2 \rightarrow Br^- + HOBr + H^+$	1	9.7E1,	7457	(Thomas et al., 2011)
$Br_2^- + O_2^- \rightarrow 2Br^- + O_2$	2	1.7E8	0	(Thomas et al., 2011)

$Br_2^- + HO_2 \rightarrow Br_2 + H_2O_2$	2	4.4E9	0	(Thomas et al., 2011)
$Br_2^- + H_2O_2 \rightarrow 2Br^- + H^+$ $+ HO_2$	2	5.0E2	0	(Thomas et al., 2011)
$Br_2^- + Br_2^- \rightarrow Br^- + Br_2$	2	1.9E9	0	(Thomas et al., 2011)
$Br_2^- + CH_3O_2H$ $\rightarrow Br^- + H^+ CH_3O_2$	2	1.0E5	0	(Thomas et al., 2011)
$Br_2^- + NO_2^- \rightarrow 2Br^- + NO_2$	2	1.7E7	-1720	(Thomas et al., 2011)
$BrOH^- \rightarrow Br^- + OH$	1	3.3E7	0	(Thomas et al., 2011)
$BrOH^- + H^+ \rightarrow Br$	2	4.4E10	0	(Thomas et al., 2011)
$BrOH^- + Br^- \rightarrow Br_2^- + OH^-$	2	1.9E8	0	(Thomas et al., 2011)
$HOBr + HO_2 \rightarrow Br + O_2$	2	1.0E9	0	(Thomas et al., 2011)

$H\text{OBr} + \text{O}_2^- \rightarrow \text{Br}^- + \text{H}^+ + \text{O}_2$	2	3.5E9	0	(Thomas et al., 2011)
$H\text{OBr} + \text{H}_2\text{O}_2 \rightarrow \text{Br}^- + \text{H}^+ + \text{O}_2$	2	1.2E6	0	(Thomas et al., 2011)
$\text{Br}_2 + \text{HO}_2 \rightarrow \text{Br}_2^- + \text{H}^+ + \text{O}_2$	2	1.1E8	0	(Thomas et al., 2011)
$\text{Br}_2 + \text{O}_2^- \rightarrow \text{Br}_2^- + \text{O}_2$	2	5.6E9	0	(Thomas et al., 2011)
$\text{Br}^- + \text{HNO}_4 \rightarrow \text{HOBr} + \text{NO}_3^-$	2	5.4E-1	0	(Thomas et al., 2011)
$\text{Br}^- + \text{O}_3 + \text{H}^+ \rightarrow \text{HOBr} + \text{O}_2$	2	1.17E1	0	(Thomas et al., 2011)
$\text{Br}^- + \text{HOCl} + \text{H}^+ \rightarrow \text{BrCl}$	3	1.3E6	0	(Thomas et al., 2011)
$\text{Cl}^- + \text{HOBr} + \text{H}^+ \rightarrow \text{BrCl}$	3	2.3E10	0	(Thomas et al., 2011)
$\text{BrCl} \rightarrow \text{Cl}^- + \text{HOBr} + \text{H}^+$	1	3.0E6	0	(Thomas et al., 2011)

$Br^- + ClO^- + H^+$ $\rightarrow BrCl + OH^-$	3	3.7E10	0	(Thomas et al., 2011)
$Cl_2 + Br^- \rightarrow BrCl_2^-$	2	7.7E9	0	(Thomas et al., 2011)
$BrCl_2^- \rightarrow Cl_2 + Br^-$	1	1.83E3	0	(Thomas et al., 2011)

Table 4.5 Aqueous photolysis chemistry

HO _x and O _x Reactions	Comments	Reference
$O_3 + hv \xrightarrow{H_2O} H_2O_2 + O_2$	$\lambda < 320\text{nm}$	(DeMore, 1997; Graedel, 1981)
$H_2O_2 + hv \rightarrow 2OH$	$\lambda < 380\text{nm}$	(DeMore, 1997; Graedel, 1981)
NO _y Reactions		
$NO_3^- + hv \rightarrow NO_2 + OH$	$300 < \lambda < 340 \text{ nm}$	(Graedel, 1981; Warneck, 1988; Zellner et al., 1990)
$NO_2^- + hv \rightarrow NO + OH$	$290 < \lambda < 410 \text{ nm}$	(Graedel, 1981; Warneck, 1988; Zellner et al., 1990)
$NO_3^- + hv \rightarrow NO_2^- + O$	$300 < \lambda < 340 \text{ nm}$	(Graedel, 1981; Warneck, 1988; Zellner et al., 1990)
$NO_3 + hv \rightarrow NO + O_2$	$470\text{-}700\text{nm}$	(Graedel, 1981)

$NO_3 + hv \rightarrow NO_2 + O$	470-700nm	(Graedel, 1981)
$HOBr + hv \rightarrow OH + Br$	Equal to gas phase	(Thomas et al., 2011)
$HOCl + hv \rightarrow OH + Cl$	Equal to gas phase	(Thomas et al., 2011)
$BrCl \rightarrow Br + Cl$	Equal to gas phase	(Thomas et al., 2011)
$Br_2 \rightarrow 2Br$	Equal to gas phase	(Thomas et al., 2011)
$Cl_2 \rightarrow 2Cl$	Equal to gas phase	(Thomas et al., 2011)

Table 4.6 Modifications of gas phase chemistry

NO _y Chemistry	n-order	A [(mole/cm ³) ¹⁻ⁿ s ⁻¹]	-E _a / R [K]	Reference
$HNO_4 \rightarrow NO_2 + HO_2$	1	1.4E-14	-1.0E4	(Graham et al., 1977)
$NO_2 + HO_2 \rightarrow HNO_4$	3			(DeMore, 1997)
Halogen Chemistry	n-order	A [(mole/cm ³) ¹⁻ⁿ s ⁻¹]	-E _a / R [K]	Reference
$Cl + O_3 \rightarrow ClO + O_2$	2	2.8E-11	-250	(Thomas et al., 2011)
$ClO + HO_2 \rightarrow HOCl + O_2$	2	2.2E-12	-340	(Thomas et al., 2011)
$BrO + ClO \rightarrow BrCl + O_2$	2	4.1E-13	-290	

$Cl + HO_2 \rightarrow HCl + O_2$	2	1.83E-11	170	(Thomas et al., 2011)
$Cl + HO_2 \rightarrow ClO + OH$	2	4.1E-11	-450	(Thomas et al., 2011)
$Cl + H_2O_2 \rightarrow HCl + HO_2$	2	1.1E-11	-980	(Thomas et al., 2011)
$Cl + CH_3O_2 \rightarrow \frac{1}{2}(ClO + HCHO + HO_2 + HCl + CO + H_2O)$	2	1.6E-10	0	(Thomas et al., 2011)
$Cl + ClNO_3 \rightarrow Cl_2 + NO_3$	2	6.5E-12	135	(Thomas et al., 2011)
$ClO + NO_2 \rightarrow ClNO_3$	3			(DeMore, 1997)

$\text{ClNO}_3 + \text{OH} \rightarrow \frac{1}{2}(\text{ClO} + \text{HNO}_3 + \text{HOCl} + \text{NO}_3)$	2	1.2E-12	-330	(Thomas et al., 2011)
$\text{ClNO}_3 \rightarrow \text{ClO} + \text{NO}_2$	1	2.754E-6	1.14E4	(Thomas et al., 2011)
$\text{Br} + \text{BrNO}_3 \rightarrow \text{Br}_2 + \text{NO}_3$	2	4.9E-11	0	(Thomas et al., 2011)
$\text{BrO} + \text{NO}_2 \rightarrow \text{BrNO}_3$	3			(DeMore, 1997)
$\text{BrNO}_3 \rightarrow \text{BrO} + \text{NO}_2$	1	6.1E-4	0	(Thomas et al., 2011)

Table 4.7 Aqueous equilibrium constants

Equilibrium Reactions	K_{298}	$-\Delta H/R$ [K]	Reference
$CO_2 \leftrightarrow H^+ + HCO_3^-$	4.3E-7	-913	(Thomas et al., 2011)
$HCO_3^- \leftrightarrow CO_3^{2-} + H^+$	4.68E-11	-1760	(Martell, 1977)
$H_2O_2 \leftrightarrow HO_2^- + H^+$	2.2E-12	-3730	(Martell, 1977)
$NH_3 \leftrightarrow OH^- + NH_4^+$	1.7E-5	-4325	(Thomas et al., 2011)
$H_2O \leftrightarrow H^+ + OH^-$	1.0E-14	-6716	(Thomas et al., 2011)
$HCOOH \leftrightarrow H^+$ $+ HCOO^-$	1.8E-4		(Thomas et al., 2011)
$HO_2 \leftrightarrow O_2^- + H^+$	1.6E-5		(Thomas et al., 2011)
$HNO_3 \leftrightarrow H^+ + NO_3^-$	1.5E1		(Thomas et al., 2011)
$HONO \leftrightarrow H^+ + NO_2^-$	5.1E-4	-1260	(Thomas et al., 2011)
$HNO_4 \leftrightarrow NO_4^- + H^+$	1.0E-5	8700	(Thomas et al., 2011)

$HBr \leftrightarrow H^+ + Br^-$	1.0E9		(Thomas et al., 2011)
$HCl \leftrightarrow H^+ + Cl^-$	1.7E-6		(Thomas et al., 2011)
$HOBr \leftrightarrow H^+ + BrO^-$	2.3E-9	-3091	(Thomas et al., 2011)
$HOCl \leftrightarrow H^+ + ClO^-$	3.2E-8		(Thomas et al., 2011)
$C_2H_4O_2 \leftrightarrow C_2H_3O_2^- + H^+$	1.7E-5		(Benjamin, 2010)

Table 4.8 Initial chemical conditions

Species	Concentration in atmosphere	Concentration in snowpack	Reference / Comment
CH_4	1800 ppb _v	1800 ppb _v	(Dibb et al., 2007)
CO	80 ppb _v	80ppb _v	
NO	2 ppt _v		
NO_2	2 ppt _v		
Br	1 ppt _v	1 ppt _v	Halogens are initialized to produce levels reported in (Thomas et al., 2011)
BrO	1 ppt _v	1 ppt _v	Halogens are initialized to produce levels reported in (Thomas et al., 2011)
$HOBr$	1 ppt _v	1 ppt _v	Halogens are initialized to produce levels reported in

			(Thomas et al., 2011)
<i>Cl</i>	2 ppt _v	2 ppt _v	
<i>ClO</i>	2ppt _v	2 ppt _v	
<i>HOCl</i>	2 ppt _v	2 ppt _v	
<i>HCOOH</i>	1.25 ppb _v	1.25 ppb _v	(Dibb and Arsenault, 2002)
<i>CH₃COOH</i>	5 ppb _v	5 ppb _v	(Dibb and Arsenault, 2002)
<i>HNO₄</i>		1.1 ppb _v	Initialized starts 10 cm into the snowpack to prevent large fluxes of NO ₂
<i>HNO₃</i>		50 ppt _v	Used to initialize nitrate concentration. Initialization start 2 cm into the snowpack to prevent large fluxes of NO ₂

<i>HONO</i>		50 ppt _v	Initialization start 2 cm into the snowpack to mirror HNO ₃ initialization
<i>NO₂⁻</i>		10 nM	(Chu and Anastasio, 2007)

References

- Benjamin, M.M., 2010. Water Chemistry. Waveland Press, Incorporated.
- Chameides, W.L., 1984. The photochemistry of a marine stratiform cloud. *J. Geophys. Res.* 89, 4739-4755.
- Chu, L., Anastasio, C., 2007. Temperature and Wavelength Dependence of Nitrite Photolysis in Frozen and Aqueous Solutions. *Environmental Science & Technology* 41, 3626-3632.
- Cunningham, J., Waddington, E.D., 1993. Air flow and dry deposition on non-sea salt sulfate in polar firn: Paleoclimatic implications. *Atmos. Environ. Part A.* 27A, 2943-2956.
- DeMore, W.B., Sander, S.P., Golden, D.M., Hampson, R.F., Kurylo, M.J., Howard, C.J., Ravishankara, A.R., Kolb, C.E., and Molina, M.J., 1997. Chemical Kinetics and Photochemical Data for Use in Stratospheric Modeling., Tech. Rep. JPL Publications. Jet Propulsion Laboratory, Pasadena, CA.
- Dibb, J.E., Albert, M., Anastasio, C., Atlas, E., Beyersdorf, A.J., Blake, N.J., Blake, D.R., Bocquet, F., Burkhardt, J.F., Chen, G., Cohen, L., Conway, T.J., Courville, Z., Frey, M.M., Friel, D.K., Galbavy, E.S., Hall, S., Hastings, M.G., Helmig, D., Greg Huey, L., Hutterli, M.A., Jarvis, J.C., Lefer, B.L., Meinardi, S., Neff, W., Oltmans, S.J., Sherwood Rowland, F., Sjostedt, S.J., Steig, E.J., Swanson, A.L., Tanner, D.J., 2007. An overview of air-snow exchange at Summit, Greenland: Recent experiments and findings. *Atmospheric Environment* 41, 4995-5006.

- Dibb, J.E., Arsenault, M., 2002. Shouldn't snowpacks be sources of monocarboxylic acids? *Atmospheric Environment* 36, 2513-2522.
- Dogliotti, L., and Hayon, E., 1967. Flash photolysis of persulfate ions in aqueous solutions. Study of sulfate and ozonide radical ions. *J. Phys. Chem.* 71, 2511-2516.
- Domine, F., Albert, M., Huthwelker, T., Jacobi, H.W., Kokhanovsky, A.A., Lehning, M., Picard, G., Simpson, W.R., 2008. Snow physics as relevant to snow photochemistry. *Atmos. Chem. Phys.* 8, 171-208.
- Fried, A., Henry, B.E., Calvert, J.G., Mozurkewich, M., 1994. The reaction probability of N₂O₅ with sulfuric acid aerosols at stratospheric temperatures and compositions. *Journal of Geophysical Research: Atmospheres* 99, 3517-3532.
- Galbavy, E.S., Anastasio, C., Lefer, B., Hall, S., 2007. Light penetration in the snowpack at Summit, Greenland: Part 2 Nitrate photolysis. *Atmospheric Environment* 41, 5091-5100.
- Graedel, T.E., and Weschler, C.J., 1981. Chemistry within aqueous atmospheric aerosols and raindrops. *Rev. Geophys.* 19, 505-539.
- Graham, R.A., Winer, A.M., Pitts Jr, J.N., 1977. Temperature dependence of the unimolecular decomposition of pernitric acid and its atmospheric implications. *Chemical Physics Letters* 51, 215-220.
- Hoigne, J., Bader, H., 1983. Rate constants of reactions of ozone with organic and inorganic compounds in water. 2 Dissociating organic compounds. *Water Research* 17, 185-194.

- Jacob, D.J., 1986. Chemistry of OH in remote clouds and its role in the production of formic acid and peroxymonosulfate. *J. Geophys. Res.* 91, 9807-9826.
- Martell, A.E., and Smith, R.M., 1977. *Critical Stability Constants*, Plenum, New York.
- Régimbal, J.-M., Mozurkewich, M., 1997. Peroxynitric Acid Decay Mechanisms and Kinetics at Low pH. *The Journal of Physical Chemistry A* 101, 8822-8829.
- Rettich, T.R., 1978. Some photochemical reactions of aqueous nitric acid. *Diss. Abst. Int. B.* 38, 5968.
- Ross, A.B., and Neta, P., 1979. *Rate Constants for Reactions of Inorganic Radicals in Aqueous Solutions*, NSRDS-NBS. U.S. Department of Commerce, Washington, D.C.
- Schmidt, K.H., 1972. Electrical conductivity techniques for studying the kinetics of radiation induced chemical reactions in aqueous solutions. *Int. J. Radiat. Phys. Chem.* 4, 439-468.
- Thomas, J.L., Dibb, J.E., Huey, L.G., Liao, J., Tanner, D., Lefer, B., von Glasow, R., Stutz, J., 2012. Modeling chemistry in and above snow at Summit, Greenland - Part 2: Impact of snowpack chemistry on the oxidation capacity of the boundary layer. *Atmospheric Chemistry and Physics* 12, 6537-6554.
- Thomas, J.L., Stutz, J., Lefer, B., Huey, L.G., Toyota, K., Dibb, J.E., von Glasow, R., 2011. Modeling chemistry in and above snow at Summit, Greenland – Part 1: Model description and results. *Atmospheric Chemistry and Physics* 11, 4899-4914.

- Warneck, P., and Wurzinger, C., 1988. Product Quantum Yield for the 305-nm Photodecomposition of NO_3^- in Aqueous Solution. *J. Phys. Chem. A.* 92, 6278-6283.
- Wild, O., Zhu, X., Prather, M., 2000. Fast-J: Accurate Simulation of In- and Below-Cloud Photolysis in Tropospheric Chemical Models. *Journal of Atmospheric Chemistry* 37, 245-282.
- Zellner, R., Exner, M., Herrmann, H., 1990. Absolute OH Quantum Yield in the Laser Photolysis of Nitrate, Nitrite, and Dissolved H_2O_2 at 308 and 351 nm in the temperature range 278-353K. *J. Atmos. Chem.* 10, 411-425.

Chapter 5. Modeling Dynamics of Ozone and Nitrogen Oxides at Summit, Greenland with a 1-D Process-Scale Model. II. Temporal Variations of Snowpack Chemistry^a

Keenan A. Murray¹, Louisa J. Kramer^{2,3}, Paul V. Doskey^{1,3,4,*}, Laurens Ganzeveld⁵, Brian Seok⁶, Brie Van Dam⁶, and Detlev Helmig⁶

¹Department of Civil and Environmental Engineering, Michigan Technological University, Houghton, MI, USA

²Department of Geological and Mining Engineering and Sciences, Michigan Technological University, Houghton, MI, USA

³Atmospheric Sciences Program, Michigan Technological University, Houghton, MI, USA

⁴School of Forest Resources and Environmental Science, Michigan Technological University, Houghton, MI, USA

⁵Department of Environmental Sciences, Wageningen University, Wageningen, Netherlands

⁶Institute of Arctic and Alpine Research, University of Colorado at Boulder, CO, USA

kmurray@mtu.edu, lkramer@mtu.edu, pvdoskey@mtu.edu*, Laurens.Ganzeveld@wur.nl, seok@Colorado.edu, Brie.Vandam@Colorado.EDU, Detlev.Helmig@Colorado.EDU

*Corresponding author. Phone: +1 906-487-2745

^a The material contained in this chapter is part of a planned submission to the Atmospheric Environment Journal.

Abstract

A 1-D process-scale model was used to analyze temporal variations in the snowpack chemistry at Summit, Greenland for 15-30 March and 15-30 May 2009. There was general agreement between model simulations and observation for the March time period; however, mixing ratios of the chemical species were underestimated. Nighttime production of nitrogen dioxide (NO_2) at the surface of the snowpack from thermal decomposition of peroxyxynitric acid (HNO_4), which is an important source of nighttime NO_2 during April, is hindered by lower production of HNO_4 during the day. Estimates of NO_2 production via nitrate (NO_3^-) photolysis created overestimates of NO_2 mixing ratios, which also led to overestimates of NO levels. Model simulations captured the observed intrusions of ozone (O_3); however, the diurnal cycle was skewed and not well defined due to modeled ozone production at the surface of the snowpack. The model reproduced measured trends in the dynamics of NO_2 , NO , and O_3 for the May time period. About 60% of the NO_2 produced at solar noon was attributed to photolysis of NO_3^- , however, the daytime NO_2 is consumed in the snowpack to form gas phase NO and gas and aqueous phase HNO_4 . Peaks of NO were underestimated, which implies a missing source of NO in addition to photolysis of NO_2 or the rate of consumption of NO via reaction with methyl peroxy radical (CH_3O_2) needs to be reduced. Peak production of NO_2 and NO during the night were 10^6 and 10^4 molec $\text{cm}^{-3} \text{ s}^{-1}$, respectively. Rates of O_3

consumption were relatively uniform ($10^8 \text{ molec cm}^{-3} \text{ s}^{-1}$) throughout the snowpack with the exception of rates near the surface at solar noon where the rate of O_3 production was similar to the consumption rate.

Keywords: 1-D process-scale model, Summit, Greenland, nitrate photolysis, peroxyxynitric acid, NO_x , nitrogen dioxide, nitrogen monoxide, ozone

1. Introduction

A comprehensive suite of continuous measurements of nitrogen oxides (NO_x), ozone (O_3), temperature, wind speed, wind direction, and irradiance at Summit, Greenland were recorded in and above snowpack over glacial ice from 2008-2010 (Van Dam et al., 2014). Mixing ratios of NO_x in snowpack increased from $\sim 10 \text{ ppt}_v$ in late winter to summertime levels of $\sim 100 \text{ ppt}_v$. Concentrations continued to rise until late summer when NO_x production diminished. The observations imply nitrogen is stored in reservoir species (NO_y) within snowpack and are recycled to NO_x during sunlit periods. The diurnal profiles of nitrogen dioxide (NO_2) contained 2 distinct peaks, the first was located in the upper $\sim 30 \text{ cm}$ of the snowpack and the second in the evening was observed from 30 cm to 2 m deep in the snowpack. Peaks in the profile of nitric oxide (NO) mirrored the peaks of NO_2 at solar noon. Snowpack acted as a sink for O_3 throughout the year. The diurnal

profile of O₃ exhibited a minimum occurring at solar noon with maximums in the evening and intrusions to 2 m. The intrusions were weakly correlated with high surface wind speed (Helmig et al., 2007).

Modeling experiments have been conducted to replicate observations of NO_x, O₃, and halogen chemistry in snowpack at Summit, Greenland during short time periods (Murray et al., 2014; Thomas et al., 2011). *Thomas et al. (2011)* successfully replicated measurements of NO, O₃, and bromine monoxide (BrO) at 1.5 meters above the surface of the snowpack for 10-13 June 2008. *Murray et al. (2014)* modeled NO_x and O₃ mixing ratios from the snowpack surface down to 2 m for 15-30 April 2009 that agreed with observations (Van Dam et al., 2014) and identified key processes that explained NO_x production and O₃ consumption within sunlit snowpack. Photolysis of nitrate (NO₃⁻) was responsible for about 80% of the NO₂ production, which was approximately 10⁸ molec cm⁻³ s⁻¹ at solar noon. Peak NO₂ production during the night was approximately 10⁸ molec cm⁻³ s⁻¹ and production rates were greatest closer to the snowpack surface. Nearly 100% of the nighttime NO₂ production was from thermal decomposition of peroxyntic acid (HNO₄). The rate of NO production during the day was similar to the rate of NO₂ production and was linked directly to NO₂ photolysis. Aqueous-phase reaction with formic acid within the Liquid-Like Layer (LLL) of snowpack consumed O₃ at a rate of 10⁶-10⁷ molec cm⁻³ s⁻¹ and represented the principal sink of O₃.

Here we use a 1-D process-scale model of snowpack chemistry to reproduce observations of chemical dynamics of O₃ and NO_x in snowpack for 11-30 March 2009 and 15-30 May 2009 at Summit, Greenland (Van Dam et al., 2014) . The March and May time periods were chosen as they represent times of the year when irradiance was small before the sunlit season and when the sun does not set, respectively. Analysis will include discussion of temporal shifts of chemical dynamics between the months.

2. Methods

The model uses observations made by *Van Dam et al. (2014)* to calculate or guide many chemical and physical processes described in detail by *Murray et al. (2014)*. A brief overview of the model is as follows: (1) the model assumes aqueous-phase chemistry occurs on the surface of snowflakes and mass transfer of chemical species between the aqueous and gas phases occurs, (2) transport of chemical species in the interstitial air of snowpack is modeled with diffusion and wind pumping parameterizations that are driven by measurements of wind speed in the overlying atmosphere, (3) transport of chemical species in the overlying atmosphere is driven by gradients in the mixing ratios of chemical species based on estimated eddy-diffusivity coefficients derived from meteorological measurements, (4) variations in snowpack temperature with depth are derived by calculating the thermal flux, which is guided by interpolated measurements of surface temperatures, (5) measurements of O₃ measurements in the overlying atmosphere

represent the modeled O_3 profile, (6) photolysis rates are calculated with FAST-JX (Wild et al., 2000) and are adjusted according to the measured irradiance, and (6) the percent production or consumption of a chemical species is calculated by considering all pertinent reactions for the chemical species and adjusting for reverse reactions when necessary. Mixing ratios of species in snowpack interstitial air are assumed to be in equilibrium with the aqueous phase at initialization. Nitric and nitrous acid (HNO_3 ;HONO) are initialized at a snowpack depth of 2 cm rather than the surface of the snowpack. Similarly, peroxyntic acid (HNO_4) is initialized at 10 cm deep. Modeled fluxes of NO_x to the overlying atmosphere are larger than observed in measurements when mixing ratios of NO_y species are initialized at the snowpack interface and were not diminished by limiting transport to molecular diffusion.

3. Results and discussion

Chemical and meteorological observations during March (15-30 March 2009) and May (15-30 May 2009) periods of the modeling experiment are described in detail by *Van Dam et al. (2014)*. Irradiance during the March episode did not exceed 350 W m^{-2} . Nearly clear sky conditions are observed in the irradiance profile throughout the period with the exception of 18-20 March when a slight decrease in peak irradiance was observed. Wind speeds did not exceed 10 m s^{-1} . Temperatures at the surface of the snowpack reflected temperatures in the overlying atmosphere and were 215-250 K. However, temperatures 1-2 m deep in snowpack were about 230 K and relatively constant. Atmospheric

temperatures were lower than temperatures in the snowpack except during the day on 18 March and for a 24 h period starting on morning of 20 March. The March period was free of pollution originating from the investigator camp except at midnight on 25 March and the evening of 29 March. Peak concentrations of NO and NO₂ at solar noon in the top 50 cm of the snowpack and are ~50 and ~200 ppt_v, respectively. Nighttime peaks of NO₂ occur below 50 cm in the snowpack and are ~200 ppt_v. O₃'s diurnal pattern has minimum and maximum concentrations of 30 and 45 ppb_v, respectively, at solar noon and midnight. Nighttime O₃ intrusions vary and extend up to 2 meters into the snowpack.

Irradiance during the May period did not drop to zero and clear skies were observed throughout with a slight decrease in irradiance on 25 May. Wind speeds were 0-5 m s⁻¹ except on 15 May when wind speeds were approximately 12 m s⁻¹. Temperatures in the upper 50 cm of the snowpack reflected diurnal trends in temperature of the overlying atmosphere. Peak temperatures near solar noon were about 255-266 K and minimum temperatures were approximately 245 K at midnight when the sun remained above the horizon. Temperatures below 50 cm were approximately 245 K and were relatively constant. Pollution from the investigator camp was observed on 25 and 26 May and NO_x data is missing 20 – 22 May . Peak concentrations of NO and NO₂ at solar noon in the top 75 cm of the snowpack and are ~200 ppt_v. Nighttime peaks of NO₂ occur below 50 cm in the snowpack and are ~400 ppt_v. O₃'s diurnal pattern has minimum and maximum concentrations of 30 and 55 ppb_v, respectively, at solar noon and midnight. Nighttime O₃ intrusions vary and extend up to 2 meters into the snowpack.

Model simulation of chemical dynamics for 15-30 March

Mixing ratios of NO_y , carbon-containing species, and halogens used to initialize the model are presented in Table 5.1. For a full list of initialization conditions, refer to *Murray et al. (2014)*. Levels of formic acid (HCOOH) were reduced from the mixing ratios observed by *Dibb and Arsenault (2002)* at Summit (5 ppb_v) to 250 ppt_v. Model runs using 5 ppb_v of HCOOH completely removed O_3 in the interstitial air. Initial mixing ratios of nitric acid (HNO_3) were set lower than *Murray et al. (2014)* (50 ppt_v) at 5 ppt_v. Model experiments initialized at higher levels of HNO_3 produced NO_2 mixing ratios greater than the observed peak values. Halogens were uninitialized as bromide consumed HNO_4 in the aqueous phase near the surface of the snowpack preventing HNO_4 production in previous model runs. The temperature of the snowpack was initialized at 230 K to reflect the observations.

The NO_2 profiles produced by the model do not reflect key aspects of the observations (Fig. 5.1). The model does not produce nighttime peaks of NO_2 in snowpack. Slight increases of NO_2 in the afternoon through early morning of the following day were observed in the atmosphere; however, the model does not replicate the pattern with the exception of the evenings of 20 and 21 March. The model produces peaks of NO_2 at the snowpack surface during solar noon for 18-24 March; however peak levels on 21-23

March are overestimated despite the lower initialization of HNO₃ at 5 ppt_v. A slight dip in irradiance was observed for 18-20 March, which might explain lower levels of NO₂ at solar noon prior to 21 March. The principal daytime production mechanism for NO₂ during the March period is photolysis of NO₃⁻ (Fig. 5.2). Unlike April when the highest levels of NO₂ are observed at night (Van Dam et al., 2014) and are produced through decomposition of HNO₄ (Murray et al., 2014), peak production of NO₂ occurs during the daytime from the photolysis of nitrate at 10⁶-10⁷ molec cm⁻³ s⁻¹.

The largest modeled production of NO₂ occurs on 21-23 March and coincides with model overestimations of mixing ratios at solar noon. Snowpack temperatures increased during 21-23 March, which accelerate kinetics of chemical production and favor transfer of chemical species from the aqueous to gas phase. Production of NO₂ during the night is two orders of magnitude smaller than production during the day. Like nighttime production of NO₂ in the snowpack in April (Murray et al., 2014), NO₂ formation in March is attributed to the relative rates of HNO₄ decomposition and formation (Fig. 5.3). However, a key difference between March and April is lack of nighttime production of NO₂ from HNO₄ decomposition in the upper 10 cm of the March snowpack. Peak nighttime production of NO₂ production in April was ~10⁸ molec cm⁻³ s⁻¹, which is 3-4 magnitudes larger than modeled for the March period (Murray et al., 2014). The model estimates production levels of hydroperoxyl radical (HO₂), which is a HNO₄ precursor, to be 10⁵-10⁶ molec cm⁻³ s⁻¹ in March, which is up to 2 magnitudes smaller than the reported values for April (Murray et al., 2014). There are several modeled sources of HO₂ at the

surface of the March snowpack and include aqueous phase reactions of formaldehyde (HCHO) with hydroxyl radical (OH), O₃ with HCOOH, OH with HCOOH, and gas phase reactions of methyldioxy radical (MO₂) with NO and decomposition of organic hydroperoxides (ROOH). These sources are the same reported in Murray et al. (2014) with the exception of the aqueous reaction of OH and HCOOH. Yields of OH from photolysis of O₃ and hydrogen peroxide (H₂O₂) are likely lower in March when irradiances are low, and thus, production rates of HO₂ from reactions involving OH and MO₂ (MO₂ is produced from methane reacting with OH) are small. The initialized concentration of HCOOH was reduced an order of magnitude compared to the April time period in order to reproduce the O₃ profile, which further hindered formation of HO₂. The combination of reduced daytime production NO₂ and HO₂ in March compared to April is the cause of the model under representing nighttime NO₂.

Simulated peaks of NO generally agree with the observations; however, peak levels for 21-23 March are overestimated (Fig. 5.4). The principal sources of NO are photolysis of NO₂ in both the aqueous phase and gas phase and the photolysis of nitrite (Fig. 5.5). Production of NO occurs in the gas phase in April through photolysis of gas phase NO₂ (Murray et al., 2014), which implies peak levels of NO in the interstitial air of snowpack at solar noon in March result from transfer of NO from the aqueous to gas phase. The photolysis of nitrite to produce NO contributes to overall production peaks in the early morning, is reduced at solar noon, and peaks again in the evening. This means the

production of NO in the early morning and night is from the nitrite photolysis and shifts to NO₂ photolysis at solar noon.

Model simulations of the diurnal cycle of O₃ do not agree with the observations; however, the deeper intrusions of O₃ in the measurements are reflected in the modeled profile (Fig. 5.6). The model did not reproduce peak levels of O₃ observed on 17 and 21 March and simulations of O₃ intrusions on 18, 20, 22, 23, 26, 29, and 30 were premature to the observed intrusions. Disagreement between the simulations and observations are likely due to O₃ production at the surface of the snowpack at solar noon, similar to the findings in Murray et al. (2014). Modeled production of O₃ in April was a result of NO_x cycling (Murray et al., 2014), however, in March ~50% of the ozone production is a result of the aqueous reaction of singlet oxygen with diatomic oxygen forming aqueous ozone. This implies ozone is produced in the aqueous phase and transported to the interstitial air. The principle sources of aqueous singlet oxygen in the model are the photolysis of NO₂ and nitrate. The rate of production of O₃ from the aqueous-phase reaction is approximately 10⁶ molec cm⁻³ s⁻¹, which is similar in magnitude to the observed consumption of snowpack O₃ by HCOOH (Fig. 5.7).

Model simulation of chemical dynamics for 15-30 May

Mixing ratios of NO_y , carbon-containing species, and halogens that were used to initialize the model are presented in Table 5.2. Levels of HNO_3 and HNO_4 are initialized at 30 ppt_v and 600 ppt_v, respectively, which are 40% and 45% lower than the concentrations that were used to initialize the model for the April simulation (Murray et al., 2014). Larger initial concentrations of HNO_3 and HNO_4 resulted in overestimation of NO_2 and NO in the interstitial air of the snowpack. Previous model runs for May revealed a missing NO source at the surface of the snowpack at solar noon. In an attempt to produce NO , the model is initialized with nitrite at 10^{-4} M concentrations compared to the estimated steady state concentration of 12 nM (Chu and Anastasio, 2007). Temperature of the snowpack was initialized at 240 K.

Simulated profiles during the period reflected the observations (Fig. 5.8). The simulated profile of NO_2 in the atmosphere overlying the snowpack more correctly represents the measurements during May than the simulations of observations during the April (Murray et al., 2014). About 65% of NO_2 produced in the upper 50 cm of the May snowpack at solar noon is attributed to photolysis of NO_3^- , which produces hydroxide (OH^-) in addition to NO_2 (Fig. 5.9). The remaining source of NO_2 is the reaction of MO_2 with NO . Total NO_2 production is limited to the immediate surface of the snowpack, unlike the

depth simulated for April (~25 cm). Peak production rates in April (10^8 molec $\text{cm}^{-3} \text{s}^{-1}$) are two orders of magnitude larger than May (10^6 molec $\text{cm}^{-3} \text{s}^{-1}$). The subplot of total production of NO_2 in Fig. 5.10 shows the snowpack is a large sync of NO_2 during the day. The principle syncs of NO_2 are the aqueous and gas phase formation of HNO_4 and NO_2 photolysis.

Midnight sun peaks of NO_2 are primarily produced from thermal decomposition of HNO_4 with production rates of about $\sim 10^6$ molec $\text{cm}^{-3} \text{s}^{-1}$ in the top 50 cm of the snowpack (Fig. 5.10). Other sources of NO_2 at nighttime are magnitudes lower in production supporting the hypothesis in Murray et al. (2014) that observed nighttime peaks of NO_2 are a result of HNO_4 decomposition near the surface of the snowpack and is transported deeper into the snowpack. Reaction of NO_2 with HO_2 in both the gas and aqueous phases produces HNO_4 . Production of HNO_4 in the aqueous phase at the surface of snowpack is regulated by production of NO_2 by NO_3^- photolysis and was about 10^8 molec $\text{cm}^{-3} \text{s}^{-1}$ at solar noon. Production of HO_2 in the upper 10 cm of the snowpack was attributed to aqueous-phase reaction of OH with HCHO and was about 10^7 - 10^8 molec $\text{cm}^{-3} \text{s}^{-1}$. In snowpack layers where HO_2 was produced from decomposition of ROOH and oxidation of NO by MO_2 , rates of production were 10^6 - 10^7 molec $\text{cm}^{-3} \text{s}^{-1}$, which links the chemistry of MO_2 and NO chemistry to both nighttime and daytime production of NO_2 .

Contributions of the reaction of nitrite (NO_2^-) with O_3 and thermal decomposition of peroxyacetyl nitrate (PAN) and dinitrogen pentoxide (N_2O_5) to production of NO_2 in snowpack interstitial air during nighttime in April were insignificant (Murray et al., 2014). With high initialized concentrations of nitrite, we expect nitrite production of NO_x to be significant. However, production of NO_2 via reaction of NO_2^- with O_3 and decomposition of PAN and N_2O_5 in May was also insignificant. Production of NO_2 via reaction of NO_2^- with OH contributes 10^3 - 10^5 molec cm^{-3} s^{-1} deep in the snowpack where NO_2 production from thermal decomposition of HNO_4 is insignificant. Even with the large concentrations of nitrite in the snowpack, production of NO_2 from nitrite reactions are not on the same order of magnitude as HNO_4 . Simulated levels of PAN above and within snowpack are about 40 ppt_v. Measurements of PAN within the snowpack exhibited increasing levels with depth and were approximately 200 ppt_v at a depth of 25 cm (Ford et al., 2002), which indicates the model underestimates PAN production. However, thermal decomposition does not make a significant contribution to production of NO_2 during the night. Levels of N_2O_5 are about 400 ppt_v and are higher in the snowpack than the overlying atmosphere; however, contributions to NO_2 production are insignificant.

Trends of NO observations are represented by the model simulations (Fig. 5.11), but the magnitudes are underrepresented. The principal source of NO during May is photolysis of NO_2 (Fig. 5.12), however, production of NO is only observed at nighttime coinciding with the nighttime production of NO_2 and is on the order of 10^4 molec cm^{-3} s^{-1} . The sinks

of NO_2 in the snowpack are formation of HNO_4 and NO_2 photolysis while the principle sink of NO is the reaction of MO_2 with NO , which produces NO_2 . Combined with the fact that during the day NO and NO_2 production does not occur except at the very surface of the snowpack, the majority of the NO_x produced in the day is stored as HNO_4 . However, peaks in NO production at the surface of the snowpack are underestimated in the model simulations, implying a missing source of NO separate from NO_2 formed from nitrate photolysis as the NO_2 modeled profile properly represents the observations.

The concentration of nitrite was increased from $1.2 \times 10^{-8} \text{ M}$ to 10^{-4} M for the May time period in an attempted to increase NO production near solar noon. However, photolysis of HONO and NO_2^- are out competed by NO_2 photolysis during the day and only contribute to NO production near midnight sun. Simulated levels of HONO and NO_2^- near the surface of the snowpack are about 800 ppt_v and 10^{-5} M , respectively, which is 4 times larger than observations for HONO and about 10^3 times greater than estimated values for NO_2^- (Chu and Anastasio, 2007; Dibb et al., 2007). Hence, excessive nitrite and HONO are present in the model to produce NO , and implies produced NO rapidly interchanges between NO_2 and NO near the surface of the snowpack during the day and is stored as HNO_4 . Therefore, an additional source of NO is needed or the conversion of NO to NO_2 by the reaction with MO_2 needs to be reduced to allow more accumulation of NO near solar noon at the surface of the snowpack.

Model simulations of the O₃ profiles somewhat agree with the observed profiles (Fig. 5.13). Simulated and observed intrusions of O₃ into the snowpack were 1 and 2 m, respectively. Intrusions were observed more frequently in May when surface wind speeds were 0-5 m s⁻¹ than April when wind speeds were 15 m s⁻¹ (Van Dam et al., 2014). Wind pumping is driven by surface wind, and thus, O₃ intrusions in May were expected to be less frequent than intrusions during April. The primary sink of O₃ in the snowpack is aqueous-phase reaction of HCOOH that produces carbon dioxide (CO₂), OH, and HO₂ (Fig. 5.14). The O₃ consumption rate in May is 10⁸ molec cm⁻³ s⁻¹, which is larger than the estimated consumption rate in April. Oxidation of NO by HO₂ at the surface of the snowpack near solar noon allows O₃ to accumulate and the simulated production is the same order of magnitude as the simulated consumption. Similar the March and April time periods, the production of ozone near solar noon creates small intrusions of daytime ozone and skews nighttime intrusions (Murray et al., 2014).

4. Conclusions

A 1-D process-scale model was used to simulate the snowpack chemistry of NO_x and O₃ at Summit, Greenland for 15-30 March and 15-30 May 2009. Model simulations indicated that a nighttime peak of NO₂ production is not observed in March due to reduced daytime production of HNO₄, which is an important precursor of nighttime NO₂. Peaks of NO₂ during the day were adequately simulated; however, the levels were

overestimate. Simulated profiles of NO mirrored NO₂ profiles and exhibited peak mixing ratios at solar noon. The principal sources of daytime NO₂ and NO were the photolysis of nitrate and gas and aqueous phase photolysis of NO₂, respectively, which implies NO produced in the aqueous phase is transferred to the interstitial air of the snowpack where NO is oxidized to NO₂. Intrusions of O₃ were simulated with the model; however, the diurnal cycle was skewed and temporal variations in mixing ratios were not well defined.

The model adequately reproduced trends in NO₂, NO, and O₃ mixing ratios in the May snowpack. Photolysis of NO₃⁻ produces NO₂, which is subsequently photolyzed and yields NO. However, the model underestimated peak levels of NO, which implies there is an undetermined source of NO or the reaction rate of NO with MO₂ must be reduced to allow accumulation of NO. High initial concentrations of nitrite were used to initialize the model in an attempt to produce more NO, resulting in 4 times the measured values of HONO (Dibb et al., 2007) and 10³ times estimated nitrite concentrations (Chu and Anastasio, 2007) without any significant increase in NO production, implying a missing source of NO within the model. The principal sink of O₃ was reaction with HCOOH in the aqueous phase. Production rates of O₃ in small zones of the surface snowpack near solar noon are similar to consumption rates and alter the ozone profile as discussed in Murray et al. (2014). Rates of peak production of NO₂ at solar noon and midnight were 10⁷-10⁸ and 10⁶ molec cm⁻³ s⁻¹, respectively. The peak production of NO₂ at midnight occurred in the upper 50 cm of the snowpack, which implies downward transport of NO₂ from the surface of the snowpack. Production of NO coincided with nighttime NO₂

production from HNO_4 decomposition and was $\sim 10^4$ molec $\text{cm}^{-3} \text{s}^{-1}$. Consumption of O_3 within snowpack is relatively uniform and was about 10^8 molec $\text{cm}^{-3} \text{s}^{-1}$.

Acknowledgements

Keenan A. Murray acknowledges assistance from V. Rao Kotamarthi (Argonne National Laboratory) with modeling chemical dynamics of the atmospheric boundary layer and partial funding through teaching assistantships provided by Michigan Technological University. The Arctic System Science Program of the National Science Foundation provided funding for the study through grant NSF-OPP-07-13992.

References

- Chu, L., Anastasio, C., 2007. Temperature and wavelength dependence of nitrite photolysis in frozen and aqueous solutions. *Environmental Science & Technology* 41, 3626-3632.
- Dibb, J.E., Albert, M., Anastasio, C., Atlas, E., Beyersdorf, A.J., Blake, N.J., Blake, D.R., Bocquet, F., Burkhardt, J.F., Chen, G., Cohen, L., Conway, T.J., Courville, Z., Frey, M.M., Friel, D.K., Galbavy, E.S., Hall, S., Hastings, M.G., Helmig, D., Greg Huey, L., Hutterli, M.A., Jarvis, J.C., Lefer, B.L., Meinardi, S., Neff, W., Oltmans, S.J., Sherwood Rowland, F., Sjostedt, S.J., Steig, E.J., Swanson, A.L., Tanner, D.J., 2007. An overview of air-snow exchange at Summit, Greenland: Recent experiments and findings. *Atmospheric Environment* 41, 4995-5006.
- Dibb, J.E., Arsenault, M., 2002. Shouldn't snowpacks be sources of monocarboxylic acids? *Atmospheric Environment* 36, 2513-2522.
- Ford, K.M., Campbell, B.M., Shepson, P.B., Bertman, S.B., Honrath, R.E., Peterson, M., Dibb, J.E., 2002. Studies of Peroxyacetyl nitrate (PAN) and its interaction with the snowpack at Summit, Greenland. *Journal of Geophysical Research: Atmospheres* 107, ACH 6-1-ACH 6-10.
- Helmig, D., Bocquet, F., Cohen, L., Oltmans, S.J., 2007. Ozone uptake to the polar snowpack at Summit, Greenland. *Atmospheric Environment* 41, 5061-5076.
- Murray, K., B., V.D., Doskey, P.V., Seok, B., Ganzeveld, L., Kramer, L., Helmig, D., 2014. Modeling Dynamics of Ozone and Nitrogen Oxides at Summit, Greenland

with a 1-D Process-Scale Model. I. Model Presentation and Chemical Dynamics
During a Spring Ozone Intrusion Event.

Thomas, J.L., Stutz, J., Lefer, B., Huey, L.G., Toyota, K., Dibb, J.E., von Glasow, R.,
2011. Modeling chemistry in and above snow at Summit, Greenland – Part 1:
Model description and results. *Atmospheric Chemistry and Physics* 11, 4899-
4914.

Van Dam, B., Helmig, D., Doskey, P.V., Kramer, L., Murray, K., Ganzeveld, L., Toro,
C., Seok, B., 2014. Multi-year observations of O₃ and NO_x dynamics in the
Summit, Greenland snowpack.

Wild, O., Zhu, X., Prather, M., 2000. Fast-J: Accurate Simulation of In- and Below-
Cloud Photolysis in Tropospheric Chemical Models. *Journal of Atmospheric
Chemistry* 37, 245-282.

Tables

Table 5.1 March 15th – 30th model chemical initialization

NO _y species	Concentration
<i>HNO</i> ₃	5 ppt _v
<i>HNO</i> ₄	600 ppt _v
<i>HONO</i>	10 ppt _v
<i>NO</i> ₂ ⁻	12 nM
Organic Carbon	
<i>CH</i> ₄	1.8 ppm _v
<i>HCOOH</i>	250 ppt _v
<i>C</i> ₂ <i>H</i> ₄ <i>O</i> ₂	5 ppb _v
Halogens	
<i>Cl</i>	0 ppt _v

<i>ClO</i>	0 ppt _v
<i>HOCl</i>	0 ppt _v
<i>Br</i>	0 ppt _v
<i>BrO</i>	0 ppt _v
<i>HOBr</i>	0 ppt _v

Table 5.2 May15th -30th model chemical initialization

NOy species	Concentration
<i>HNO₃</i>	30 ppt _v
<i>HNO₄</i>	600 ppt _v
<i>HONO</i>	0 ppt _v
<i>NO₂⁻</i>	10E-4 M
Organic Carbon	
<i>CH₄</i>	1.8 ppm _v
<i>HCOOH</i>	1 ppb _v
<i>C₂H₄O₂</i>	5 ppb _v
Halogens	
<i>Cl</i>	2 ppt _v
<i>ClO</i>	2 ppt _v
<i>HOCl</i>	2 ppt _v
<i>Br</i>	1 ppt _v

<i>BrO</i>	1 ppt _v
<i>HOBr</i>	1 ppt _v

Figures

Fig. 5.1

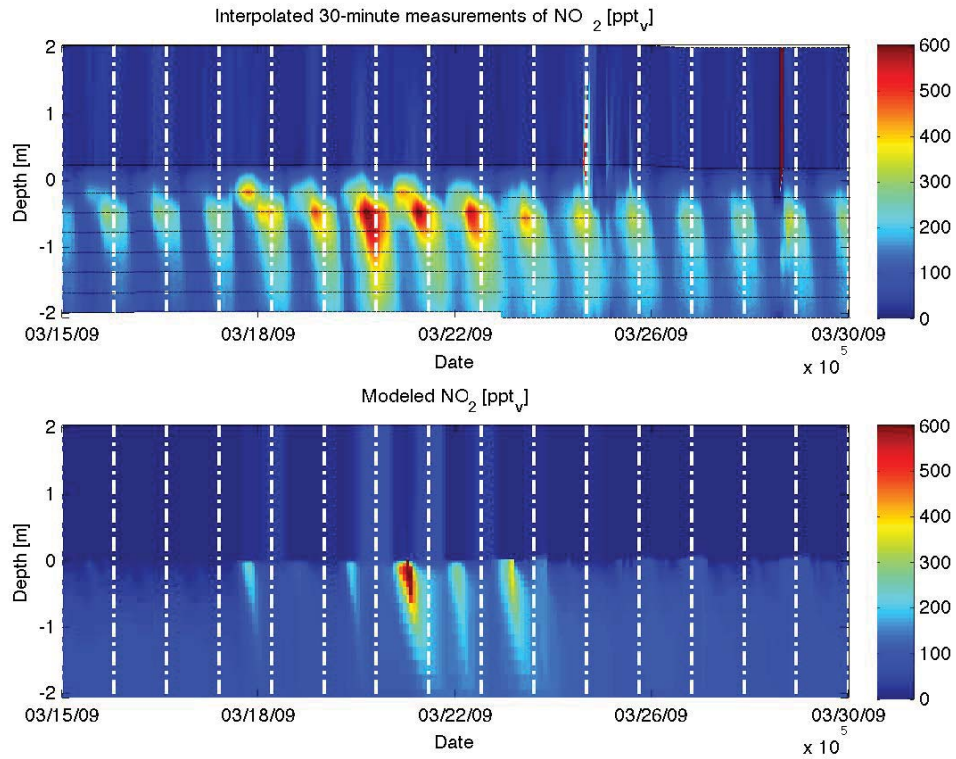


Fig. 5.1. Comparison of modeled and measured NO₂ profile in and above snowpack March 15th–30th at Summit, Greenland. Horizontal black lines represent the heights where measurements of chemical species and temperature were made. Vertical dashed white lines represent midnight of each day. Negative depths represent snowpack.

Fig. 5.2

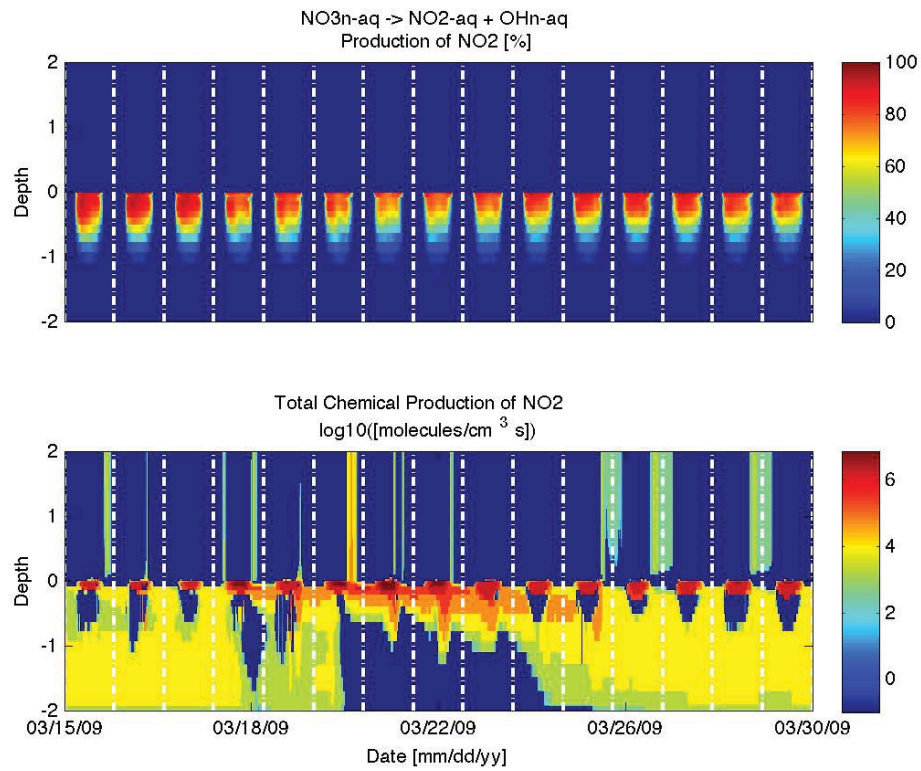


Fig. 5.2. Modeled production of NO₂ from the photolysis of nitrate for March 15th -30th, 2009 at Summit, Greenland. The top graph shows the percent contribution of the reaction to production rates depicted in the bottom graph. Vertical dashed white lines represent midnight of each day. Negative depths represent snowpack.

Fig. 5.3

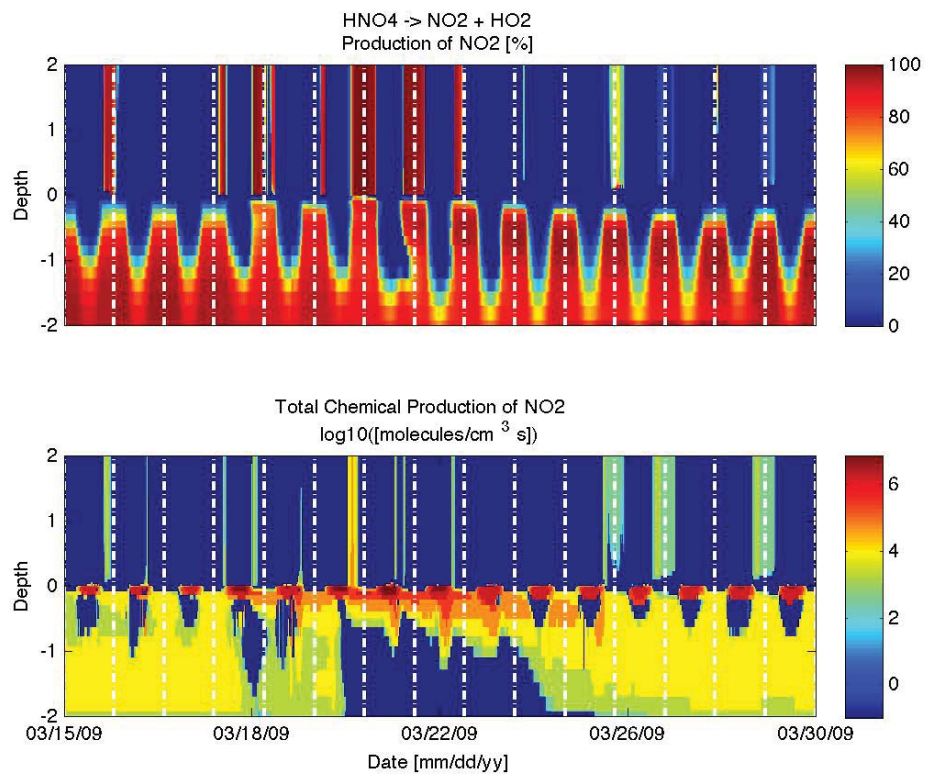


Fig. 5.3. Modeled production of NO₂ from the decomposition of peroxyntic acid for March 15th -30th, 2009 at Summit, Greenland. The top graph shows the percent contribution of the reaction to production rates depicted in the bottom graph. Vertical dashed white lines represent midnight of each day. Negative depths represent snowpack.

Fig. 5.4

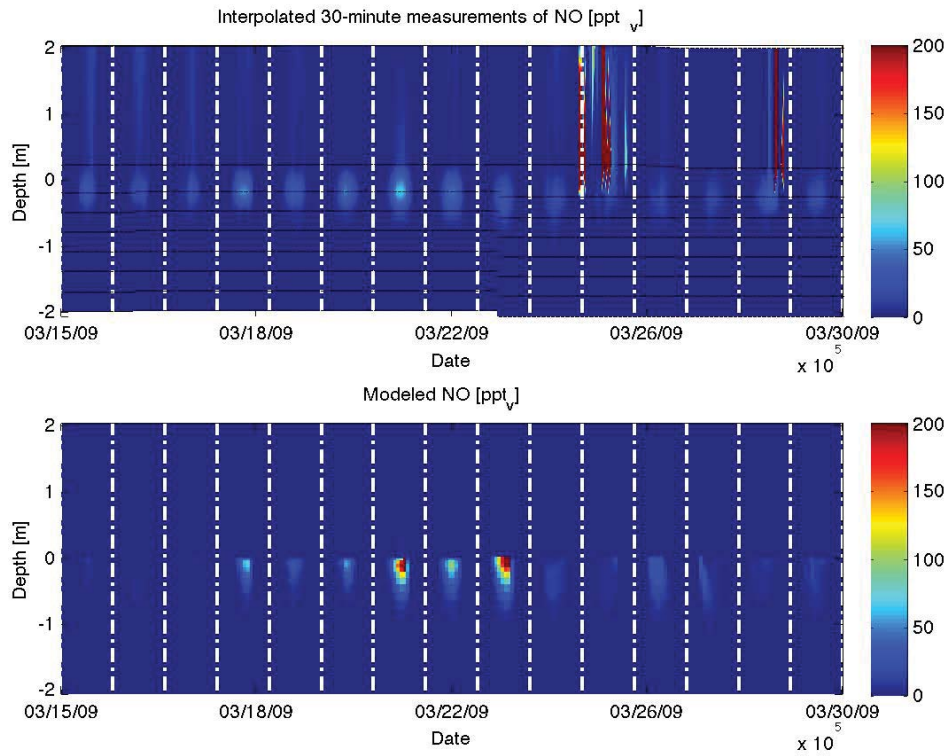


Fig. 5.4. Comparison of modeled and measured NO profile in and above snowpack March 15th-30th at Summit, Greenland. Horizontal black lines represent the heights where measurements of chemical species and temperature were made. Vertical dashed white lines represent midnight of each day. Negative depths represent snowpack.

Fig. 5.5

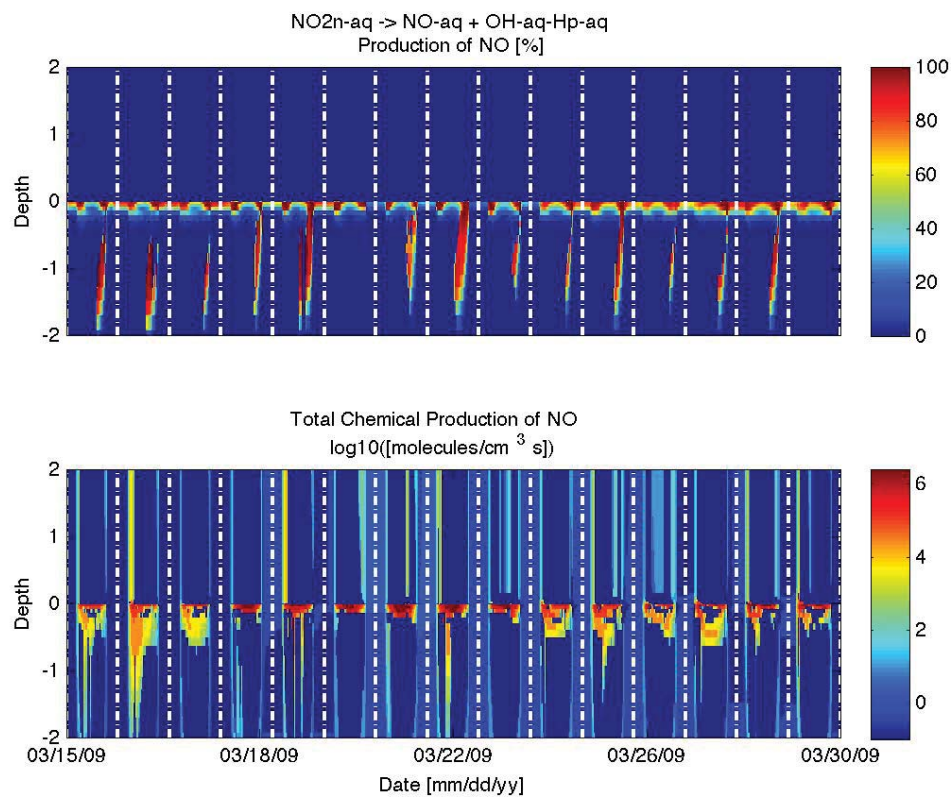


Fig. 5.5. Modeled production of NO from the photolysis of nitrite for March 15th - 30th, 2009 at Summit, Greenland. The top graph shows the percent contribution of the reaction to production rates depicted in the bottom graph. Vertical dashed white lines represent midnight of each day. Negative depths represent snowpack.

Fig. 5.6

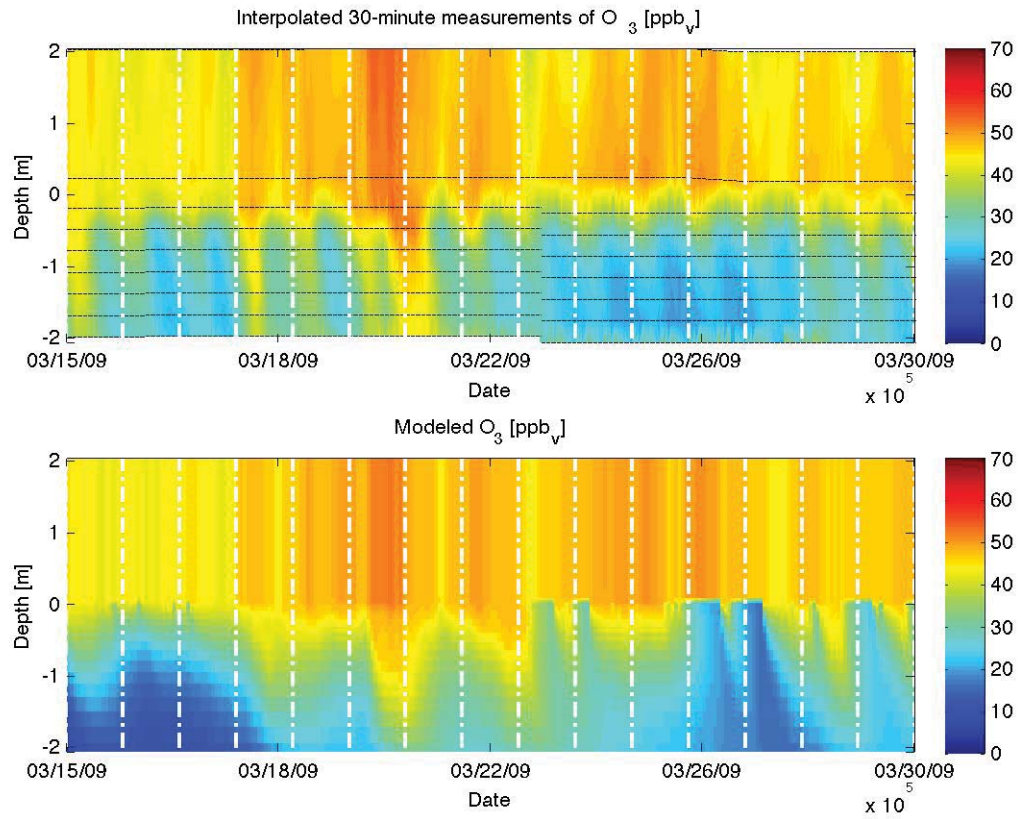


Fig. 5.6. Comparison of modeled and measured O_3 profile in and above snowpack March 15th -30th at Summit, Greenland. Horizontal black lines represent the heights where measurements of chemical species and temperature were made. Vertical dashed white lines represent midnight of each day. Negative depths represent snowpack.

Fig. 5.7

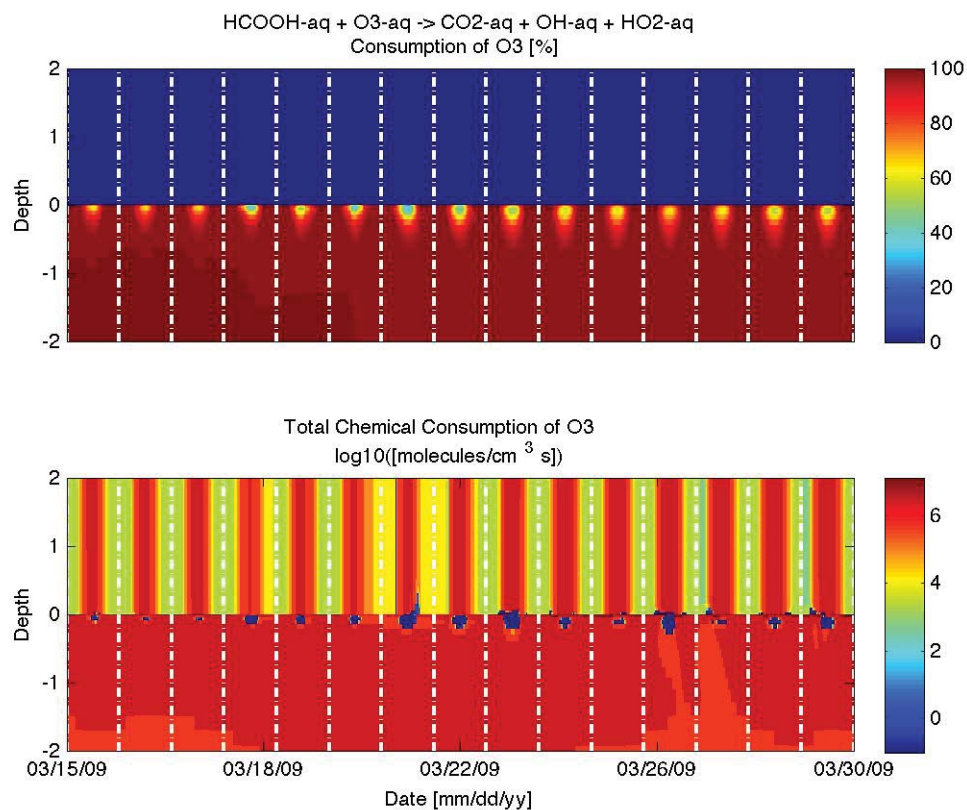


Fig. 5.7. Modeled consumption of O_3 from reaction of aqueous formic acid with ozone for March 15th -30th , 2009 at Summit, Greenland. The top graph shows the percent contribution of the reaction to production rates depicted in the bottom graph. Vertical dashed white lines represent midnight of each day. Negative depths represent snowpack.

Fig. 5.8

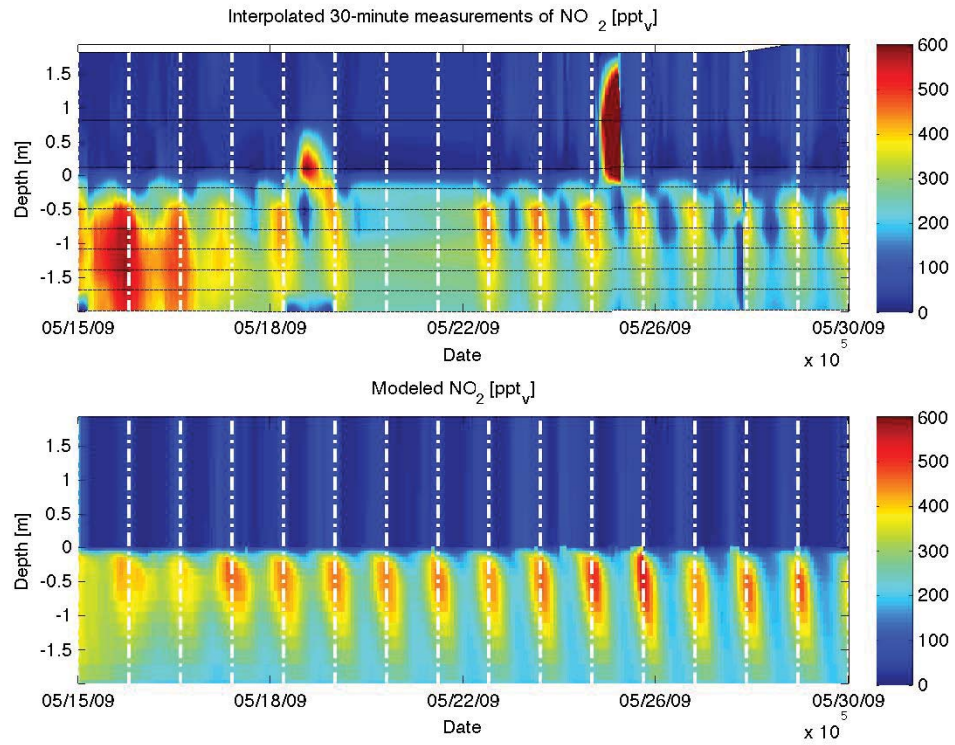


Fig. 5.8. Comparison of modeled and measured NO₂ profile in and above snowpack May 15th-30th at Summit, Greenland. Horizontal black lines represent the heights where measurements of chemical species and temperature were made. Vertical dashed white lines represent midnight of each day. Negative depths represent snowpack.

Fig. 5.9

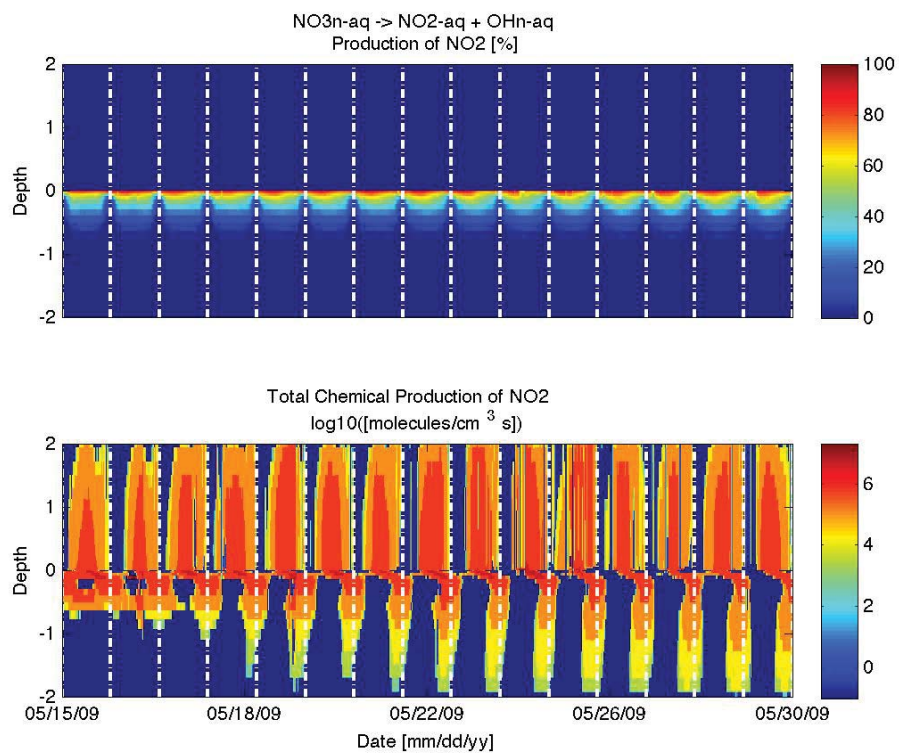


Fig. 5.9. Modeled production of NO₂ from the photolysis of nitrate for May 15th -30th, 2009 at Summit, Greenland. The top graph shows the percent contribution of the reaction to production rates depicted in the bottom graph. Vertical dashed white lines represent midnight of each day. Negative depths represent snowpack.

Fig. 5.10

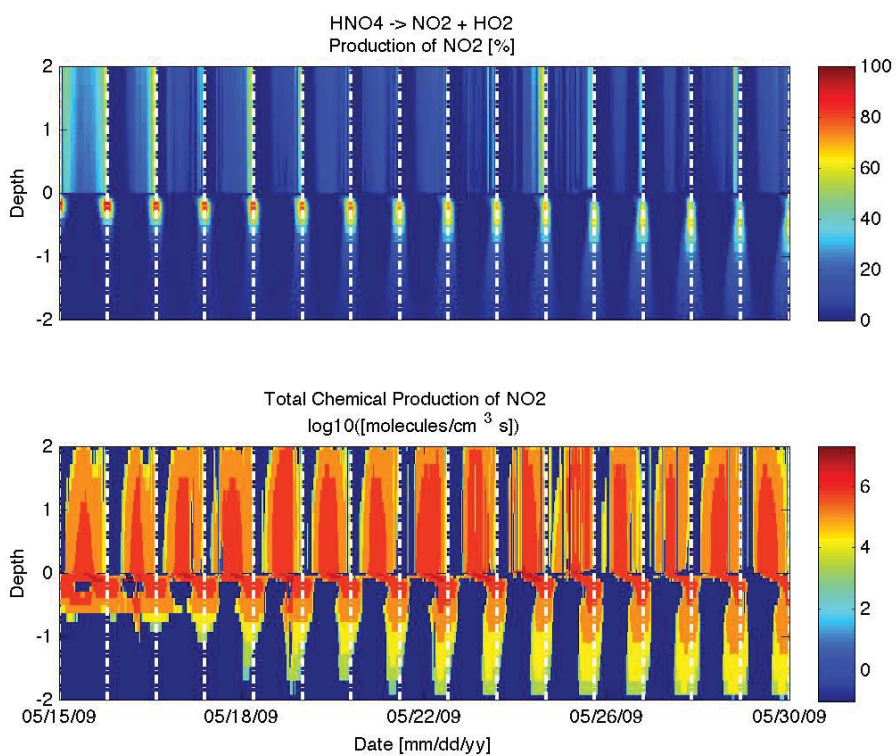


Fig. 5.10. Modeled production of NO₂ from the decomposition of peroxyntic acid for May 15th -30th, 2009 at Summit, Greenland. The top graph shows the percent contribution of the reaction to production rates depicted in the bottom graph. Vertical dashed white lines represent midnight of each day. Negative depths represent snowpack.

Fig. 5.11

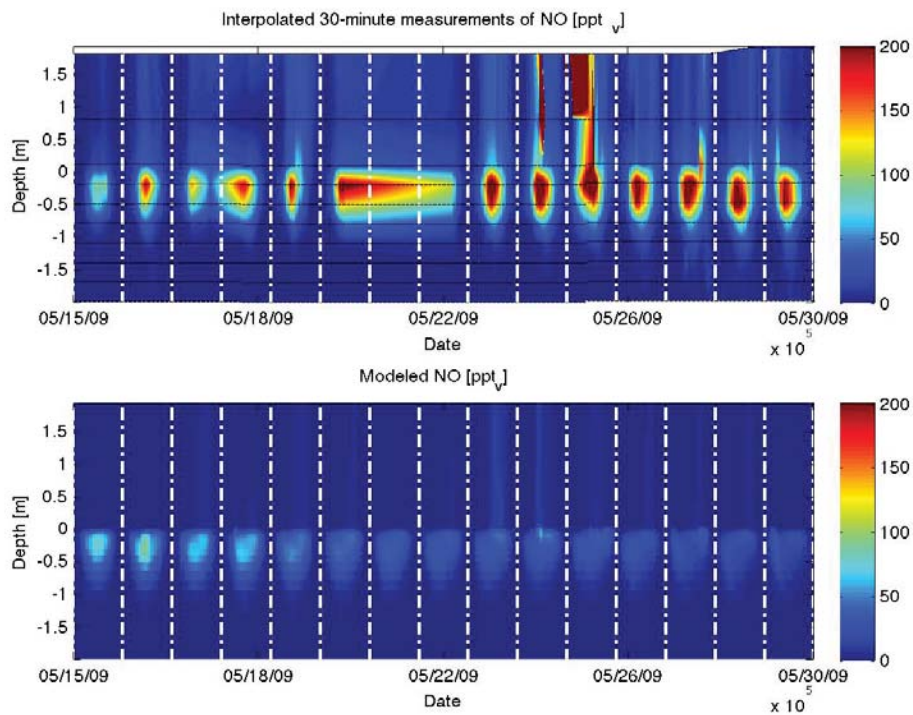


Fig. 5.11. Comparison of modeled and measured NO profile in and above snowpack May 15th-30th at Summit, Greenland. Horizontal black lines represent the heights where measurements of chemical species and temperature were made. Vertical dashed white lines represent midnight of each day. Negative depths represent snowpack.

Fig. 5.12

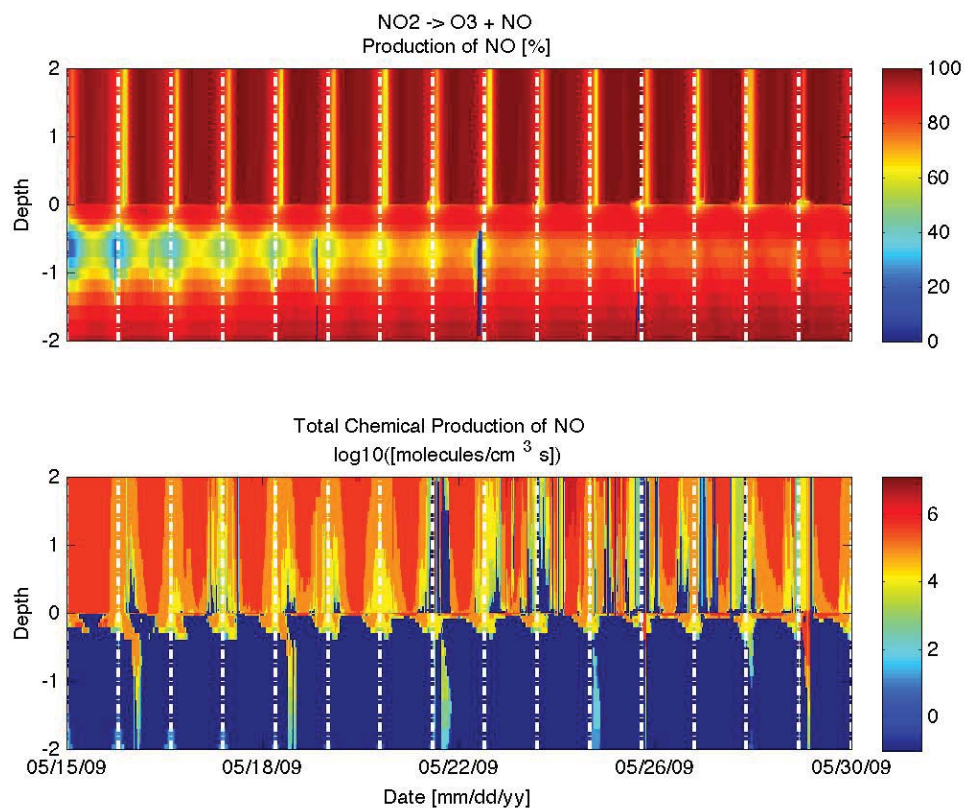


Fig. 5.12. Modeled production of NO from the photolysis of NO₂ for May 15th - 30th, 2009 at Summit, Greenland. The top graph shows the percent contribution of the reaction to production rates depicted in the bottom graph. Vertical dashed white lines represent midnight of each day. Negative depths represent snowpack.

Fig. 5.13

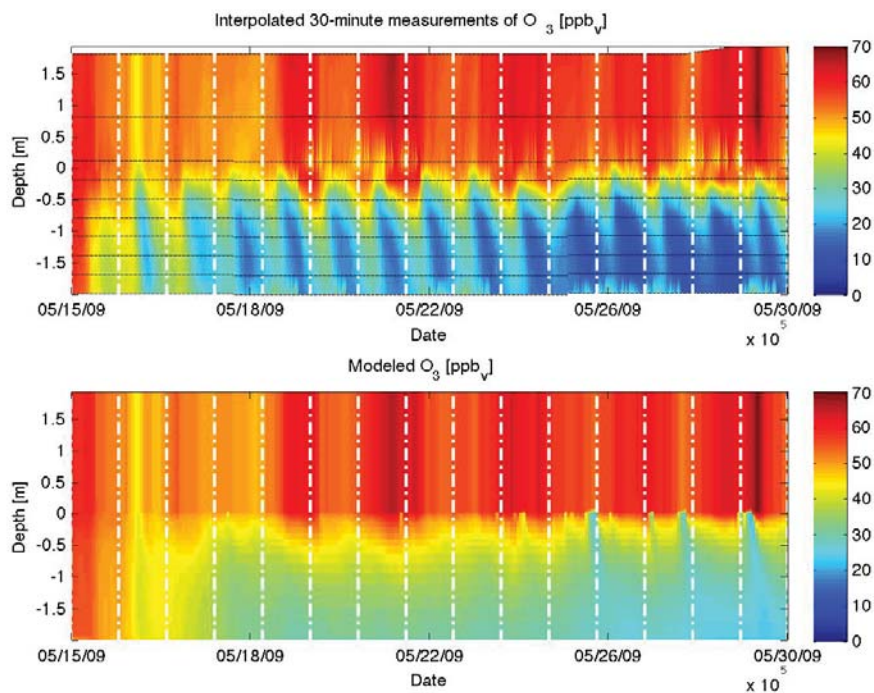


Fig. 5.13. Comparison of modeled and measured O₃ profile in and above snowpack May 15th-30th at Summit, Greenland. Horizontal black lines represent the heights where measurements of chemical species and temperature were made. Vertical dashed white lines represent midnight of each day. Negative depths represent snowpack.

Fig. 5.14

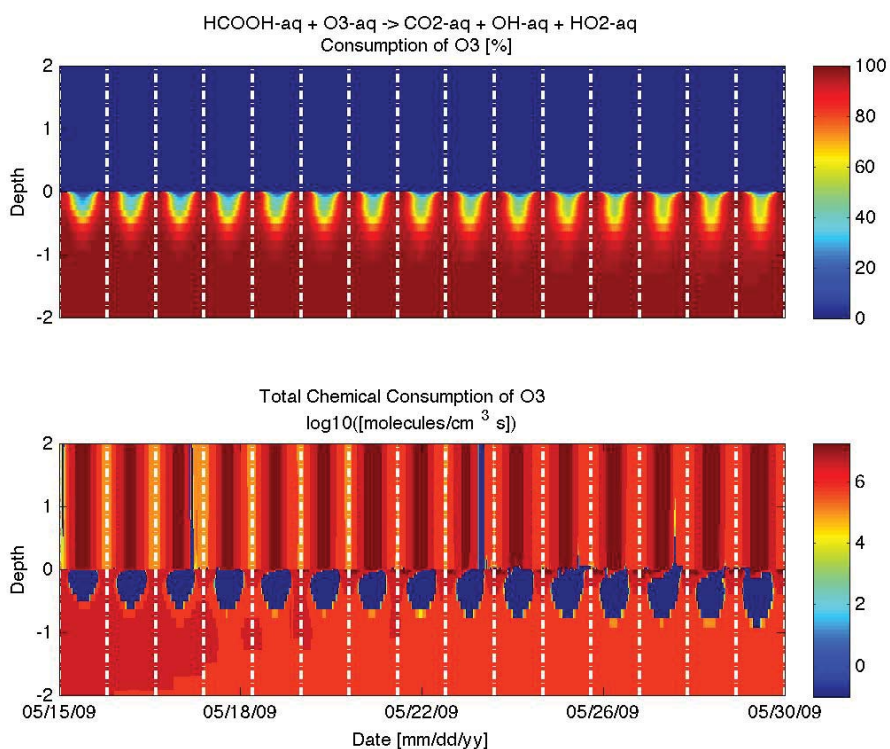


Fig. 5.14. Modeled consumption of O_3 from reaction of aqueous formic acid with ozone for May 15th -30th , 2009 at Summit, Greenland. The top graph shows the percent contribution of the reaction to production rates depicted in the bottom graph. Vertical dashed white lines represent midnight of each day. Negative depths represent snowpack.

Chapter 6. Modeling Dynamics of Ozone and Nitrogen Oxides at Summit, Greenland with a 1-D Process-Scale Model. III. Comparison of Measured Fluxes with Modeled Exchange with Snow^a

Keenan A. Murray¹, Louisa J. Kramer^{2,3}, Paul V. Doskey^{1,3,4,*}, Laurens Ganzeveld⁵, Brian Seok⁶, Brie Van Dam⁶, and Detlev Helmig⁶

¹Department of Civil and Environmental Engineering, Michigan Technological University, Houghton, MI, USA

²Department of Geological and Mining Engineering and Sciences, Michigan Technological University, Houghton, MI, USA

³Atmospheric Sciences Program, Michigan Technological University, Houghton, MI, USA

⁴School of Forest Resources and Environmental Science, Michigan Technological University, Houghton, MI, USA

⁵Department of Environmental Sciences, Wageningen University, Wageningen, Netherlands

⁶Institute of Arctic and Alpine Research, University of Colorado at Boulder, CO, USA

kmurray@mtu.edu, lkramer@mtu.edu, pvdoskey@mtu.edu*, Laurens.Ganzeveld@wur.nl, seok@Colorado.edu, Brie.Vandam@Colorado.EDU, Detlev.Helmig@Colorado.EDU

*Corresponding author. Phone: +1 906-487-2745

^a The material contained in this chapter is part of a planned submission to the Atmospheric Environment Journal.

Abstract

Measured 24-h fluxes of NO_x in April and May 2009 are bidirectional and ranged 2×10^{10} - 9×10^{12} molec $\text{m}^{-2} \text{s}^{-1}$. Modeled 24-h emissions from the snowpack (surface exchange) are always upwards at $2\text{-}7 \times 10^{11}$ molec $\text{m}^{-2} \text{s}^{-1}$ in April and May. “Cleaning” of NO_x fluxes to remove downward fluxes of NO and NO_2 resulted in good agreement between the clean NO_x fluxes and the modeled surface exchanges in April. Cleaned NO_x fluxes in May are an order of magnitude larger than the modeled surface exchange and are similar to previously reported values. By analyzing the surface exchange calculation, it was determined the model cannot produce the clean NO_x fluxes within the parameters of the environment. Modeled fluxes of NO_x in the surface layer in May show an order of magnitude increase of fluxes in the first 50 cm of the atmosphere during the day and is attributed to modeled production of NO_x from the thermal decomposition and photolysis of peroxyntic acid to form NO_2 during the day with minor contributions from the photolysis of HONO to form NO in the early morning. Hence, it is likely that NO_x fluxes in May were increased by chemical production of NO_x near the surface of the snowpack.

Keywords: 1-D process-scale model, flux, NO_x , NO_2 , NO, surface exchange, flux divergence, Summit, Greenland

1. Introduction

Activities of many photo-sensitive chemical species in Arctic snowpack are enhanced during the sunlit season (Dibb et al., 2007). Mixing ratios of nitrogen oxides (NO_x) in snowpack interstitial air are several orders of magnitude larger than atmospheric levels during the sunlit period (Beine, 2002; Honrath et al., 1999; Van Dam et al.). The primary formation mechanism for NO_x within the snowpack is photolysis of nitrate (NO_3^-) in a Liquid-Like Layer (LLL) at the surface of snowflakes (Honrath et al., 2000 ; Murray et al., 2014a). The production of NO_x in the snowpack is large enough to influence ambient NO_x concentrations in remote areas (Davis et al., 2001; Ridley et al., 2000). In the Summer 2000 at Summit, Greenland, the average 24-h upward fluxes of NO_x , nitrous acid (HONO), and nitric acid (HNO_3) were 2.52×10^{12} , 4.64×10^{11} , and 7.16×10^{11} molecules $\text{m}^{-2} \text{s}^{-1}$, respectively, which might indicate reservoir species of NO_x (i.e., NO_y) in snowpack are a source of NO_x to the Arctic atmosphere (Honrath et al., 2002).

Gradient flux measurements are made in the surface layer of the atmospheric boundary layer due to similarity theory. Similarity theory dictates physical and chemical fluxes in the surface layer are constant with height, validating the use of concentrations measurements at two different heights in flux calculations. However, NO_x chemistry involving the NO_x cycle is rapid, implying chemical interchanging between nitrogen monoxide (NO) and nitrogen dioxide (NO_2). The effect of the chemical transformations

on flux measurements is called flux divergence and is a change of chemical fluxes due to chemistry occurring on timescales shorter than transportation timescales (De Arellano et al., 1993). In an attempt to minimize flux divergence, measured fluxes of NO_x are reported instead of fluxes of NO and NO_2 as the quick chemistry of NO_x cycle does not consume or produce NO_x . However, chemical sources and sinks of NO_x can still impact NO_x flux measurements if the chemistry is rapid.

Here we compare measured fluxes of NO_x from the snowpack at Summit, Greenland with model estimates of the atmosphere-surface exchange derived from a 1-D process-scale model (Murray et al., 2014a) . Atmosphere-surface exchange of NO_x will be evaluated for 15-30 April and 15-30 May 2009. Details of the observations and modeling of snowpack chemistry for the 2 periods are reported by Van Dam et al. (2014) and Murray et al. (2014a); (2014b), respectively.

2. Methods

Calculations of atmospheric fluxes are based upon a comprehensive suite of continuous chemical and meteorological measurements at Summit, Greenland Van Dam et al. (2014). Fluxes are calculated using the gradient method as follows (Businger et al., 1971; Dyer, 1974; Honrath et al., 2002):

$$F = -K_H \frac{\partial C}{\partial z} \quad (23)$$

$$K_H = \frac{1}{z_2 - z_1} \int_{z_1}^{z_2} \frac{u_* k z}{\phi(L, z)} dz \quad (24)$$

$$\phi = \left(1 - 15 \frac{z}{L}\right)^{-\frac{1}{2}} \quad L < 0 \quad (25)$$

$$\phi = 1 + \frac{4.7z}{L} \quad L > 0 \quad (26)$$

$$\phi = 1 \quad L = 0 \quad (27)$$

Where F is the flux ($\text{molec m}^{-2} \text{s}^{-1}$) with negative values indicating a downward flux, K_H is the eddy diffusivity ($\text{m}^2 \text{s}^{-1}$), C is concentration (molec m^{-3}), z is the height above the surface (m), u_* is friction velocity (m s^{-1}), k is the Von Karman constant assumed to be 0.4, and L is the Monin-Obuhkov length (m). Equation (24) uses the definition of the calculus average to determine average values of K_H between the two measurement heights that were located at z_1 and z_2 . Meteorological data used to calculate fluxes from the measurements is not filtered based on L to eliminate bias in the comparison with model, which used the raw data to calculate fluxes of chemical species above the snowpack. Raw fluxes were plotted against L to determine bias of the magnitude or direction of the fluxes related to stability of the atmospheric boundary layer (ABL);

however, no biases were indicated. In this paper, references to “measured flux” or “flux” imply measured NO_x fluxes above the surface of the snowpack.

Exchange of chemical species with the snow surface is defined in the 1-D process-scale model as follows:

$$SE = uC_s - \frac{D_g(C_{j+1} - C_j)}{dz} \quad (28)$$

where SE is the modeled exchange of chemical species with the surface ($\text{molec m}^{-2} \text{ s}^{-1}$), u is the vertical velocity of wind at the surface of the snowpack caused by windpumping (m s^{-1}), D_g is the molecular diffusion coefficient ($\text{m}^2 \text{ s}^{-1}$), C_{j+1} and C_j are the concentrations of the species immediately above and below the surface of the snowpack in the model (molec m^{-3}), dz is the distance between C_{j+1} and C_j (m), and C_s is the linearly interpolated concentration of the chemical species at the surface of the snowpack (molec m^{-3}). If C_{j+1} is larger than C_j , the magnitude of u is set to a negative value to create transport in the direction of the gradient. The use of the term “surface exchange” in this paper refers to the modeled exchange of NO_x at the snow-atmosphere interface.

Fluxes and surface exchange of NO_x are calculated using 10 minute measurements and 15 minute modeled data of NO and NO_2 , respectively, and are presented as 24-h averages. The objective of the paper is to compare the surface exchange, or emission, of NO_x from the snowpack to fluxes measured above the snowpack. Modeled 15-min surface exchanges of NO_x are almost always upward, implying emission of NO_x from the snowpack at all times of the day. To perform the comparison between the surface exchange and fluxes, “cleaned” 24-h NO_x , NO, and NO_2 fluxes are calculated using only upward measured fluxes of NO and NO_2 . By “cleaning” the fluxes, we can identify the feasibility of the model misrepresenting surface exchange of NO_x or the possibility of flux divergence impacting flux measurements near the surface of the snowpack.

3. Results and Discussion

3.1. 15-30 April 2009

Measurements of the NO_x fluxes show bidirectional exchange in April and range in magnitude from 2×10^{10} - 1×10^{12} molec $\text{m}^{-2} \text{s}^{-1}$ (Fig. 6.1). Pollution is observed in the NO_x measurements on 18 and 21 of April and on these days’ fluxes should be ignored.

Downward fluxes of NO_x are observed on 16, 19-25, and 28-29 April. Surface exchanges

of NO_x ranges $2\text{-}7 \times 10^{11}$ molec $\text{m}^{-2} \text{s}^{-1}$ over the April episode and agree well with fluxes on 15, 17, 26, and 27 of April. Cleaning of the NO_x fluxes represents upward NO_x fluxes from below the measurement heights. Since the heights of the gradient NO_x measurements in April were roughly at 0 and 2 meters high, the cleaned NO_x fluxes should represent the surface exchange of NO_x from the snowpack, which is confirmed with comparison of the cleaned NO_x flux and surface exchange (Fig. 6.1). Ignoring pollution events, the cleaned NO_x fluxes range $10^{11}\text{-}10^{12}$ molec $\text{m}^{-2} \text{s}^{-1}$. *Honrath et al.* (2002) reported a summertime 24-h NO_x flux of 2.52×10^{12} molec $\text{m}^{-2} \text{s}^{-1}$, which is roughly one magnitude larger than the NO_x fluxes and surface exchange presented for April.

The measured 24-hr fluxes of NO are always downward and range from $10^{11}\text{-}2 \times 10^{12}$ molec $\text{m}^{-2} \text{s}^{-1}$ except on April 21 when pollution is observed in the NO profile (Fig. 6.2). The cleaned NO flux profile has excellent agreement with the modeled NO surface exchange and is roughly an order of magnitude smaller than the measured downward fluxes of NO, implying the downward transport of NO from the atmosphere is larger than NO emissions from the snowpack. On April 16, 19, 24, 25, and 29 the downward flux of NO is the major component of the NO_x flux, meaning transport of NO_x in the surface layer is dominated by downward NO transport from the atmosphere on these days. Similarly, on April 20-23, 29, downward fluxes of NO_2 from the atmosphere dominates the transport of NO_x in the surface layer. The cleaned NO_2 fluxes are similar to the cleaned NO_x fluxes, as NO_2 tends to be the dominant species of NO_x .

3.2. 15-30 May

May NO_x fluxes are mostly upward with downward fluxes occurring on 17-18 and 24 – 27 (Fig. 6.4) and range in magnitude from 2×10^{11} - 9×10^{12} molec m⁻² s⁻¹. Pollution on 24-25 and 27 April is observed in the measurements and these fluxes are ignored. No data is available for flux measurements on May 18 and 21. The surface exchanges in May ranged from 2 - 7×10^{11} molec m⁻² s⁻¹ and are always upward. Fluxes of NO_x are typically less than a magnitude larger than surface exchange except on 29 April when there is good agreement between the flux and surface exchange. Cleaning of the NO_x fluxes creates closer agreement between the fluxes and surface exchanges on 18 and 26 April, however, it also increases the NO_x fluxes on other days (Fig. 6.4). Raw upward and cleaned NO_x fluxes are on the same magnitude measured by *Honrath et al. (2002)*, but the surface exchange is roughly a magnitude lower. This implies either the model underestimates surface exchange of NO_x or NO_x flux measurements capture both the emissions from the snowpack and chemical production below the lower gradient measurement.

Measurements of the NO_x gradients occurred at 0.75 – 1.75 m 15- 27 May and 0.75 - ~2 m 28-29 May, which differs from April when the lower gradient measurement occurred at the surface of the snowpack. Hence, it is possible that production of NO_x below the lower gradient measurement contributes to the deviation between the NO_x surface exchanges and fluxes.

The 24-hr fluxes of NO in May are always downwards and range from 10^{11} - 4×10^{12} molec $m^{-2} s^{-1}$, which are approximately an order of magnitude larger than observed in April (Fig. 6.5). This implies there is larger downward transport of NO from the atmosphere in May compared to April. Downward transportation of NO from the atmosphere dominates the NO_x fluxes on May 24-26, however, May 24 and 25 are pollution events and should be ignored. Cleaning of the NO fluxes results in a cleaned profile that is typically several times larger than the modeled surface exchange except on May 17 when there is excellent agreement. These deviations can be easily explained by the underrepresentation of NO in the modeled profile (Fig. 6.5), but are not a significant portion of NO_x fluxes and surface exchange. On May 19 and 20 the upward fluxes of NO are small and are not depicted in the cleaned NO profile.

Cleaning of the NO_2 fluxes did not produce any significant changes in the flux profile on non-pollution days (Fig. 6.6), implying NO_2 fluxes are primarily composed of upwards fluxes with very little transport of NO_2 downwards from the atmosphere. This behavior is significantly different than April when on several days' downward transportation of NO and NO_2 from the atmosphere dominated NO_x transport in the surface layer. The raw and cleaned NO_2 profiles are up to a magnitude larger than the modeled surface exchange of NO_2 , implying the model either underrepresents production of NO_x in the snowpack or there is significant production of NO_2 between the surface of the snowpack and the lower

gradient measurements. Due to the larger downward fluxes of NO in May and the better agreement between the raw measured fluxes and modeled surface exchange of NO_x, it is possible the larger downward fluxes of NO are partially responsible for the production of NO₂ between the snowpack and lower gradient measurement shown in the cleaned NO_x fluxes.

Increasing the surface exchange of NO_x by an order of magnitude would bring the surface exchange in good agreement with cleaned NO_x fluxes. In order to create the increase, the NO_x gradient or concentration at the snow-atmosphere interface would need to be increased an order of magnitude (Eq. (28)). The modeled NO_x gradients at the interface fluctuates in May, but the mean gradient is ~20 ppt_v. Increasing the gradient an order of magnitude would imply a gradient of 200 ppt_v across the snow-atmosphere interface, which in the model is ~1.5 cm. A NO_x gradient on the same order as observed measurements over a finite distance is unrealistic (Fig. 6.4). The modeled surface concentration of NO_x is diurnal, reaching peaks of ~150 ppt_v at solar noon. Increasing the modeled surface concentration an order of magnitude would create peak surface concentrations of ~1.5 ppb_v, which is vastly larger than any observation in measurements (Fig. 6.4). Hence, the deviation between NO_x fluxes and surface exchange is not from underestimation of surface exchange, but is most likely from NO_x production occurring between the snowpack and the lower gradient measurements. The modeled transport of NO_x above the snowpack supports this theory (Fig. 6.7). During the day, upward modeled NO_x fluxes at the surface of the snowpack increases an order of magnitude in the first 50

cm of the atmosphere, implying the production of NO_x near the surface of the snowpack. The model contributes the majority of the NO_x production above the snowpack to the thermal decomposition and photolysis of peroxyacetic acid to produce NO_2 with a minor contribution from the photolysis of HONO in the early morning producing NO. Therefore, it is likely that flux divergence is occurring near the surface of the snowpack.

3 Conclusion

Fluxes of NO_x in April and May 2009 are bidirectional while modeled NO_x surface exchanges are always upwards. “Cleaning” of NO_x fluxes to remove downward fluxes of NO and NO_2 resulted in good agreement between the clean NO_x fluxes and the modeled surface exchanges in April and ranged $2\text{-}7 \times 10^{11}$ molec m^{-2} s^{-1} . Modeled surface exchanges of NO_x in May are in the same range as April, but cleaned NO_x fluxes deviated an order of magnitude larger and are similar to previously reported values. By analyzing the surface exchange calculation, it was determined the model cannot produce the NO_x fluxes within the parameters of the environment and the deviations between the cleaned NO_x fluxes and surface exchange are most likely a result of flux divergence occurring near the surface of the snowpack in May. Modeled transport of NO_x above the snowpack in May supports this hypothesis with NO_x fluxes increasing of an order of magnitude in the first 50 cm of the atmosphere during the day. The model contributes the majority of the NO_x production to the thermal decomposition and photolysis of

peroxyntic acid to form NO_2 during the day with minor contributions from the photolysis of HONO to form NO in the early morning. Hence, it is likely that NO_x fluxes in May were increased by chemical production of NO_x between the snowpack and the lower gradient measurements.

Acknowledgments

Keenan A. Murray acknowledges assistance from V. Rao Kotamarthi (Argonne National Laboratory) with modeling chemical dynamics of the atmospheric boundary layer and partial funding through teaching assistantships provided by Michigan Technological University. The Arctic System Science Program of the National Science Foundation provided funding for the study through grant NSF-OPP-07-13992.

References

- Beine, H.J., Honrath, R.E., Domine, F., Simpson, W., Fuentes, J.D., 2002. NO_x during background and ozone depletion periods at Alert: Fluxes above the snow surface. *J. Geophys. Res.* 107, 4584.
- Businger, J.A., Wyngaard, J.C., Izumi, Y., Bradley, E.F., 1971. Flux-Profile Relationships in the Atmospheric Surface Layer. *Journal of the Atmospheric Sciences* 28, 181-189.
- Davis, D., Nowak, J.B., Chen, G., Buhr, M., Arimoto, R., Hogan, A., Eisele, F., Mauldin, L., Tanner, D., Shetter, R., Lefer, B., McMurry, P., 2001. Unexpected high levels of NO observed at South Pole. *Geophysical Research Letters* 28, 3625-3628.
- De Arellano, J.V.-G., Duynkerke, P.G., Builtjes, P.J.H., 1993. The divergence of the turbulent diffusion flux in the surface layer due to chemical reactions: the NO-O₃-NO₂ system. *Tellus B* 45, 23-33.
- Dibb, J.E., Albert, M., Anastasio, C., Atlas, E., Beyersdorf, A.J., Blake, N.J., Blake, D.R., Bocquet, F., Burkhardt, J.F., Chen, G., Cohen, L., Conway, T.J., Courville, Z., Frey, M.M., Friel, D.K., Galbavy, E.S., Hall, S., Hastings, M.G., Helmig, D., Greg Huey, L., Hutterli, M.A., Jarvis, J.C., Lefer, B.L., Meinardi, S., Neff, W., Oltmans, S.J., Sherwood Rowland, F., Sjostedt, S.J., Steig, E.J., Swanson, A.L., Tanner, D.J., 2007. An overview of air-snow exchange at Summit, Greenland: Recent experiments and findings. *Atmospheric Environment* 41, 4995-5006.

- Dyer, A.J., 1974. A review of flux-profile relationships. *Boundary-Layer Meteorol* 7, 363-372.
- Honrath, R.E., Guo, S., Peterson, M.C., Dziobak, M.P., Dibb, J.E., Arsenault, M.A., 2000. Photochemical production of gas phase NO_x from ice crystal NO₃⁻. *Journal of Geophysical Research* 105, 24183.
- Honrath, R.E., Lu, Y., Peterson, M.C., Dibb, J.E., Arsenault, M.A., Cullen, N.J., Steffen, K., 2002. Vertical fluxes of NO_x, HONO, and HNO₃ above the snowpack at Summit, Greenland. *Atmospheric Environment* 36, 2629-2640.
- Honrath, R.E., Peterson, M.C., Guo, S., Dibb, J.E., Shepson, P.B., Campbell, B., 1999. Evidence of NO_x production within or upon ice particles in the Greenland snowpack. *Geophysical Research Letters* 26, 695-698.
- Murray, K., B., V.D., Doskey, P.V., Seok, B., Ganzeveld, L., Kramer, L., Helmig, D., 2014a. Modeling Dynamics of Ozone and Nitrogen Oxides at Summit, Greenland with a 1-D Process-Scale Model. I. Model Presentation and Chemical Dynamics During a Spring Ozone Intrusion Event.
- Murray, K., Van Dam, B., Doskey, P.V., Seok, B., Ganzeveld, L., Kramer, L., Helmig, D., 2014b. Modeling Dynamics of Ozone and Nitrogen Oxides at Summit, Greenland with a 1-D Process-Scale Model II. Temporal Variations of Snowpack Chemistry.

Ridley, B., Walega, J., Montzka, D., Grahek, F., Atlas, E., Flocke, F., Stroud, V., Deary, J., Gallant, A., Boudries, H., Bottenheim, J., Anlauf, K., Worthy, D., Sumner, A.L., Splawn, B., Shepson, P., 2000. Is the Arctic Surface Layer a Source and Sink of NO_x in Winter/Spring? *Journal of Atmospheric Chemistry* 36, 1-22.

Van Dam, B., Helmig, D., Doskey, P.V., Kramer, L., Murray, K., Ganzeveld, L., Toro, C., Seok, B., 2014. Multi-year observations of O₃ and NO_x dynamics in the Summit, Greenland snowpack.

Figure

Fig. 6.1

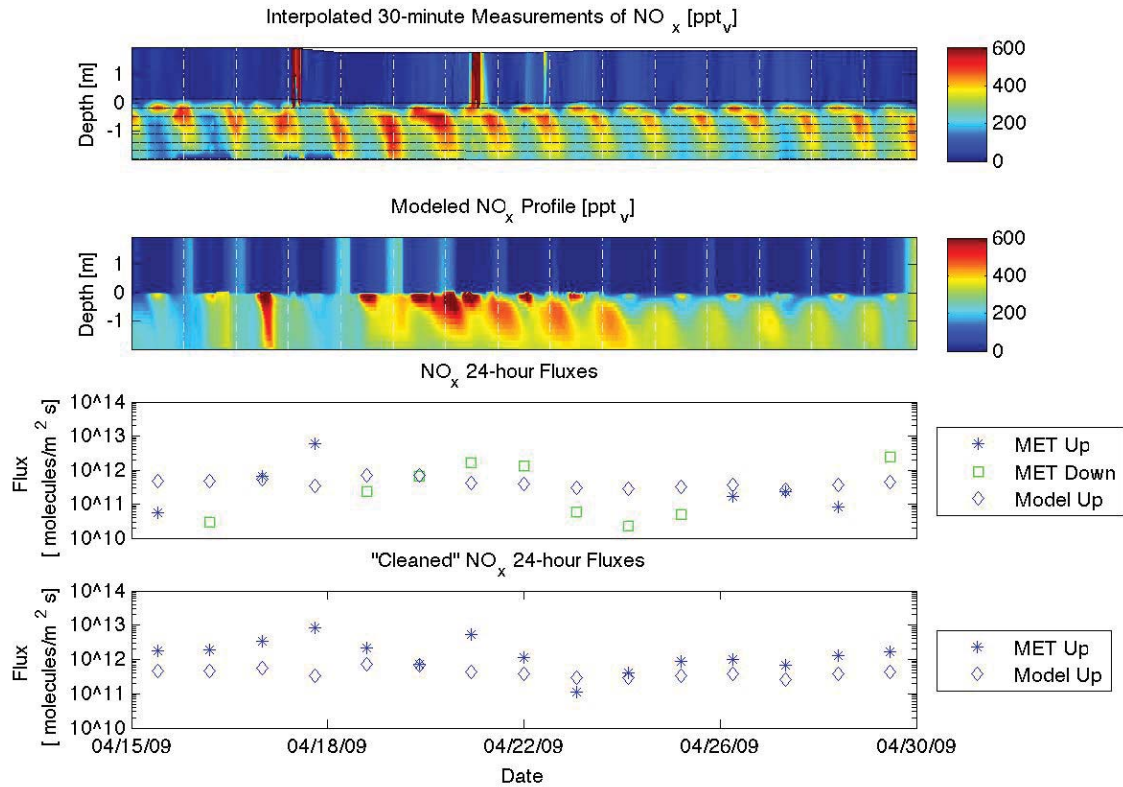


Fig. 6.1. Measured flux and modeled surface exchange of NO_x for April 15th-30th, 2009. The top plot shows the 30-min interpolated measurements of NO_x as a function of time and depth in ppt_v . The second subplot is the modeled NO_x profile from the 1-D process scale model. The NO_x 24-hr flux plot shows the measured fluxes and modeled surface exchange. A subplot of “Cleaned” NO_x 24-h fluxes represents NO_x fluxes with downward fluxes of NO and NO_2 removed. Vertical white lines on the contour graphs represent midnight of each day while horizontal dashed black lines represent heights in which measurements were made. The flux legend contains 3 entries. Entries prefaced of “MET” and “Model” are measured fluxes from a meteorological tower and modeled surface exchanges, respectively, while entries with “Up” and “Down” refer to directionality of the flux.

Fig. 6.2

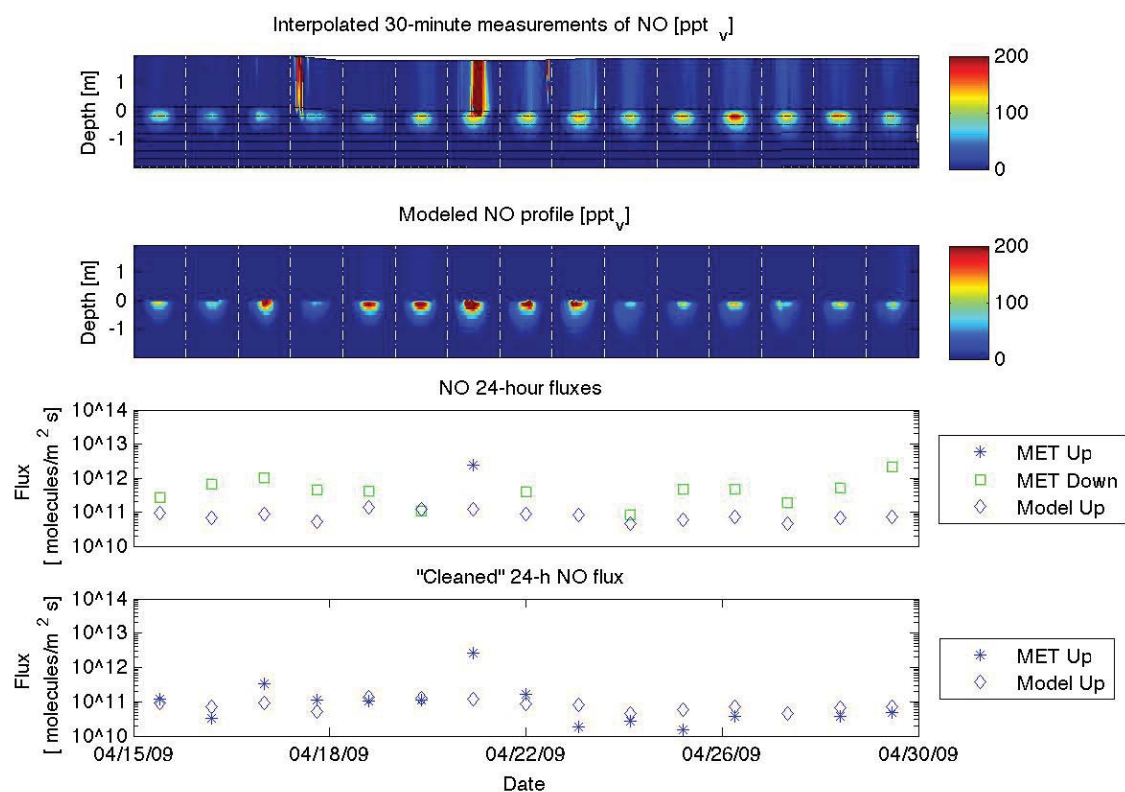


Fig. 6.2. Measured flux and modeled surface exchange of NO for April 15th-30th, 2009. The top plot shows the 30-min interpolated measurements of NO as a function of time and depth in ppt_v. The second subplot is the modeled NO profile from the 1-D process scale model. The NO 24-hr flux plot shows the measured fluxes and modeled surface exchange. A subplot of “Cleaned” NO 24-h fluxes represents upward measured NO fluxes. Vertical white lines on the contour graphs represent midnight of each day while horizontal dashed black lines represent heights in which measurements were made. The flux legend contains 3 entries. Entries prefaces of “MET” and “Model” are measured fluxes from a meteorological tower and modeled surface exchanges, respectively, while entries with “Up” and “Down” refer to directionality of the flux.

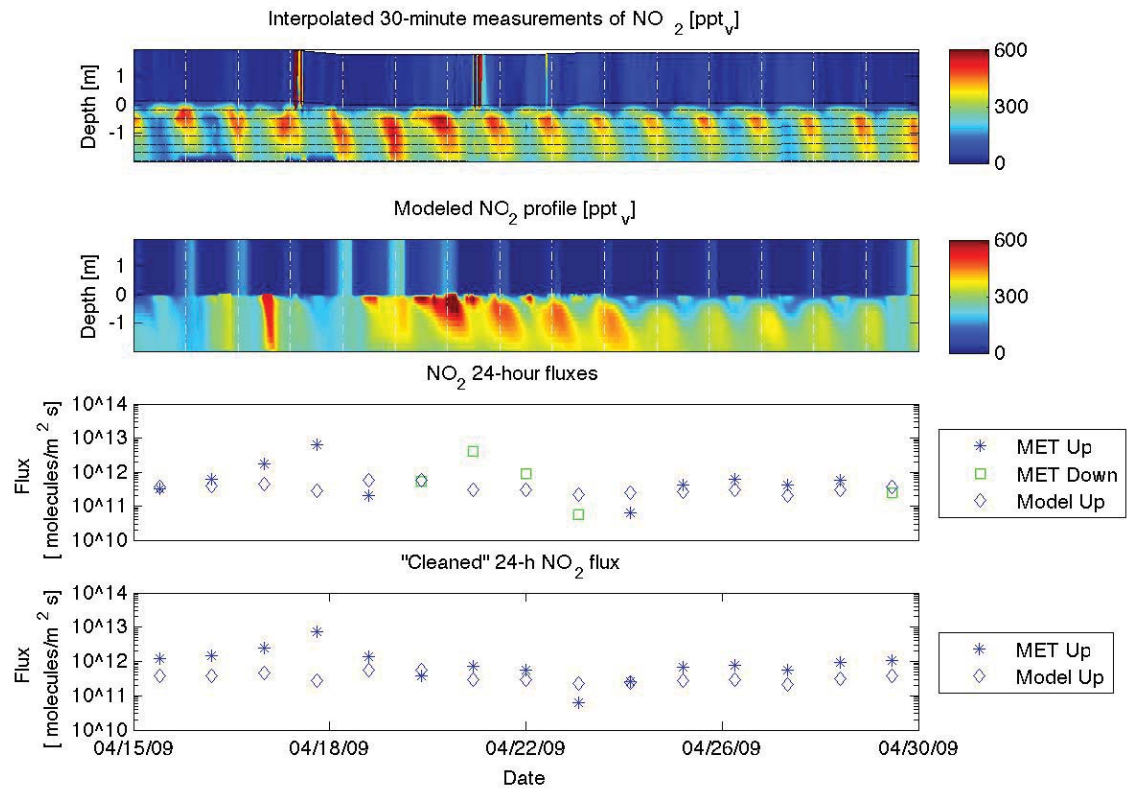


Fig. 6.3

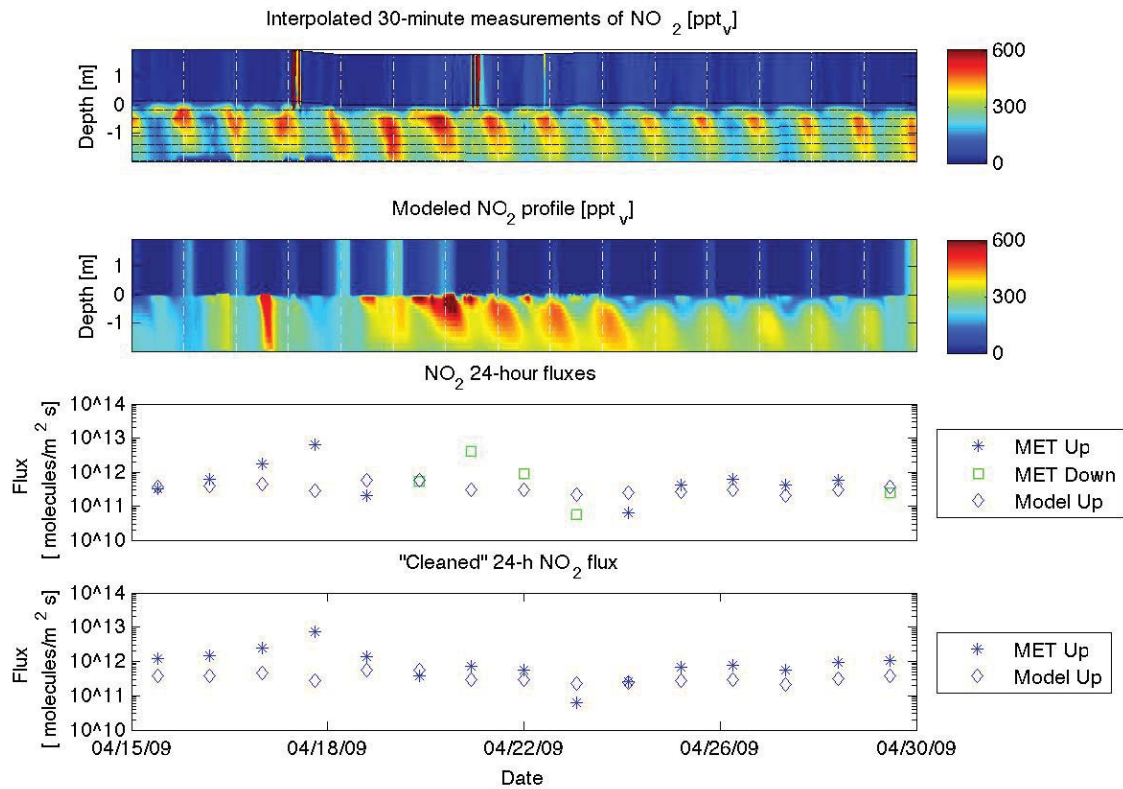


Fig. 6.3. Measured flux and modeled surface exchange of NO_2 for April 15th-30th, 2009. The top plot shows the 30-min interpolated measurements of NO_2 as a function of time and depth in ppt_v . The second subplot is the modeled NO_2 profile from the 1-D process scale model. The NO_2 24-hr flux plot shows the measured fluxes and modeled surface exchange. A subplot of “Cleaned” NO_2 24-h fluxes represents upward measured NO_2 fluxes. Vertical white lines on the contour graphs represent midnight of each day while horizontal dashed black lines represent heights in which measurements were made. The flux legend contains 3 entries. Entries prefaces of “MET” and “Model” are measured fluxes from a meteorological tower and modeled surface exchanges, respectively, while entries with “Up” and “Down” refer to directionality of the flux.

Fig. 6.4

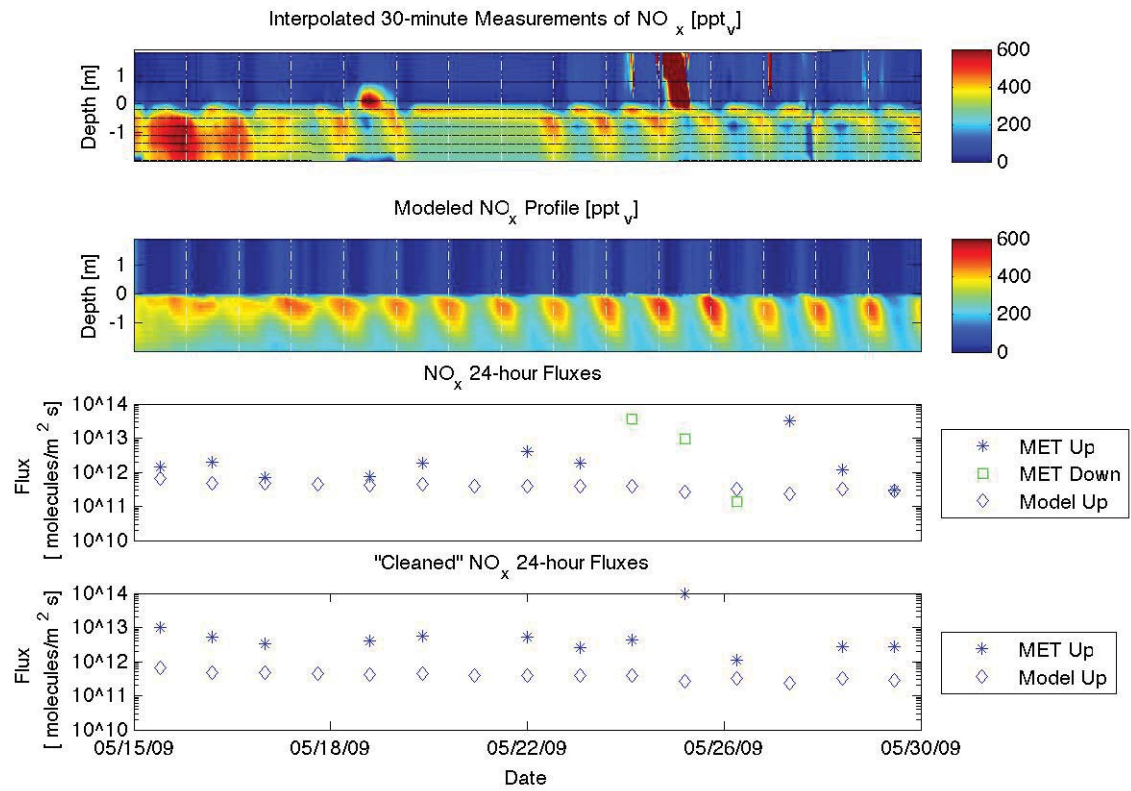


Fig. 6.4. Measured flux and modeled surface exchange of NO_x for May 15th-30th, 2009. A subplot of “Cleaned” NO_x 24-h fluxes represents NO_x fluxes with downward fluxes of NO and NO_2 removed. Vertical white lines on the contour graphs represent midnight of each day while horizontal dashed black lines represent heights in which measurements were made. The flux legend contains 3 entries. Entries prefaces of “MET” and “Model” are measured fluxes from a meteorological tower and modeled surface exchanges, respectively, while entries with “Up” and “Down” refer to directionality of the flux.

Fig. 6.5

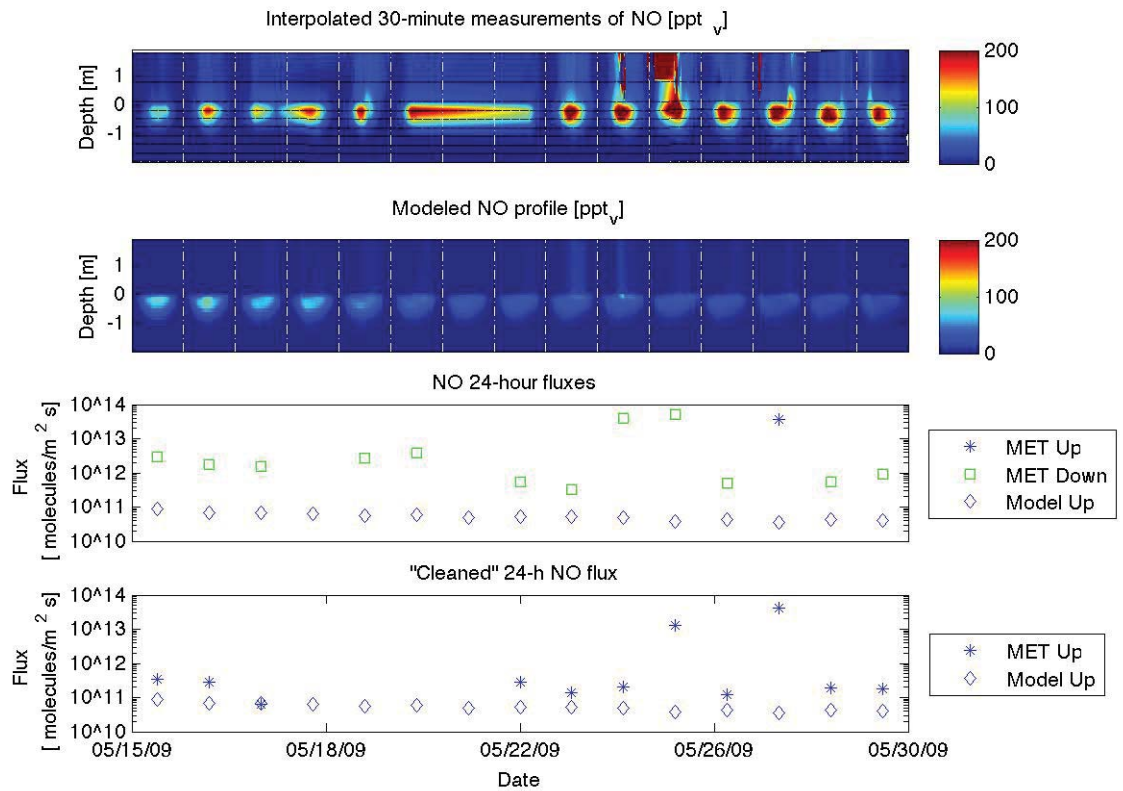


Fig. 6.5 Measured flux and modeled surface exchange of NO for May15th-30th, 2009. The top plot shows the 30-min interpolated measurements of NO as a function of time and depth in ppt_v. The second subplot is the modeled NO profile from the 1-D process scale model. The NO 24-hr flux plot shows the measured fluxes and modeled surface exchange. A subplot of “Cleaned” NO 24-h fluxes represents upward measured NO fluxes. Vertical white lines on the contour graphs represent midnight of each day while horizontal dashed black lines represent heights in which measurements were made. The flux legend contains 3 entries. Entries prefaces of “MET” and “Model” are measured fluxes from a meteorological tower and modeled surface exchanges, respectively, while entries with “Up” and “Down” refer to directionality of the flux.

Fig. 6.6

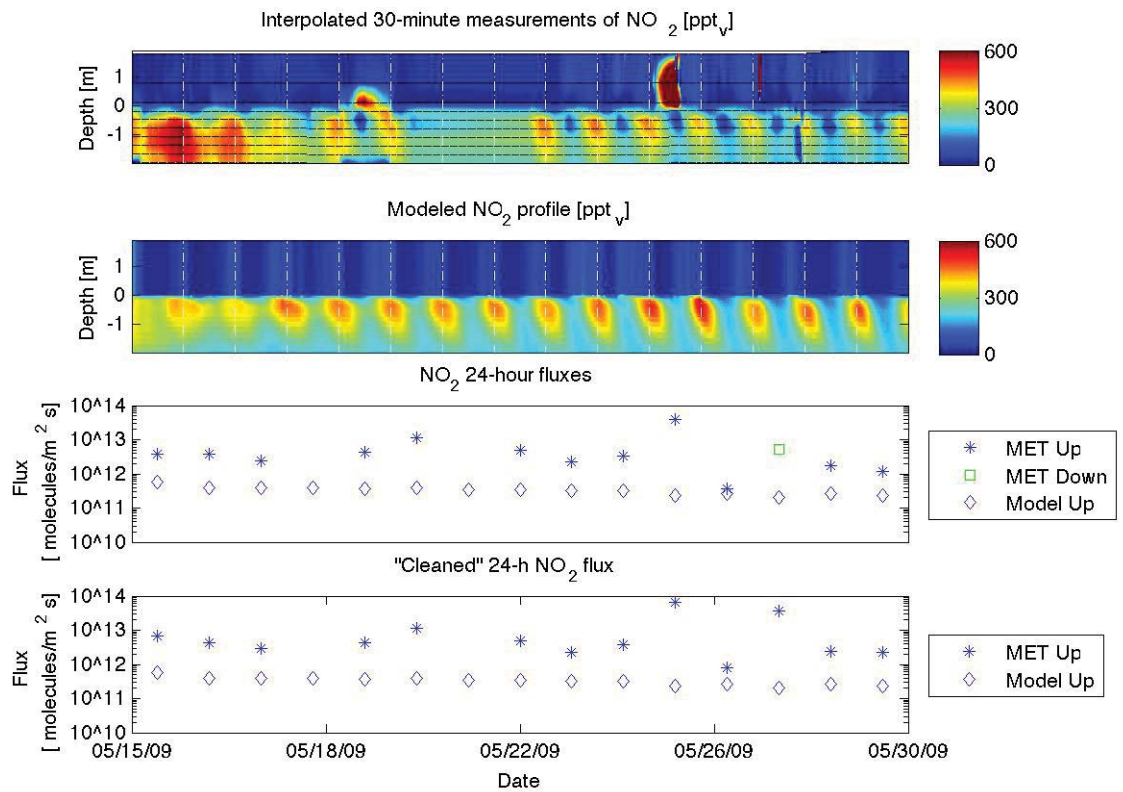


Fig. 6.6 Measured flux and modeled surface exchange of NO_2 for May 15th-30th, 2009. The top plot shows the 30-min interpolated measurements of NO_2 as a function of time and depth in ppt_v . The second subplot is the modeled NO_2 profile from the 1-D process scale model. The NO_2 24-hr flux plot shows the measured fluxes and modeled surface exchange. A subplot of “Cleaned” NO_2 24-h fluxes represents upward measured NO_2 fluxes. Vertical white lines on the contour graphs represent midnight of each day while horizontal dashed black lines represent heights in which measurements were made. The flux legend contains 3 entries. Entries prefaced of “MET” and “Model” are measured fluxes from a meteorological tower and modeled surface exchanges, respectively, while entries with “Up” and “Down” refer to directionality of the flux.

Fig. 6.7

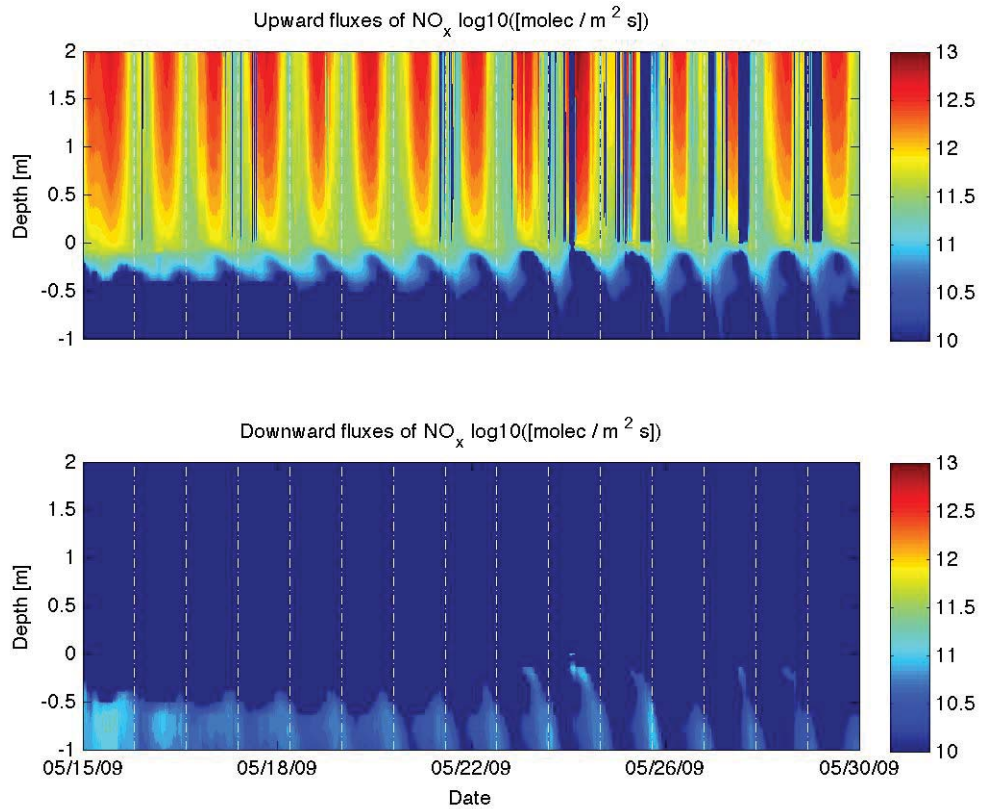


Fig. 6.7 Modeled fluxes of NO_x for May 15th-30th, 2009. The top and bottom graph shows the upward and downward fluxes of NO_x on a log₁₀ scale as a function of depth and time, respectively. Vertical white lines on the contour graphs represent midnight of each day.

Chapter 7. Conclusions

The process-scale model presented in this work is capable of reproducing trends of NO_x and O_3 observed in the snowpack for the April and May time periods. The photolysis of nitrate in the top 50 cm of the snowpack is responsible for production of NO_2 at solar noon and peaked at 10^8 and 10^7 - 10^8 molec cm^{-3} s^{-1} in April and May, respectively. NO_2 production in May was limited to the surface of the snowpack due to fast NO_x cycling and storage of NO_x as HNO_4 . The model run for the March episode overestimated NO_2 peaks despite the lower initialization concentration of nitrate. Nighttime profiles of NO_2 in April and May episodes are from HNO_4 produced in the aqueous phase decomposing in the gas phase to produce NO_2 , which is transported up to 2 m deep in the snowpack. The nighttime production rates of NO_2 peaks in the top 50 cm of the snowpack at 10^8 and 10^6 molec cm^{-3} s^{-1} in April and May, respectively. Lower production of HNO_4 in the aqueous phase caused by a decrease in HO_2 production resulted in an underestimated nighttime NO_2 profile in March.

Production of NO in the top 50 cm of the snowpack near solar noon is related to the photolysis of NO_2 for March-May. In the March episode the NO profile is a result of the photolysis of NO_2 in the gas and aqueous phases and implies mass transfer of NO from the aqueous to gas phase to produce the NO profile. Production of NO in April and May is from gas phase photolysis of NO_2 and peaked at 10^6 molec cm^{-3} s^{-1} and 10^4 molec cm^{-3} s^{-1} , respectively. The peak production of May NO occurred in the evening during HNO_4

decomposition to form NO_2 . Consumption of NO and NO_2 was modeled at solar noon in May implying quick conversions between NO and NO_2 and storage of NO_x as HNO_4 , resulting in underestimated peaks of NO . Based upon these model observations, there is missing source of NO separate from NO_2 photolysis or the rate of conversion of NO to NO_2 needs to be reduced to accumulate NO at solar noon. Unreasonably high initial concentration of nitrite was used in the May model run in an attempt to provide a source of NO , but failed to produce NO at solar noon.

The major sink of O_3 in all time periods is the aqueous reaction of formic acid with O_3 to form CO_2 , OH , and HO_2 . Consumption rates of O_3 in the snowpack were estimated at 10^6 , 10^6 - 10^7 , and 10^8 molec cm^{-3} s^{-1} in March, April, and May, respectively, and occurred throughout the snowpack except at the surface of the snowpack near solar noon when production of O_3 was modeled. The O_3 production was a result of high concentrations of HO_2 and NO_x near the surface of the snowpack and produced small ozone intrusions during the day that are not observed in measurements. This implies either an excess of NO_x and HO_x in the snowpack at solar noon or a missing ozone sink. The latter is more likely as NO_x and HO_x are responsible for the day and nighttime profiles of NO and NO_2 .

Fluxes of NO_x in April and May 2009 are bidirectional while NO_x surface exchanges are always upwards. "Cleaning" of NO_x fluxes to remove downward fluxes of NO and NO_2 resulted in good agreement between the clean NO_x fluxes and the modeled surface

exchanges in April and ranged $2-7 \times 10^{11}$ molec $m^{-2} s^{-1}$. Surface exchanges of NO_x in May are in the same range as April, but cleaned NO_x fluxes deviated an order of magnitude larger and are similar to previously reported values. By analyzing the surface exchange calculation, it was determined the model cannot produce the NO_x fluxes within the parameters of the environment. Modeled transport of NO_x above the snowpack shows an order of magnitude increase of NO_x fluxes in the first 50 cm of the snowpack and is attributed to the production of NO_2 during the day from the thermal decomposition and photolysis of peroxyntic acid with minor contributions of NO from $HONO$ photolysis in the early morning. Hence, it is likely that NO_x fluxes in May were increased by chemical production of NO_x between the snowpack and the lower gradient measurements.

Moving forward with the model, further temporal analyses of NO_x chemistry should be performed to further verify the findings in this dissertation. Specifically, it would be beneficial to determine the chemical dynamics to produce observed NO_x profiles during early spring when irradiance is low. The model may also be used to analyze other chemical species and dynamics at Summit such as halogens and HO_x . Comparisons of measured fluxes of NO_x above the snowpack to modeled surface exchange at the atmosphere-snowpack interface should be further pursued to determine the impact of flux divergence caused by temporal variations of measurements and spatial variations in flux measurement heights.